CAPILLARY SCALE REAGENT INTRODUCTION AND OPTICAL DETECTORS FOR CAPILLARY SCALE ANALYSIS

by

SANTOSH K. MISHRA

Presented to the Faculty of the Graduate School of
The University of Texas at Arlington in Partial Fulfillment
of the Requirements
for the Degree of

DOCTOR OF PHILOSOPHY

THE UNIVERSITY OF TEXAS AT ARLINGTON
August 2011

ACKNOWLEDGEMENTS

Though only my name appears on the cover of this dissertation, a great many people have contributed to its production. I owe my gratitude to all those people without whom my graduate experience would not be one that I will cherish forever.

I will always be proud to be a graduate student of The University of Texas at Arlington - Chemistry and Biochemistry Doctoral program, and I will be eternally grateful to my esteemed advisor, Prof. Purnendu (Sandy) Dasgupta who trusted in my intellectual capacity, supervised my graduate work from the onset to the end. This dissertation would not have been possible without his excellent guidance. Not only was he readily available to me, as he so generously is for all of his students, but he always read and responded to the drafts of each chapter of my work more quickly than I could have hoped. His oral and written comments are always extremely perceptive, helpful, and appropriate. He has enlightened me through his wide knowledge, helped me to see life and science in their full depth, and taught me how to appreciate the good scientific work that helps other researchers to build on it. I thank him for all his moral and financial support, caring nature, patience and providing me with an excellent atmosphere for conducting research. I would like to thank the National Science Foundation (Grant # CHE-0731792) for funding the entire research discussed in this dissertation.

The members of my dissertation committee, Dr. Kevin A. Schug and Dr. Xiyun (Richard) Guan have generously given their time and expertise to better my work. I thank them for their contribution and their ongoing support. I also thank Prof. Daniel W. Armstrong, Prof. Dasgupta and Dr. Schug for their lectures in 2007, which gave me the resources essential in my doctoral research. I am grateful to Dr. Brian Edwards, the department Scientific Apparatus Engineer, who maintained all the equipment in my lab so efficiently that I never had to worry about viruses, losing files, creating backups or installing software. Special thanks to Mr. Howard

Bailiff for his assistance in machining various devices for this research. Speaking of coffee, I'd like to thank the staff of Chemistry Department for tolerating my presence twice a day for the past five years. Their stimulant infusion provided the necessary boost to keep me operating through the night.

It was a pleasure to share doctoral studies and life with lab mates like Dr. Mrinal Sengupta, Dr. Ignacio Villanueva, Dr. Bingcheng Yang, Dr. Masaki Takeuchi, Dr. Shin-ichi Ohira, Dr. Andrea Kirk, Jason Dyke and Charles Phillip Shelor. Many good friends, especially Mr. Gaurav Arora and Dr. Jiney Jose, have helped me stay sane through these difficult years. Their support and care helped me overcome setbacks and stay focused on my graduate study. I greatly value their friendship and I deeply appreciate their belief in me.

I would like to thank my family—my father, Mr. Asha Pal Mishra, my mother, Mrs. Asha Mishra, my sister, Mrs. Ragini Shukla, my brother, Mr. Pradeep Mishra, my father-in-law, Mr. Murlidhar Rashinkar, my mother-in-law, Mrs. Pramila Rashinkar, my extended family and Mrs. Kajori Dasgupta—for their trust, love and warm support during my odyssey at the University of Texas at Arlington.

Last but not least, I am deeply thankful to my life partner, my beloved wife, Shilpa, who was also my colleague at the University of Texas at Arlington. She has always given me courage to overcome any obstacles and stood by my side through thick and thin. Were it not for her I would be a very different person today, and without *her* this achievement could not be accomplished. I dedicate this dissertation to my wife, Shilpa and to my son, Sushrut Mishra for their motivation, unconditional love and sacrifice. It has been a great journey for us all.

July 18, 2011

ABSTRACT

CAPILLARY SCALE REAGENT INTRODUCTION

AND OPTICAL DETECTORS FOR

CAPILLARY SCALE

ANALYSIS

Santosh K. Mishra, PhD

The University of Texas at Arlington, 2011

Supervising Professor: Purnendu K. Dasgupta

Atmospheric aerosols are of great interest as they have the potential to perturb the earth's radiative energy balance, influence the climate, reduce visibility, and adversely affect human health. The composition of atmospheric particulate matter, especially the concentrations of metals and their ratios, provide insights into sources of the aerosol. Capillary scale ion chromatography systems have several advantages over conventional chromatographic analysis systems like low reagent consumption, small sample requirement, higher efficiencies and better absolute mass detection limits. Hence, to achieve source identification and source apportionment, optical detector based capillary ion chromatography systems are proposed to perform qualitative and quantitative analysis of metal ions in a continuous fashion.

Optical absorption detection is the most common mode of detection in analytical chemistry and chromatography. A simple, economical, versatile, light emitting diode based capillary scale multi-reflection absorbance detector was investigated. The detector performance is better than

commercial absorbance detectors and the fabrication cost for the detector is a small fraction of the cost of commercial absorbance detectors.

The sensitivity of fluorescence detection is often much better than that of absorbance detection. A capillary ion chromatography compatible, simple, versatile, liquid-core waveguide-based fluorescence detector was developed. A commercially available Teflon® AF coated fused silica capillary was used as a liquid core waveguide detection cell; this was transversely excited. Very high detection sensitivities (low picomol to low femtomol level detection limits) were achieved with very good reproducibility.

Postcolumn reagent addition is a very common technique utilized in liquid/ion chromatography because the detection selectivity and sensitivity can be increased considerably thanks to the derivatization reaction. A capillary scale, low volume, dilutionless, pulseless, electrodialytic reagent introduction device was investigated for large ionizable ligands such as 2-(4-pyridyl azo) resorcinol that can form intensely colored metal chelates. The electrodialysis current is easily controlled and governs the amount of reagent introduced.

TABLE OF CONTENTS

LIST OF ILLUSTRATIONS

CHAPTER 1

INTRODUCTION

1.1 Aerosols

The term ‘aerosol’, originally coined in 1920 as an analog of ‘hydrosol’ (stable liquid suspension of solid particles), connotes two phase systems consisting of solid or liquid particles in gas [1]. Aerosols, also called suspended particulate matter, aero colloidal systems or dispersions, are simply defined as solid or liquid particles suspended in gas [1]. The atmosphere, whether urban or rural, contains high concentration of aerosol particles (approximately 10^7-10^8 cm^{-3}) [2]. The chemical composition of aerosols as a function of size is different as aerosol formation can occur via different possible routes like chemical reaction, nucleation, condensation, coagulation, cloud/fog processing, evaporation of gases, mechanical disruption and suspension of solids [3]. The stability of aerosols varies from a few seconds to a year or more [1]. The concentration of aerosols, depending on meteorological conditions and the source of emission, varies considerably spatially and temporally [4]. Also, the composition of atmospheric particulate matter for a given location changes during the year depending on the weather [4].

The size, shape and density are important parameters of aerosol particles (often called atmospheric/airborne particulate matter (PM)) for characterizing their behavior [1]. The mean diameter of aerosol particles span over five orders of magnitude, from 0.001 to 100 μm [1]. Atmospheric PM are mostly non-spherical, whose size is represented by equivalent *Stokes diameter* or *aerodynamic diameter* [5]. *Stokes diameter* is the diameter of the sphere that has the same settling velocity (rate at which the particle settles in still fluid) and the same density as that of the particle while *aerodynamic diameter* (AD) is the diameter of the unit density (1 g/cm^3) sphere that has the same settling velocity as that of the particle [5]. Aerodynamic diameter is

the more commonly used term for representing the particle size [5]. Particles less than 2.5 μm diameter ($PM_{2.5}$) are generally called “fine” while those greater than 2.5 μm in diameters are called “coarse” [1].

The physical and chemical properties as well as the lifetime of the particle are affected by its size [2]. Source of atmospheric aerosol particles can either be natural like windblown dust, pollens, plant fragments and sea-salt or anthropogenic (e.g., automobile exhaust, wood combustion, power generation), etc. [2]. Atmospheric particulate matter is a complex mixture of small solid particles and it consists of various components like salts (sulfates, nitrates and ammonium), organic material (like carbon compounds, aromatic compounds and polyaromatic hydrocarbons), crustal species, sea salt, metal oxides, hydrogen ions, water, etc. [4]. Coarse particles contain crustal elements like magnesium, aluminum, silicon, calcium and iron and biogenic organic materials like pollen, spores, plant fragments, etc. [4]. Fine particles usually contain sulfates, nitrates and ammonium salts along with organic and elemental carbon and certain transition metals [4].

Particles may be either directly emitted into the atmosphere (primary particles) or formed there by chemical reactions (secondary particles) [6]. Primary fine mode particles are largely generated by combustion and high temperature processes while coarse mode particles are usually originate from mechanical processes like grinding and entrainment of soil and dust [6].

Various trace elements have been routinely detected in atmospheric particulate matter [6]. These may originate from different sources including dust, waste incineration, smelters, boilers, steel furnaces, combustion of coal, vehicle exhaust and brake wear [6].

1.2 Health hazards associated with particulate matter and metals in particulate matter

The average amount of air inhaled by a human is 13 m^3/day [7,8]. Impact on human health by a specific source is calculated by the equation: impact = emissions x intake fractions x toxicity, where, emissions is mass emitted (per unit time), intake fraction is mass inhaled per

mass emitted, toxicity is health impact (like disease rate or numerical risk of adverse outcomes) per mass inhaled [8]. Parameters like population density, wind speed and atmospheric mixing height affect the intake fraction [8]. The height of an emission source plays an important role in fate and exposure to the PM emitted from that source. Hence emission sources can be categorized as high stack (100 m), low stack (25 m) and ground level sources [8].

United States Environment Protection Agency (U.S. EPA) is currently concerned about particulate matter 10 μm and smaller as this size range particle passes through the throat, nose and enter into the respiratory system [9]. EPA categorizes inhalable particles according to their sizes viz., PM_{10} (particles with aerodynamic diameter $\leq$ 10 μm), $PM_{10-2.5}$ ("coarse" particles with aerodynamic diameter between 10-2.5 μm), $PM_{2.5}$ ("fine" particles with aerodynamic diameter $\leq$ 2.5 μm) and $PM_{0.1}$ ("ultrafine" particles with aerodynamic diameter less than 0.1 μm) [9]. $PM_{2.5}$ intake fraction is 4 times higher for ground level (mobile) sources as compared to elevated stationary sources (s.g., stacks) [8]. Coarse and fine particles differ in their composition [10]. Fine and ultrafine particles have carbonaceous core (with metals and organics adsorbed on the surface cavities) while coarse particles typically consist of insoluble crustal minerals, biological material, sea salt, etc. [10]. PM shape and size determine the location of deposition in the respiratory system. $PM_{2.5-10}$ i.e., coarse particles deposit in the upper respiratory tract while fine particles ($PM_{2.5}$) reach the alveolar region [11]. Water soluble metals can be released into lung alveoli and can get deposited in the lung parenchyma [10]. Water insoluble metals stay in the lower respiratory tract for a longer duration compared to water soluble metals [12]. Because of its small size and large surface area, $PM_{2.5}$ sorbs more toxic chemicals per unit mass and can be easily deposited in the body and is hence closely related to morbidity and mortality [11,13]. Metals can be present as water-soluble salts, or as water-insoluble oxides or can be complexed to soluble or insoluble components [12]. Metals present as insoluble oxides can have natural or anthropogenic origin whereas, water soluble metals can be originated from certain emission source pollution particles [12]. In general, metals originating from anthropogenic sources are

more soluble than those from crustal sources [14].

US EPA classifies Cr, Cd, As, Ni, Mn and Pb as mobile source air toxics (MSAT) [15]. Cu and Fe are redox-active metals and are linked to reactive oxygen species (ROS) generation *in-vivo,* detrimental to health [15]. PM (containing transition metals like Fe, Zn and Cu) are toxic because they may dissolve in lung fluid and cause cellular inflammation via release of free radicals due to Fenton's or like reactions [16]. The soluble fraction of PM containing transition metals can cause oxidative damage (due to reactive oxygen species like hydroxyl and superoxide anion radicals) to proteins, enzymes, cellular membrane lipids and DNA [10]. Water soluble transition metals with that easily undergo redox changes adversely affect membrane lipid peroxidation and initiate oxidative DNA damage [10]. Soluble metals (Fe, Ni, V, Co, Cu, Cr) in/on inhaled particles are linked to cellular oxidative stress in airway epithelial cells of the respiratory system [10]. A study was carried out to investigate the adverse effect of $PM_{2.5}$ constituents on DNA damage induction in A549 human lung cells [17]. The extent of oxidative damage was proportional to qualitative and quantitative composition of metals in $PM_{2.5}$ [17]. Zn has been correlated to lung problems [18]. Water soluble metals in PM adversely affect the blood coagulation times and exacerbate thrombotic diseases like atherosclerosis [19]. A recent study suggests that ambient air pollution affects the birth weight of full term infants [20]. $PM_{2.5}$ water soluble metals and other components were associated with small reduction in birth weights [20]. These metals might deposit in fetal tissues and consequently affect fetal growth [20]. Ni, Cr and Cd (human carcinogens) salts have clastogenic and/or uneugenic properties [21].

As particulate matter metals may cause severe damage to human health, it is very important to identify the emission sources that normally emit characteristic metals (singly or in specific ratio (isotopically within metals) and among metals) and accordingly apportion the metals to their respective sources i.e., carry out a source apportionment study.

1.3 PM source apportionment

Source identification helps policy makers and modelers develop control strategies to reduce PM concentrations [22]. Correct sampling procedures, chemical analysis methods and knowledge of predominant anthropogenic sources are important for successful source identification as well as source apportionment studies. Source apportionment is performed to validate the data, establish the relationship between emission sources and ambient air quality and update the emissions inventory [22]. Various sources may contribute to a specific event and their contribution will typically vary from event to event. Chemical speciation assists in determining the contribution of known emission sources as well as identification of new particle emission sources [22].

If a constant ratio is obtained between the concentrations of two chemical species for multiple studies, then the two chemical species can be considered to come from the same source. Also, if a constant ratio is obtained between two chemicals, then one chemical can be used as the indicator (or surrogate) for the other chemical [23]. When a specific ratio of chemicals is used to identify the sources, extreme caution has to be observed as chemicals undergo degradation at different rates [24]. Metals, however, cannot be transmuted. Also chemicals, which are ubiquitously present in large concentrations, should not be used for determining the ratio [24].

To determine the adequacy and completeness of the collected data, a statistical evaluation must be performed, which must be consistent with data quality objectives. However, if statistical methods are not applied or interpreted correctly, then it might lead to flawed, even fatally flawed opinions [25]. To evaluate and demonstrate measurement trends, researchers use regression, correlation and multivariate statistical techniques like Principal Component Analysis (PCA) [25].

Two basic techniques to compare and evaluate relationships between multiple

constituents (or variables) from a given data set are regression and correlation [26]. The correlation coefficient is primarily used for exploratory data analysis [27-32]. It is advisable to establish a correlation matrix if multiple species are considered. Depending on favorable quantitative value of the correlation coefficients, they can be termed to have ‘high’ correlation, ‘close’ correlation and ‘significant’ correlation in decreasing order of significance [26].

Some particles formed via atmospheric chemical reactions may undergo chemical transformations leading to the changes in their chemical and physical properties. Hence, receptor models (like PCA) are used for source identification and source apportionment [33]. Correlation and regression also form the backbone of more sophisticated techniques like Principal Component Analysis and Receptor Modeling [26]. Receptor models quantify source contribution using a theoretical and mathematical framework [33]. Multivariate statistical methods can be utilized (only if a source exhibits one or more characteristic chemical fingerprints) to determine the number of fingerprints of a given source, chemical composition of each fingerprint and relative contribution of each fingerprint in each collected sample [34]. PCA mainly includes following 4 steps viz., (1) data transformation, (2) singular value or eigenvector decomposition, (3) determination of number of significant eigenvectors and (4) visual display of loading plots and scores [34]. PCA reduces the number of correlated variables in a given data set by transforming the variables to a new set of principal components (PCs) or uncorrelated reference variables. PCs are then sorted out so that almost all variability between the samples can be accounted for by a small number of PCs and the relationships between multivariate samples can be assessed easily using visual scores and plots [34]. PCA is a commonly used method used in source apportionment studies [13,34-41].

1.4 PM metal determination techniques

Atmospheric transportation of metals largely occurs via the aerosol phase. The concentrations of metals in atmospheric aerosols depend on their sources. Throughout this document by metal aerosols we mean aerosol particles that contain metals, in whatever form,

elemental or combined or a mixture thereof. Natural metal aerosol sources include crustal minerals (from soil or dust resuspension, erosion, surface winds, volcanic eruptions), volcanic eruptions, forest fires and oceans. Anthropogenic sources of metal aerosols include incineration, fossil-fuel combustion, industrial activities, vehicle tire and brake lining abrasions, etc.

Several techniques have been utilized for the determination of metals in atmospheric aerosols. These techniques include particle-induced X-ray emission (PIXE) [40], inductively coupled plasma mass spectrometry (ICPMS) [15, 16, 17, 30, 32, 37, 39, 41, 43,45, 47, 52, 54], inductively coupled plasma optical emission spectroscopy (ICP-OES) [12, 42, 44, 46, 48, 51, 54],ion chromatography (IC) [16,27,37, 43,45, 49, 51],energy dispersive X-ray fluorescence (XRF) [44, 49, 53], atomic absorption spectrophotometry (AAS) [11, 29, 35, 36],laser ablation coupled to inductively coupled plasma mass spectrometry (LA-ICPMS) [28].

1.5 Need for on-line study

Normally, heavy metals, found in particulate matter and aerosols, are present in the concentration range of low to sub ng/m^3 and hence long sampling periods (usually many hours) are required for the collection before sufficient sample is available for analysis [13]. Inertial methods such as gravitational settling, centrifugation and electrostatic/thermal precipitation as well as filtration are available for ambient aerosol collection. Filtration is the most common approach for sampling aerosols. Air sampling is usually performed for long duration (6-24 h) to accumulate an easily measurable amount of the samples; many different filter types like mixed cellulose esters, polycarbonate, polyvinyl chloride, glass or quartz fiber and silver membrane filters may be used [39,40,55,56].

The field-collected sample is typically transported to the laboratory and then analyzed. Depending on the analyte sought, the composition of the sample may change during such transport and hence may not reflect the actual composition of the collected sample. Also, some

atmospheric species exhibit short half-lives and their concentration can change rapidly [3]. Dasgupta *et al.* have established the instrumentation for near continuous (15 min time resolution) measurement of acidic and basic atmospheric gases and simple cationic and anionic constituents of atmospheric PM as well as the acidity of atmospheric aerosols [57-67].

There has been a lack of instrumentation that could provide real time or near-real time information about the atmospheric metals in a reasonably short time. Mukhtar and Limbeck performed on-line flow-injection analysis of Zinc present on PM_{10} using flame atomic absorption spectrometry (FAAS); however, the sampling was performed separately on filter for few hours. Only the analyte was dynamically extracted from the collected sample and the extract was injected into the FIA system [18]. Dasgupta *et al.* have successfully analyzed atmospheric Cr (VI) in an automated manner wherein the air sampling time was reduced to 15 minutes and the sample (collected on one of the two filters used in the set up) was washed and preconcentrated on anion exchange minicolumn and eluted with 0.1 M sodium perchlorate followed by reaction with sym-1,5-diphenylcarbazide before being detected by a light emitting diode-based dedicated flow through absorbance detector [68].

In case of on-line or real-time analysis, sampling, sample preparation and analysis must be coupled in an integral and automated manner. This reduces the contamination due to human error, labor cost and analysis cost per sample, improving data quality, system reliability and sample throughput. To characterize metal concentrations in atmospheric aerosols with high time resolution, to prevent loss of sample integrity and to deliver accurate qualitative and quantitative information (for source identification and source apportionment purposes) on-line analysis is essential.

1.6 Capillary ion chromatography: advantages and challenges

The word Chromatography (which in Greek means “color writing”) is defined as the ‘physical method of separation in which the components to be separated are distributed between two phases, one of which is stationary (stationary phase) while the other (the mobile

phase) moves in a definite direction' [69]. The origin of chromatography can be traced back to Tswett's scientific discovery (in early 1900's) of separating chlorophyll pigments, which were adsorbed in several colored zones over the length of a glass column packed with $CaCO_3$ particles. This initial discovery led to other chromatographic techniques like paper chromatography, thin layer chromatography and ion exchange chromatography (in the 1930's), gas chromatography and gel chromatography (in the 1950's), supercritical chromatography (in the 1960's), high pressure (or performance) liquid chromatography (in the late 1960's) and ion chromatography (in the 1970s) [70]. Horvath *et al.* in late 1960's demonstrated the separation of ribonucleotides using 1.0 mm i.d. stainless steel capillary packed with 30 um particles [71]. This led to the advent of micro or capillary liquid chromatography (containing columns less than 1.0 mm i.d. and micro flow detector cells) [72]. Capillary scale liquid chromatography has several advantages over its conventional size counterparts that use 4-6 mm i.d. columns: more efficient separation, improved mass sensitivity, lower reagent consumption, small sample requirement, small footprint and easy coupling to detectors that can handle low flow rates. Micro liquid chromatography and capillary liquid chromatography has progressed rapidly and several reviews are available [73-75].

Ion chromatography is the separation of ionic or ionizable compounds wherein 'the separation is based on the differences in the ion exchange affinities of the sample components' [69]. The pioneering work in the field of ion chromatography is attributed to Small, Stevens and Baumann who published a seminal paper in 1975, which described a chromatographic system with an electrical conductivity detector and two columns (one with a low exchange capacity for separating the ionic/ionizable analytes and the other with high exchange capacity for reducing the background conductivity) [76].

Research has been carried out to perform ion chromatography on a capillary scale for a long time. Several challenges have been associated with capillary scale ion chromatography separations. These include: (a) preparation of packed capillary columns of small dimensions (<1

mm i.d.), (b) preparation and efficient use of narrow bore open tubular capillary columns (<0.01 mm), (c) reliable pumping of extremely small flow rates (< 20 µL/min), (d) reproducible injection of minuscule amounts of sample (to avoid overloading of column as well as to prevent band broadening), (e) using a small enough detection volume but have sufficient detection sensitivity to measure small amounts of an analyte, etc. [77]. Rokushika *et al.* in 1983, reported their work on the separation of anions and carboxylic acids using a capillary ion chromatography system, which was based on a capillary column (0.19 mm i.d. fused silica capillary) packed with anion exchange resin and a capillary scale Nafion® perfluorosulfonate hollow fiber tubing suppressor [78]. They also demonstrated the use of an UV detector for the detection of UV absorbing anions (like aminobenzoic acids, nucleotides and nucleobases) in capillary ion chromatography [79].

The first capillary ion chromatography system equipped with NaOH electrodialytic eluent generator (on the high pressure end) was established by Sjögren *et al.* [80]. Boring et al. successfully established capillary scale anion chromatography set up (small enough to fit in custom briefcase) and utilized it for the field study to analyze the atmospheric water soluble gases [81,82]. Capillary scale anion chromatographic separation and detection have been carried out by many researchers, but separation and detection of cations on capillary scale has remained a challenge [77]. Capillary scale separation and indirect photometric detection of monovalent cations (Li^+, Na^+, K^+, NH_4^+) has been attempted with capillary columns (0.35 mm x 50 mm, packed with 10 µm particles) and a capillary scale suppressor (0.35 mm x 35-40 mm) [83]. Alkali and alkaline earth metals have been separated using capillary open tubular chromatography using 4.6 µm i.d. polybuytadiene-maleic acid column [84]. Very recently, Dionex Corp. (now Dionex/Thermofisher) has commercialized capillary scale chromatography instrumentation and has showed its utility for the determination of alkali and alkaline earth metals viz., Li, Na, K, Mg and Ca using a suppressed conductivity detector [85]. But capillary scale cation chromatography for the detection of transition or heavy metals has not been

successfully achieved: In addition to previously mentioned limitations, it is difficult to obtain a 'metal free' chromatographic system and this hinders trace level metal detection. However, macro scale detection of many metal ions has been achieved by Dasgupta *et al*. using highly sensitive fluorescence detectors based on light emitting diodes and Teflon® AF coated fused silica capillaries [86,87].

1.7 Dissertation overview

The primary objective of this research was to improve presently existing metal analysis technique(s) so it could be utilized for source identification and source apportionment studies. This was partly accomplished by the development of capillary scale detection schemes (mainly optical detection) as optical detection is the most common method of detection used in the field of analytical chemistry.

Chapter 2 provides our initial work i.e., development of a capillary scale optical detector with high sensitivity. This chapter describes the development of a simple, inexpensive, versatile capillary scale light emitting diode based multi-reflection absorbance detector that relies on commercially available fused silica capillaries [88]. Different parameters like capillary cross-section, length of the multi-reflection coating, and the angle of light incidence were optimized for the best possible configuration. The effective pathlengths were observed to be greater at low absorbance values, indicating that the detection cells were truly multipath systems. The component cost, including data processing electronics, is a fraction of the cost of the commercial instruments and the multi-reflection detector shows over 50-fold gain in signal-to-noise (S/N) as compared to single-pass on-tube configuration with the same capillary. Under pneumatic flow (pulseless) conditions, the limit of detection (LOD) was 4.4 fmol (2.6 pg) of Bromothymol Blue (BTB).

Fluorescence detection has better detection sensitivity (about three orders of magnitude better) than the absorbance detection as the fluorescence detection of analyte takes place at a different wavelength (emission) as compared to the excitation wavelength and hence the

detection takes place in absence of bright background used for exciting the molecules. Chapter 3 provides an account of my next attempt in attaining high detection sensitivities for the detection of metals. This was achieved by the fabrication of capillary scale liquid core waveguide (LCW) based fluorescence detectors that could be utilized for capillary ion chromatography and other microflow or capillary systems [89]. I had worked on the preliminary design of the LCW based fluorescence detector wherein conventional LED was used as the light source and an economical light-to-voltage convertor (photosensor) was used as the detector. Other members of the group performed the rest of the work in this chapter. A Teflon® AF coated fused silica capillary served as the LCW and it was transversely excited with a conventional or a high power LED or a laser source. The detection sensitivity increased with the power of the light emitted by the source. The S/N=3 LOD for the constructed fluorescence detector (with high power LED and miniature photomultiplier tube (mPMT) detector) was 3.8 fmol Al with relative standard deviation of 1.5% (n=10) at the 20 fmol level.

Additionally, capillary scale post-column reagent introduction was developed to expand the horizon of capillary scale detection by introducing reagents that either form chromogenic or fluorogenic compounds with the analyte of interest [90]. Postcolumn reagent introduction is an important and one of the oldest techniques used in liquid/ion chromatography. Detection selectivity and sensitivity can be significantly improved by the introduction of a derivatization reagent. Chapter 4 of this dissertation deals with the development of a novel capillary scale electrodialytic reagent introduction device, which (in combination with the LED based multi-reflection capillary absorbance detector) was successfully utilized for the detection of several metals. This electrodialytic reagent introduction device introduced minimal band broadening effect as it had very low internal volume of 300 nL. It had the added advantage of introducing reagents without any pulsations as the reagent ions were introduced into the analyte channel under the influence of electric current, thus improving the detection limits. A limit of detection of 0.5 fmol Zn (S/N = 3) was observed with a capillary scale flow injection system with simple LED

based multi-reflection absorbance detector. I concluded that capillary scale post electrodialytic reagent introduction device can be successfully used for the trace detection of atmospheric metals.

Overall, the work documented here has contributed to the overall goal of the group to use atmospheric metals for source identification and source apportionment studies. Chapter 5 presents some conclusions and future directions of the techniques presented in this work. The work presented in Chapter 2, 3 and 4 have been published and a part of the research mentioned in this Chapter 5 (viz., on-line detection of atmospheric metals using inductively coupled plasma mass spectrometry) is currently under preparation for publication and has not been included in this dissertation.

CHAPTER 2

CAPILLARY SCALE LIGHT EMITTING DIODE BASED MULTI-REFLECTION ABSORBANCE DETECTOR

2.1 Introduction

UV–Vis absorption measurement is by far the most common detection technique in analytical chemistry especially as such measurements have been extended to optically transparent analytes by detecting them as negative peaks in separation systems that use an absorbing background. The interest in capillary scale optical absorbance detectors was originally in context with capillary electrophoresis (CE) systems. However, capillary scale analysis systems now encompass a lot more than CE systems and the same principles apply to microfluidic devices. In fact, high efficiency CE must also have very small illuminated volumes to maintain the fidelity of the separation achieved, in capillary scale flow injection analysis (FIA) etc., this is not a major requirement. As the drive to miniaturization continues, capillary scale small detectors will doubtless continue to play a more important part. However, relative to some other means of detection such as amperometry and laser-induced fluorescence, detection sensitivity is substantially poorer, this is where capillary scale absorbance detection really needs improvement [91].

2.1.1 Linearity, sensitivity and optical aperture

One of the problems with designing a conventional on-capillary detector is that great care must be exercised in designing the optical aperture; else, much of the light travels around the liquid, generating stray light and reducing the linear dynamic range and deteriorating detection limits[92,92]; the situation is particularly exacerbated with capillaries having an i.d. of $\leq$50 μm [95]. Boring and Dasgupta [95] advocated twin razor blade based slits width about the same as that of the capillary i.d. Kitagishi and Sato [92] have more recently reported on the optimized slit width for a 75 μm i.d. capillary to be 67 μm. Even when the slit width has been

properly chosen and stray light has been minimized, the sensitivity is essentially controlled by the limited path length: the light passes through the capillary radially, only once. The effective path length is somewhat less than the i.d. of the capillary; obviously an infinitely small slit width would be necessary if only the diametric path were to be strictly addressed. Methods for calculating the average pathlength from the geometry of the aperture has been discussed in the literature [96]. To improve the limit of detection (LOD), either the signal must be increased or the noise must be decreased. In the present case, the signal is directly dependent on the pathlength.

2.1.2 *Increasing the signal*

We explore efforts to obtain better signal in chronological order below. Albeit in macrosystems, the senior author explored the use of reflective cells early on [97,98]. An externally silvered helical path cell [97] resulted in increased path length but the light loss was very large. The cell effectively behaved as a multipath cell and thus as a nonlinear absorbance amplifier. Similar behavior was reported for a cell with partially reflective entrance and exit windows placed orthogonal to the light beam [98]. Tsuda et al. [99] used a rectangular capillary and absorption was monitored across the long dimension of the cross section. Axial detection, which involves launching light directly into the bore of the capillary was introduced in a preliminary form by Xi and Yeung [100] but was far too complicated to be adopted for routine use. In a subsequent paper, they advocated the use of high RI solvents in the capillary for the capillary to function as a waveguide and to transmit light efficiently [101]. Only very recently this approach has been used in a more practical fashion with aqueous solutions in Teflon AF coated silica tubes that then function as liquid core waveguides [102], This does require tees at each end resulting in additional dispersion, and use in Microsystems may be complicated.

In 1991 Wang et al. [103] were the first to use a geometry where a segment of the capillary wall is rendered reflective, a focused laser beam enters through an entrance window and is multiply reflected before exiting through the cell at another window on the opposite side

located approximately 1.2 mm away from the entrance window. The arrangement was subsequently patented [104] but to our knowledge, never commercialized. A Z-cell was patented even earlier [105] and subsequent improvements were reported by others [106]. Modest gains in pathlength are possible with a larger bore "sleeve" detection capillary connected at the end of the narrower bore main conduit but the overall gain is often modest. This approach was introduced by the senior author [94] and subsequently reinvented by others [107,108]. In a "bubble" cell, the detection area of the capillary is blown out to a bubble form and thus a larger pathlength is attained [109]; however, it was fairly immediately realized that the approach is not without problems [110].

2.1.3 Decreasing the noise

At the other end of the effort to improve S/N, noise has to be decreased. Culbertson and Jorgenson [111] have utilized a dual photodiode array detection and signal averaging arrangement to reduce noise sufficiently to obtain an LOD 6.3x lower than a comparable commercial capillary scale detector. Small apertures lead to poor light throughput creating a need to measure low photocurrent levels. Liu et al. [112] first used switched integrator based low current measuring circuitry and described fully referenced radial path capillary scale absorbance detectors with 3-10 microabsorbance units (μAU) noise levels under use conditions. Noise considerations not only include the need to measure low photocurrents but also source noise itself. Dedicated detectors meant for use at a single wavelength can use light emitting diodes (LEDs) as light sources which intrinsically have lower noise [95] and full advantage can then be taken of the switched integrator based circuitry. Our laboratory has been an advocate of the use of LEDs as spectroscopic sources in analytical chemistry for some time now [113,114]; presently there are many aficionados. Solid state light sources like LEDs also permit themselves to be easily modulated without the need for mechanical choppers and this in turn allows synchronous detection. Source light is of course exponentially extinguished as path length increases. Increased signal from increasing the pathlength is sooner or later is

thus offset by excessive noise caused by light starvation of the detector. Even so, recently Eom and Dasgupta [115] achieved a noise level of 7 μAU with a pulsed LED source, lock-in-amplifier detection for a 7 cm path length macrobore z-path cell.

2.1.4 *The multireflection cell, flow injection and refractive index (RI) artifacts*

The multireflection arrangement can be traced back to White [116] and the "White cell" is still widely used for gas phase measurements. The original work of Wang et al. [103,104] for capillary scale liquid phase adaptation was certainly promising. However, there were several shortcomings which might explain why it was never commercialized or pursued in that form by others. The account strongly suggests a focused coherent source such as a laser is essential and the number of lasers available in the UV-Vis range are limited and only a few are affordable. Moreover, they are noisy sources; the data in Wang et al. indicate a noise level of approximately 700 μAU. Second, the system was acutely dependent on the angle of the incident light. Around the sweet spot of 7°, going to either a 5° or a 10° incidence angle resulted in a approximately40% attenuation in transmitted light. Nearly a decade went by before Moosavi *et al*. [117] microfabricated devices with integral aluminum mirrors to devise multi-reflection cells with effective path length of 50-272 μm where the straight through orthogonal path lengths were 10-30 μm, i.e., a sensitivity gain of 5-10x was realized; the light source remained a He-Ne laser. More recently Ellis *et al*. [118] constructed a multi-reflection cell from 0.8 mm bore conduit where the entrance and exit apertures were placed 10 mm apart and interrogated with an optical fiber coupled LED and photodiode. The primary focus of this work was to provide a low-dispersion cell which will be more immune to refractive index artifacts compared to standard commercial Z-path cells. Results are discussed in these terms, particularly in comparison with commercial cells. The effective path length is (theoretically) computed to be approximately 17 mm compared to the light entry – exit distance of 10 mm (this would correspond to a gain of approximately 22x compared to the 0.8 mm diametric

pathlength). Our best estimate of the noise levels from the presented figures were that this was $\leq$200 μAU.

Relative to CE or chromatography where the analyte(s) is (are) typically separated from the matrix, in flow injection there is no separation. Any optical effects elicited by the matrix will be superimposed on the analyte signal, regardless of any chemistry performed. Especially for trace analysis, this is a particular problem. A suggested solution is to inject the sample into a carrier which is matrix matched [119]; obviously this is not an option when the matrix salinity is continuously changing [118]. Minimizing or eliminating RI effects has been a continuous preoccupation for us. We observed that RI effects are dramatically reduced when the light path is orthogonal to the fluid flow direction and the light path is reversed on itself [120]. This was confirmed in a somewhat different flow cell design but where the same relative geometric relationship between light and fluid flow was maintained [121]; this has since been commercialized [122]. Depending on the cell geometry, the RI effect can be much larger than one may expect. Further, even a small RI mismatch can have a large effect. For a Z-path cell, even the injection of 10 mM NaOH into a water carrier can cause a RI induced signal of approximately 1 milliabsorbance Unit (mAU) in amplitude [123]. Both refractive index and turbidity problems can be successfully solved with multiple wavelength monitoring; it has been shown that that an analyte present in a solution containing milk and alcohol can be selectively determined if the analyte is selectively made to undergo a color change or generate a differently colored product and optical absorption is monitored at a sufficient number of wavelengths before and after the color change [123]. The general approach of multiwavelength absorbance detection to compensate for RI effects was later simplified by operating different wavelength LED emitters at different frequencies and applying frequency-selective detection methods [115].

In the present chapter we wish to examine the optimum construction of an affordable multireflection-type capillary scale absorbance detector intended for miniaturized FIA use. We have deliberately chosen a conduit diameter intermediate between those used by Wang et al

[103] and Ellis et al [118] that will be well suited for capillary scale FIA use and utilize a minimalist configuration where the effect of light launching angle can be studied. We used a readily available commercial LED of medium brightness to establish attainable performance specifications and report on its immunity to RI induced effects.

2.2 Experimental

2.2.1 Reagents

All reagents were used as received. Bromthymol blue (BTB) was prepared in 1 mM NaOH. A stock solution of 0.5 mM BTB was diluted with 1 mM NaOH as needed. A saturated solution of Eriochrome Black T (EBT) was prepared in 1 mM NaOH and then filtered through 0.22 µm pore size nylon membrane syringe filters. All solutions were made in distilled deionized water.

2.2.2 Cell design and electronics

A cell holder that allows the use of different launch angles and capillary cells of different length was machined out of Aluminum and is shown in Figure 2.1(a) as a photograph. It is composed of two cylindrical parts A and B. Part B is shown separately on the right; it can slide into and fit snug inside A. A 0.6 mm dia. hole is bored straight through the cylindrical axis of both A and B through which a 375 µm o.d. fused silica capillary (silvered and epoxy coated, *vide infra*) passes. Holes 1-5 (4 and 5 are not visible in the photograph) are drilled into part A in a V-pattern and basically ends in the same general axial location, distributed radially around the central capillary passage. These holes are bored at different angles and end-polished optical fibers (0.5 mm o.d., P/N 02-532, www.edmundoptics.com) are inserted into these holes to launch light into the capillary, the choice of the specific hole governs the choice of the launch angle (15°, 30°, 45°, 60° and 75°) of the incident light. Figure 2.1(b) illustrates the geometric arrangement in which light is launched (45° launch angle is shown) into the capillary and detected. A machine drawing is provided in Appendix A in Figures A1(a) and A1(b). In B, the hollowed out area provides a space for locating a miniature hemispherical lens equipped light to

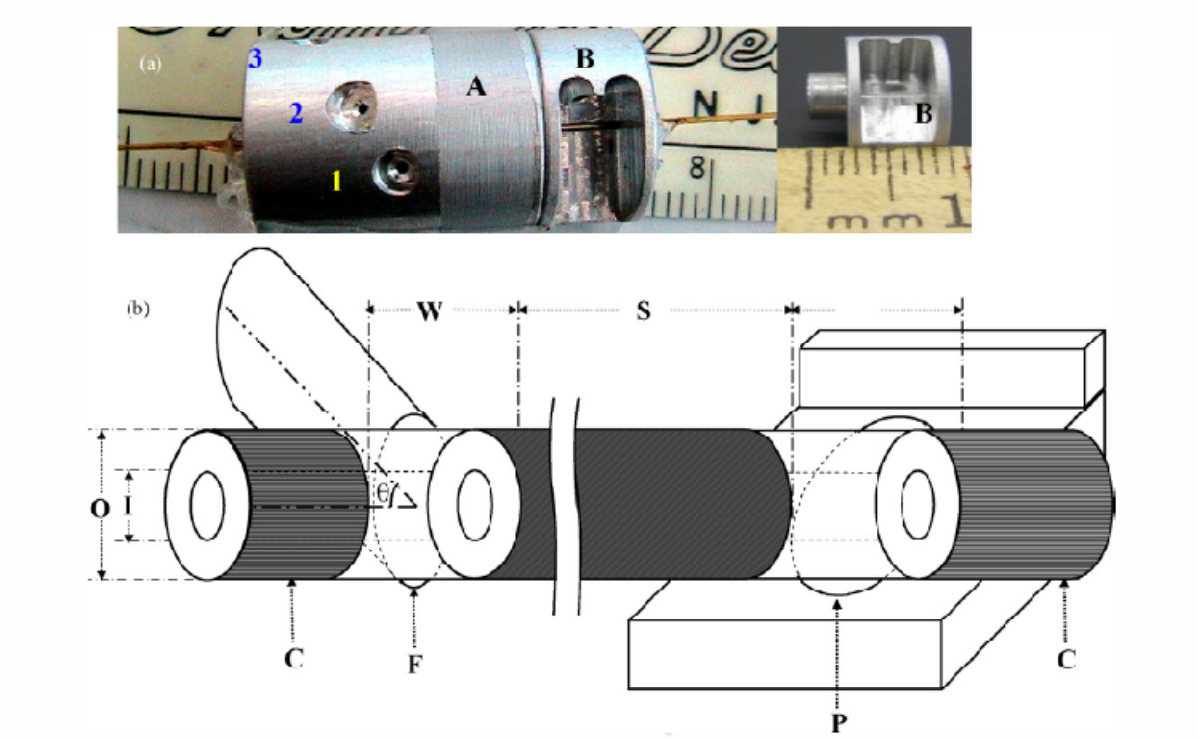

Figure 2.1 (a) Capillary detection cell holder, photographically shown. The holder is consists of two machined components A and B, the latter slides into the former. It is shown assembled on the left panel and right panel shows B alone. Holes 1, 2, 3 etc. are drilled in part A at different angles to insert an optical fiber and light launch into a capillary at different angles. (b) Schematic representation (not to scale): C-polyimide coated capillary, *F* – 0.500mm diameter optical fiber, *I* – inner diameter of capillary (0.180 mm), *O* – outer diameter of capillary (0.350 mm), *P* – 0.900mm diameter light receiving area of photo-detector, *S* – silver coated length of capillary (10.0 mm), *W* – transparent window of capillary (1.0 mm), θ – angle of incidence of optical fiber with respect to capillary axis.

voltage converter (TSL257R, www.taosinc.com) which is simply affixed by optical grade epoxy adhesive to a clear window made in a silvered capillary. The output of this photodetector was further amplified by a two-stage FET-input operational amplifier (TSL072CP, www.ti.com) before acquisition.

Sections of polyimide-coated fused silica capillaries (180 μm i.d., 375 μm o.d. TSP180375, www.polymicro.com), 9 cm in length, were taken. The polyimide coating was removed with hot concentrated sulfuric acid over a desired length (from 12-55 mm) and then treated with H_2O_2-conc. H_2SO_4 mixture. Prior to silvering this area by a commercial silvering kit (Lilly Industries, Woodbridge, CT), the intended light entry and exit windows (1.0 mm each) were protected by masking with Teflon tape banded around the capillary, thus eventually creating a ring-shaped window. The quality of the silver coating obtained is very dependent on surface cleanliness. After silvering, the coating was checked for its uniformity and protected from mechanical and chemical damage with an epoxy coating (mixed two-component epoxy adhesive was diluted with 4 volumes of acetone) being painted over the silvered and the window area, after the protective PTFE tape has been removed. Similar experiments were conducted with a square capillary (100 μm on each side, circular outer cross section with 375 μm dia, WWP100375, Polymicro Technologies).

The other end of the optical fiber bringing light to the capillary is provided with a protective sleeve and threaded into a ¼-28 threaded chromatographic union with a ¼-28 threaded male nut and ferrule. It is coupled to a clear-bodied 5 mm (T 1-$^3/_4$) LED (Stanley Electric EFA5366x, www.digi-key.com, nominal λ_{max} 609 nm, measured λ_{max} 613 nm) via a 5.0 mm diameter sapphire ball lens (NT43-646, Edmund Optics); the ball lens was found to increase the light intensity at the distal end of the fiber approximately 6-fold. The LED was powered by a 5V source via a 68 Ω resistor, resulting in a drive current of 44 mA. Another light to voltage sensor (TSL252R, TAOS, this device has less intrinsic sensitivity compared to the

detector at the light exit end) was used as the reference detector. This was cemented at the bottom of the LED; there was no need to amplify this signal.

When the cell holder part B is fully pushed into part A, the dimensions accommodate a capillary with an entrance-exit window separation of 10 mm. As longer spacing is used, part B is removed further away from part A to adjust to the necessary distance. Both components are affixed by modeling clay on an Al base plate, painted black. The capillary and cell holder are covered by an inverted box to prevent intrusion of ambient light.

For comparison purposes, a single-pass radial path cell was used, with a construction similar to that described by Boring and Dasgupta [95], using a pair of razor blades to define the slit. The cell holder is necessary only for variable length and variable incidence angle experiment. When launch angle and length parameters have been decided on, a much simpler breadboard cell construction is used which works equally well. This is described in SI for a 10 mm cell using a 45° incidence angle.

2.2.3 Experimental arrangement

The experimental setup was that of a single line flow injection system. The carrier (1 mM NaOH) was pneumatically pumped through a 1 µL external loop volume 6-port injection valve (070-0134H, www.vici.com) through which the sample (unless otherwise stated, 0-1.1 µM bromothymol blue (BTB) in 1 mM NaOH) was injected. The valve outlet terminates in a 75 mm length of a 100 µm i.d. fused silica capillary which was connected to the detection cell by a PVC sleeve tube butt-joint. The pneumatic pressure was adjusted to obtain a flow of 10 µL min^{-1}. The amplified signal detector output and the reference detector output were acquired by a laptop personal computer (PC) using a model 1608FS data acquisition module (www.measurementcomputing.com) via the universal serial bus at a frequency of 5 Hz.

A saturated solution of Eriochrome Black T (EBT) was put in the cell with a syringe and the signal detector output was measured. This relatively small value was taken as the “dark signal” and subtracted from all signal detector outputs before further processing. Absorbance

was calculated by the PC by log transformation. The stability of the LED output was indicated by the reference detector output and was found to be very stable. However, no improvement in the observed noise level resulted by ratioing the signal detector output to the reference detector output prior to log transformation and in general, the reference detector output was not further used.

The molar absorptivity BTB at 613 nm (LED λ_{max}) and at 616 nm (ε_{max}) was measured to be 40,059±32 and 40,420±54 $M^{-1}cm^{-1}$, respectively, with an Agilent XA6/350 diode array spectrometer based on 1-60 µM BTB in 1 mM NaOH (measurement on 20 separate solutions).

2.3 Results and discussion

2.3.1 Stray light

Traditionally, stray light is defined as light that does not travel through the sample but still reaches the detector. This definition assumes that the source light is essentially monochromatic with a bandwidth much less than the absorption band of the analyte. With LEDs as light sources, a good match between the analyte absorption band and the LED emission band cannot always be obtained. As a result some of the light that passes through the sample is in a wavelength domain that has no interactions with the sample. This situation is analogous to atomic absorption spectroscopy with a continuum source and a low resolution monochromator. The net effect of light reaching the detector that goes around the sample and that goes through the sample but is at a wavelength that does not interact with the sample is essentially the same. Restricting ourselves with conventionally defined stray light for the moment, based on initial experiments with water and concentrated solutions of Eriochrome Black T respectively filling the cell (as well as the LED being turned off altogether), we determined that as much as approximately 20% of the light reaching the detector does not pass through the sample. Painting the inside of the cell holder with a flat black paint reduced the stray light to approximately 5%. No efforts were made to reduce this further; it has been shown elsewhere [121] that small amounts of stray light have virtually no effects on LODs or absolute

absorbance values at low absorbance values. However, the upper range of linearity is sacrificed. The latter is not a prime concern in capillary scale detection systems where analyte signals will rarely exceed 10 mAU.

2.3.2 Pathlength and launch angle dependence

It can be readily ascertained from first principles that if an ideally collimated narrow beam was reflected between two infinitely thin parallel plates, the overall path length, without consideration of the refraction through the walls, will be L/sin θ where the light entry and exit windows are separated by distance L and θ is the angle of incidence. In other words, in this ideal and hypothetical case, as the launch angle approaches 90° (parallel to the axis of the conduit), the observed pathlength will approach L whereas as it approaches 0° (orthogonal to the capillary axis), the pathlength will approach infinity. Wang et al. [103] provided ray tracing approaches in their original exposition of the multi-reflection concept that took into account the finite thickness of the capillary wall and the refraction caused by the interface. Although Ellis et al [118] used a non-coherent LED source they also adapted the same approach. With a diverging source of significant beam diameter where the beam increasingly explores smaller traverses than the largest possible traverse (the diameter), there are of course limitations of this approach. In reality, it is doubtful, even with a laser source, how well the observed pathlengths will correspond with the values thus computed. Wang et al. state, for example, that in going from θ = 5° to θ = 3°, the pathlength should have increased by 170% but the observed increase was 2.8%. Using the ray-tracing approach, Ellis et al calculated a pathlength of 17.3 mm for θ = 30° in their system. Their calibration slope intercomparison with conventional cells and corresponding dispersion coefficient (D) data suggest an actual pathlength of 11.1±0.4 mm [118], barely larger than the 10 mm distance separating the windows. However neither Wang et al nor Ellis et al studied their systems over a broad range of light incidence angles.

Granted that illumination with non-coherent light via a fiber-optic of diameter larger than the inner bores of the capillaries (and with all the additional less-than-ideal features of the

interface) may not allow us to reach any fundamental theoretical insights, it does allow us to reach practical conclusions from practical arrangements of what may be the best angle to use. It is also important to note that the acceptance angle of the fiber (which is also the angle at which light emanates from the fiber) is substantially larger than the 15° launch angle increments studied here. A similar situation applies at the light detection end; the photodiode uses an integral hemispherical lens that has a significant acceptance angle. Figure 2.2 presents the observed absorbance –concentration best fit linear calibration curves for (a) a 180 µm bore capillary of circular cross section and (b) a capillary of 100 µm square cross section for launch angles of 15°, 30°, 45°, 60° and 75°. In (a) it is observed that 15°, 30°,and 60° illumination angles lead to virtually the same response that are barely distinguishable from each other. An illumination angle of 75° led to a slightly greater apparent pathlength and an illumination angle of 45° the pathlength is decidedly higher than the rest. In (b), all but 45° and 60° illumination angles produce nearly the same response, which is somewhat lower than the 45° and 60° illumination responses that are close to each other. A slightly different picture emerges from Cassidy plots [124] in Figure 2.3 in which sensitivity is plotted as a function of concentration. The characteristics of a multipath cell, in which light propagates in different paths of different effective lengths, is that the larger pathlengths have a greater influence at relatively low absorbance values of the solution than at higher absorbances [97]. The reason for this is simple: the detector cannot discriminate between paths through which various rays of light might come through when the attenuation is already high, further passage through a long path has little effect on the total amount of light reaching the detector. As a result, as seen in Figure 2.3, for either the round or the square capillary, the apparent sensitivity (or apparent molar absorptivity of the dye) increases at lower dye concentrations (low absolute absorbances) clearly indicating that there is some degree of multipath behavior. However, stable sensitivities (linear calibration behavior) are observed beginning at fairly low absolute absorbances, starting with about 0.4 -0.5 µM BTB - the flat regions of the plots in Figure 2.3 correspond to the slopes

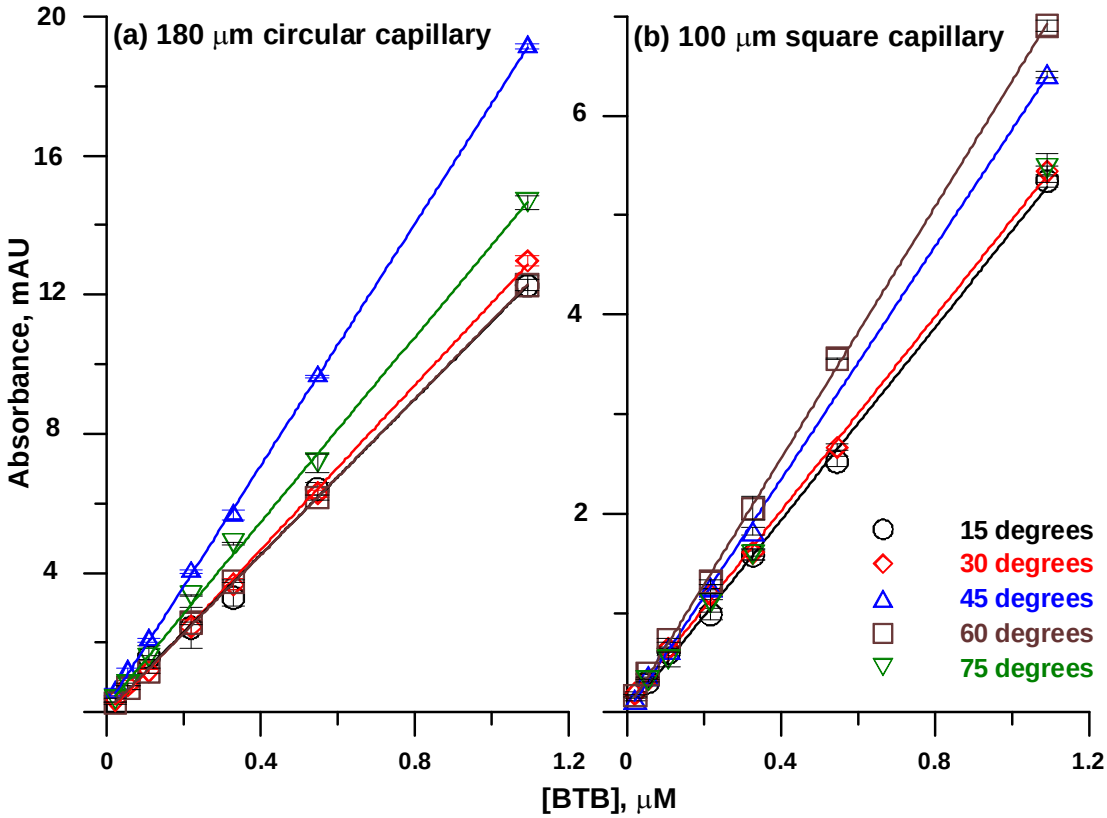

Figure 2.2 Response as a function of injected BTB concentration at different angles of incidence of launched light for (a) round and (b) square cross section capillaries.

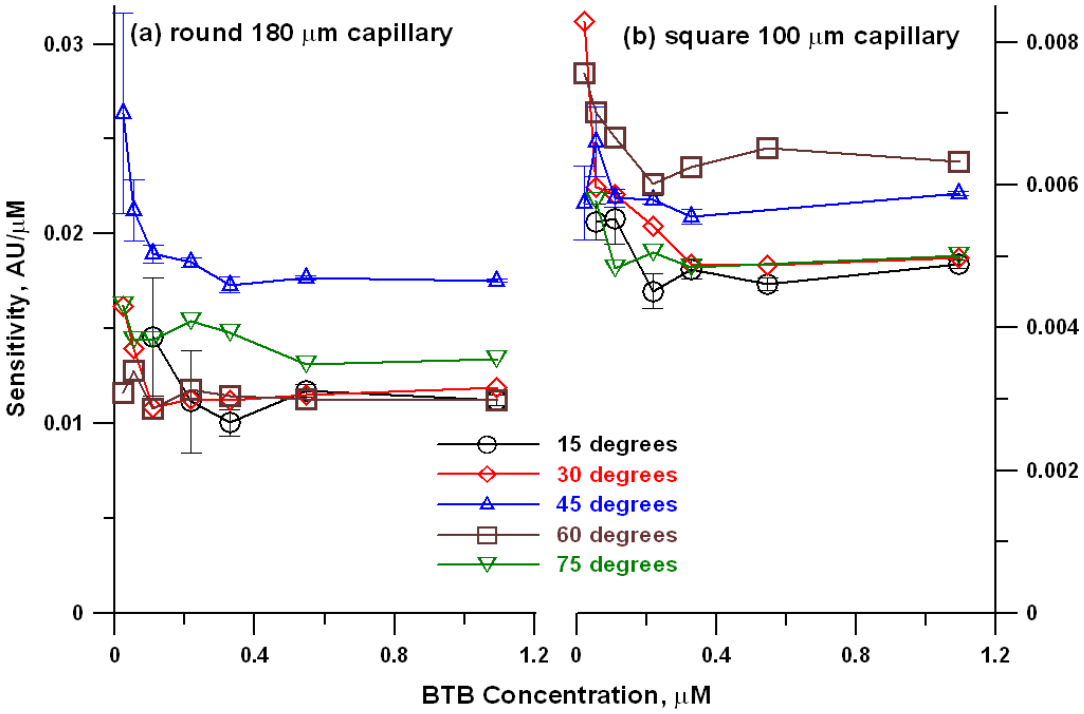

Figure 2.3 Cassidy plots, sensitivity vs. concentration, for both (a) round and (b) square capillaries. For clarity, ±1 standard deviation error bars are shown only for the 15° and 45° launch angles.

in Figure 2.2; the best fit lines in the latter are of course weighted more heavily by higher values. We have deliberately plotted Figure 2.3 with the ordinate origin starting at zero, to illustrate that while there is a dependence on the launch angle, across the range studied this difference is less than a factor of 2 whereas a $1/\sin\theta$ dependence would have resulted in a nearly 4x difference between the 15° and 75° launch angles. In fact, it would be obvious from either Figure 2.2 or 2.3 that the observed calibration slope/pathlength order does not follow the expected order of the sensitivity increasing monotonically with decreasing angle of incidence. For the square capillary, efforts were made to carefully ensure that the optical fiber was perpendicularly oriented to one of the square sides, but the same results were obtained.

Beside the multipath effect, a broadband source also contributes to greater apparent molar absorptivities at lower concentrations as discussed in the next section, albeit in the present case the analyte absorption and LED emission are particularly well matched and this effect is relatively small.

2.3.3 Effective absorptivity of solutions encountered with a broadband source

To compute the pathlengths actually attained, one requires the value of the molar absorptivity of the dye. Many investigators now use LEDs as light sources and it is well known that bandwidths of such sources are often larger than desired. Further, the match between the emission spectrum of the LED and the absorption spectrum of the analyte is rarely as good as it is in the present case ($\lambda_{max,LED}$ 613 nm; $\lambda_{max,BTB}$ 616 nm). Hauser et al. [125] originally discussed the computation of the effective absorptivity of the analyte in such a case. Since this can be useful in many applications beyond the present context, we discuss this in some detail below.

Figure 2.4 shows superimposed absorption spectra of BTB, plotted in terms of molar absorptivity (left ordinate) including ±1 standard deviation error bars compared to the LED emission spectrum (right ordinate). Also shown is the transmittance spectrum of a 10 μM solution of BTB that is transformed from the molar absorptivity data (rightmost ordinate)

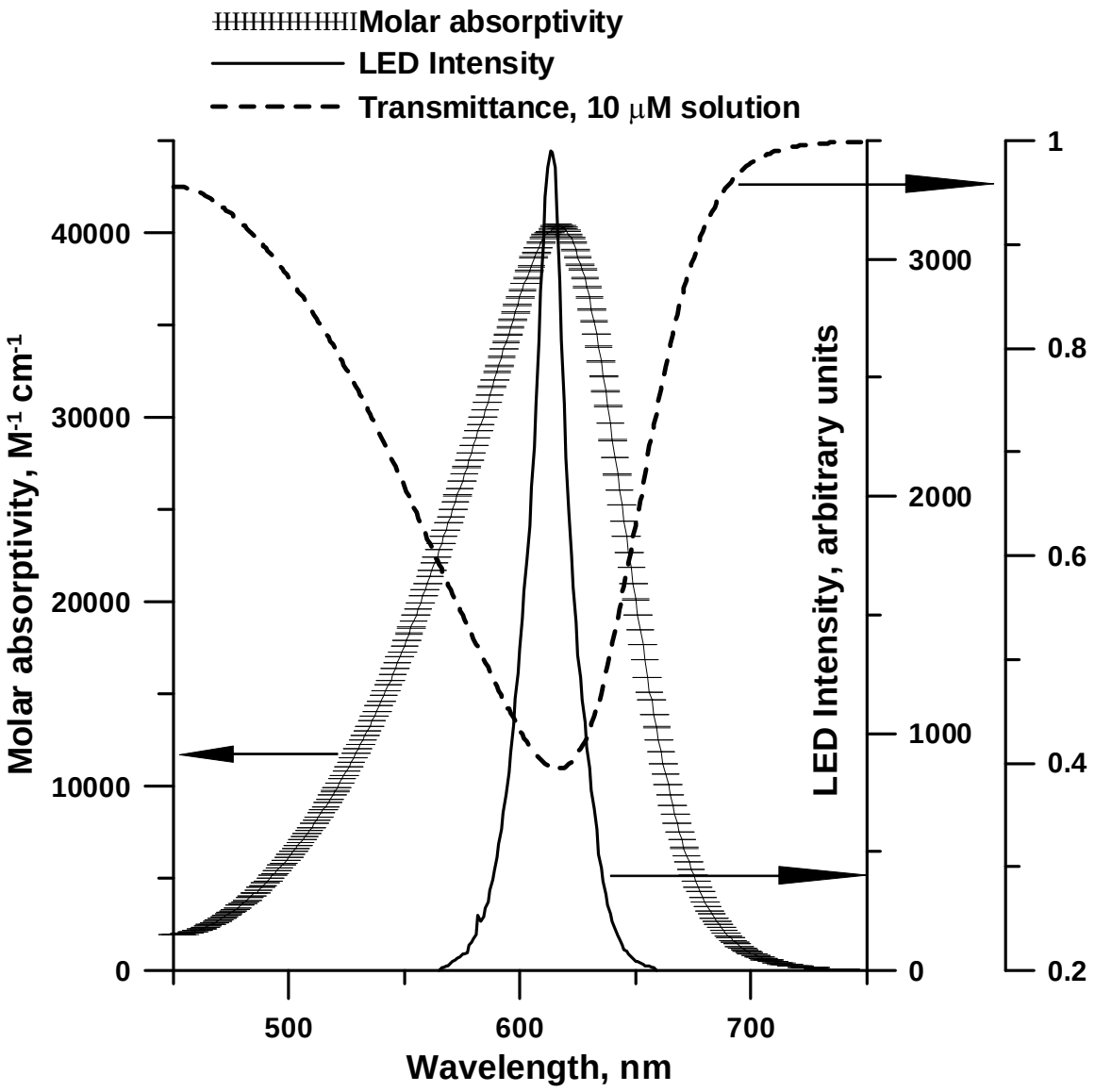

Figure 2.4 Molar absorptivity of alkaline BTB (left ordinate) transmittance of a 10 μM solution (rightmost ordinate) and LED intensity (right ordinate).

assuming a 1 cm pathlength. The LED emission occurs between 565 and 660 nm and the total incident light intensity I^0 is given by the summation of the light intensities at each of the wavelengths I^0_λ:

$$I^0 = \sum_{\lambda = 565\text{-}660} I^0_\lambda \quad \ldots(1)$$

To calculate the effective transmittance of the 10 μM solution shown, the total transmitted light I is computed by multiplying the incident light intensity at each wavelength by the corresponding transmittance value T_λ and then summing these values:

$$I = \sum_{\lambda = 565\text{-}660} I_\lambda T_\lambda \quad \ldots(2)$$

Absorbance is then calculated from the usual expression A = -log (I/I^0) and the absorptivity is then calculated in the usual manner. This exercise carried out for the data in Figure 2.4 will lead to an effective molar absorptivity of 37,820 $M^{-1}cm^{-1}$, significantly less than the 40,059 $M^{-1}cm^{-1}$ value simply taken for the LED maximum emission wavelength. Further, if the same exercise is repeated for solutions of different concentration, it will be observed that the effective molar absorptivity decreases monotonically from 37,949 $M^{-1}cm^{-1}$ for a 0.1 μM concentration to 37,094 $M^{-1}cm^{-1}$ at 50 μM. This variation occurs because it is absorbance and not transmittance that linearly scales with concentration. The change here is relatively small because within the intensity weighted bandwidth of the LED, the absorption of BTB is relatively uniform. The effective absorptivity will vary a great deal more when this is not the case. In the following we use $\varepsilon_{eff} = 3.75 \times 10^4$ $M^{-1}cm^{-1}$ as an average value.

2.3.4 Effective optical path length of the cell

We measured the dispersion coefficient (D) in our particular system, this is the factor by which an injected sample is diluted by the time it reaches the detector. For a 20 mm circular cell and 1 μL injection volume, this was found to be 1.85±0.05. For a 10 mm cell, this D-value would be comparable or lower (less dilution).

In interpreting the absolute ordinate values in Figure 2.3 (or the slopes in Figure 2.2), for a dye of ε_{eff} = 3.75 x 10^4 $M^{-1}cm^{-1}$, a D-value of 1.85, an ordinate value of 10 mAU•μM^{-1} corresponds to a pathlength of 4.6 mm. The best case pathlengths in the round and square capillary cases will this be calculated to be approximately 7.4 and 2.8 mm, respectively. These absolute values are remarkable in that they are in fact lower than the shortest path separating the entrance and exit windows (the distance between them in both the circular and square capillary cases is 10 mm). These results therefore suggest that at least in these small bore relatively thick wall capillaries, after the initial entrance, a significant, if not major, part of the light actually does *not* bounce back and forth between the entrance and exit windows as one may imagine but after a relatively finite distance of passage through the solution, finds its way into the glass wall through which it travels, resulting in a path length that is shorter than the distance between the entrance and the exit windows. In a fashion, this also explains the unexpected and non-monotonic nature of the dependence of the pathlength on the launch angle. Note that the o.d./i.d. aspect ratio of the glass tube used by Ellis et al. [119] was 1.6, in the present case it is 2.1; this is likely to further promote any light conduction through the relatively thicker glass wall.

2.3.5. Light throughput, noise and signal to noise ratio

While the absorbance signal is directly dependent on the pathlength, the analyte detectability is ultimately dependent on the signal to noise ratio. In general, at low light levels reaching the detector, the noise increases with decreasing light levels. At higher levels of light, however, there is no further decrease in noise above some threshold value of light [115]. Figure 2.5 shows this same behavior where data from (a) round capillaries at different launch angles (circles), (b) square capillaries at different launch angles (squares) and (c) round capillaries with 10-50 mm lengths and a 45° launch angle (circles with lines) are shown. It will be observed that the noise reaches a more or less constant value at primary detector output values above approximately 60 mV, regardless of the nature of the arrangement or the geometry of the cell but below this value, the detector noise begins to increase exponentially. It is also further

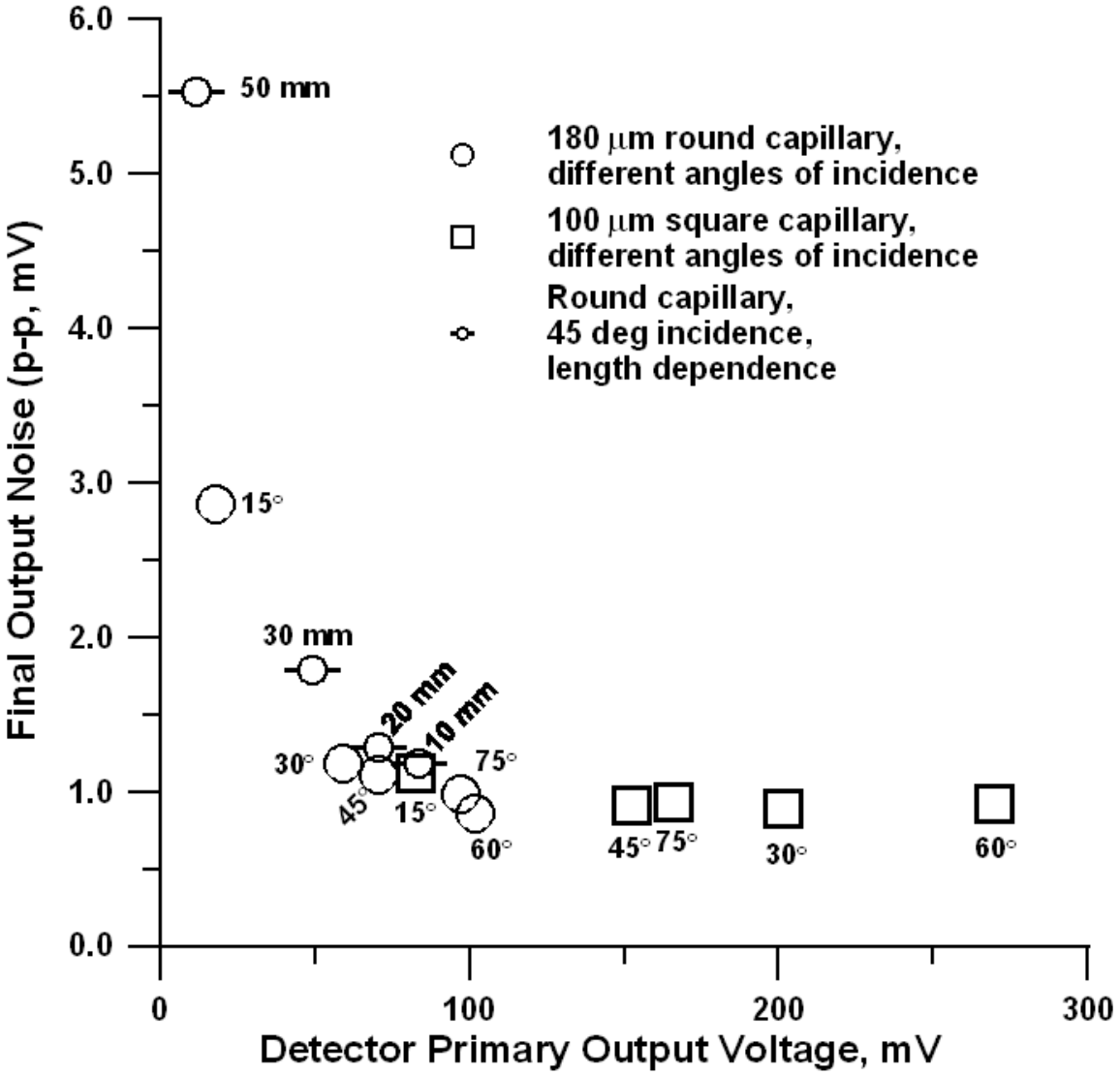

Figure 2.5 Noise as a function of light intensity reaching detector (directly proportional to detector primary output).

observed that for case (c), the noise increases monotonically with the increase in cell length. It is clear that the 50 mm cell suffers from poor light throughput and high noise and any advantage of increased pathlength will not translate into a better S/N. The angular dependence of light entry for both types of capillaries is more complex. For the capillary with a square hydraulic cross section (case (b)), there is relatively small dependence on the launch angle: while the 15° launch angle produced the highest light throughput (Figure 2.5), the actual pathlength was the lowest. For the round capillaries (case (a)), the light throughput increased and the noise decreased systematically with increasing launch angle (60° results were almost the same as that of 75°).

These factors combine to influence the observed signal to noise ratios, which are shown in Figure 2.6 for 110 nM injected BTB for the same three cases a – c previously discussed. Note that because of superior light transmission, the square capillaries provide relatively greater S/N. The best case S/N for the square capillary is only 25% lower than the best case value for the round capillary, even though the latter has a hydraulic diameter 1.6x lower. (However, the dispersion in square capillaries was not measured, if this dispersion is larger than round capillaries, significant lengths of square tubing will need to be avoided to realize the optical superiority.) The response behavior dependence on cell length is discussed in more detail below.

2.3.6. Length dependence and limits of detection

Length dependence was studied with the round capillaries using a single entrance angle of 45°. Each exhibited excellent Beer's law linearity over a range of 22-1090 nM (n=7) with a zero intercept linear r^2 value ranging from 0.9978 to 0.9994 (see Appendix 1, Figure A4). The respective effective path lengths for 10, 20, 30, and 50 mm cells were 8, 17, 28.5 and 32.6 mm. Considering that our accuracy in defining the distance between the light entry and exit points is probably no better than ±1 mm, the effective path lengths, especially for the three shorter wavelengths clearly indicate an approximately linear increase of the effective pathlength

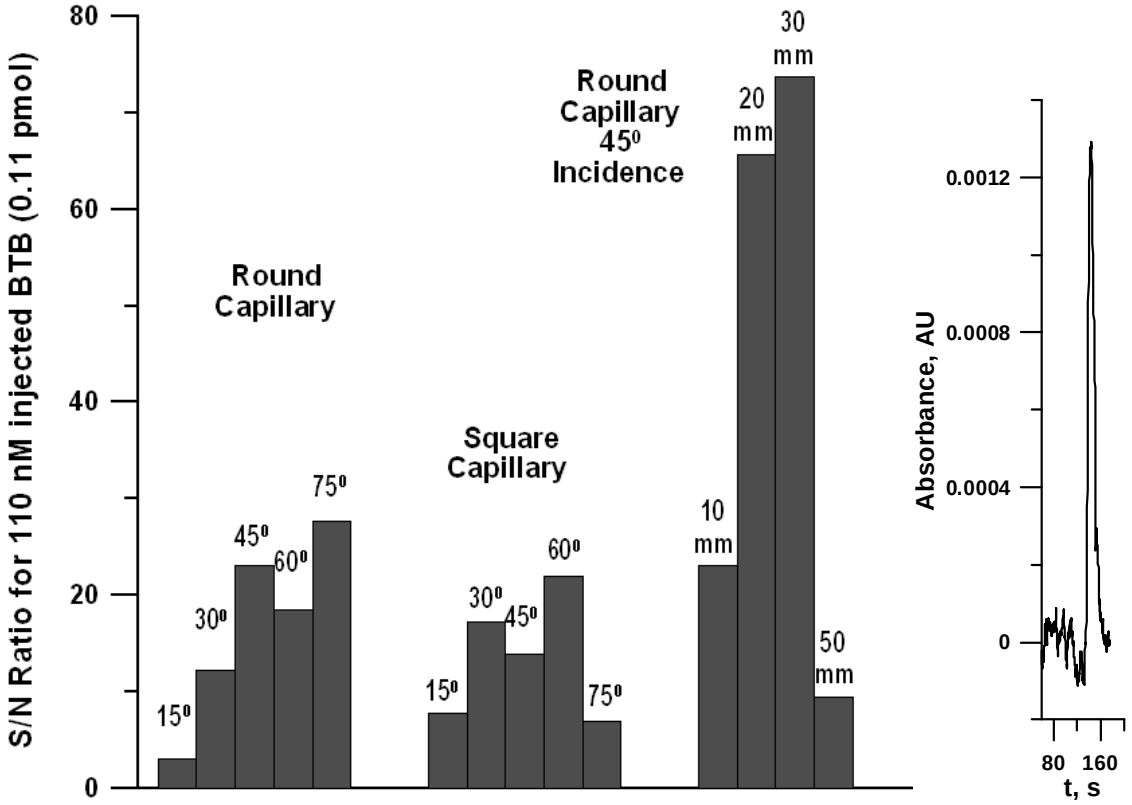

Figure 2.6 Left: signal/noise for a 110 nM injected sample for round and square capillaries as a function of light launch angle and for round capillaries as a function of light entry and exit distance. Right panel shows the response to a 22 nM injected BTB sample in a 2 cm cell.

with the physical distance between the light entrance and exit windows. Cassidy plots (see Appendix 1, Figure A5) further indicate a greater effective pathlength at lower solution concentrations, except for the longest tube where accurate measurement at low concentrations is made difficult due to increased noise and seemingly, a behavior opposite to the other cases is observed.

Returning to Figure 2.6, the increase in S/N in going from a 10-mm to a 20-mm cell is large but the 30-mm cell actually produces a S/N that is statistically no better than the 20-mm cell. The 50-mm cell clearly performs the worst. If the illuminated volume was not an issue, it is possible that a brighter light source may permit the maximum S/N at a greater physical cell length. However, what is presently attainable is very respectable. The right panel of Figure 2.6 shows the response of the 20 mm cell to 22 nM injected BTB; at the prevalent noise levels this peak has a S/N greater than 15. This corresponds to a S/N=3 LOD of 4.4 nM or 4.4 fmol, i.e., approximately 2.6 pg BTB. In the present case, the noise level is <80 µAU with an effective pathlength of 17 mm; in comparison, the single radial pass cell of Boring et al. [95] of 75 µm inner diameter exhibited a noise level of approximately 15 µAU.

2.3.7 Refractive index effects

It was of interest to determine whether the immunity to schlieren effects reported by Ellis et al [118] persist as the system is further miniaturized. We compared the behavior of a single radial pass cell with that of a multireflection cell (180 µm bore round capillary, 45° launch angle, 10 mm) when 10 µM alkaline BTB or 10 µM alkaline BTB prepared in a matrix of 100 ‰ NaCl is injected into a water carrier. Figure 2.7 will indicate that in the case of the single pass cell, due to the presence of 100 ‰ NaCl in the sample, there is very evident decrease in the peak height and there is also apparent peak broadening occurs. Hence, interference in quantitative measurement will be expected due to refractive index effects with such a cell. In contrast, the multi-reflection cell has considerable immunity to refractive index effects. We echo the sentiments of Ellis et al. [118] that such cells would be well suited for samples with variable

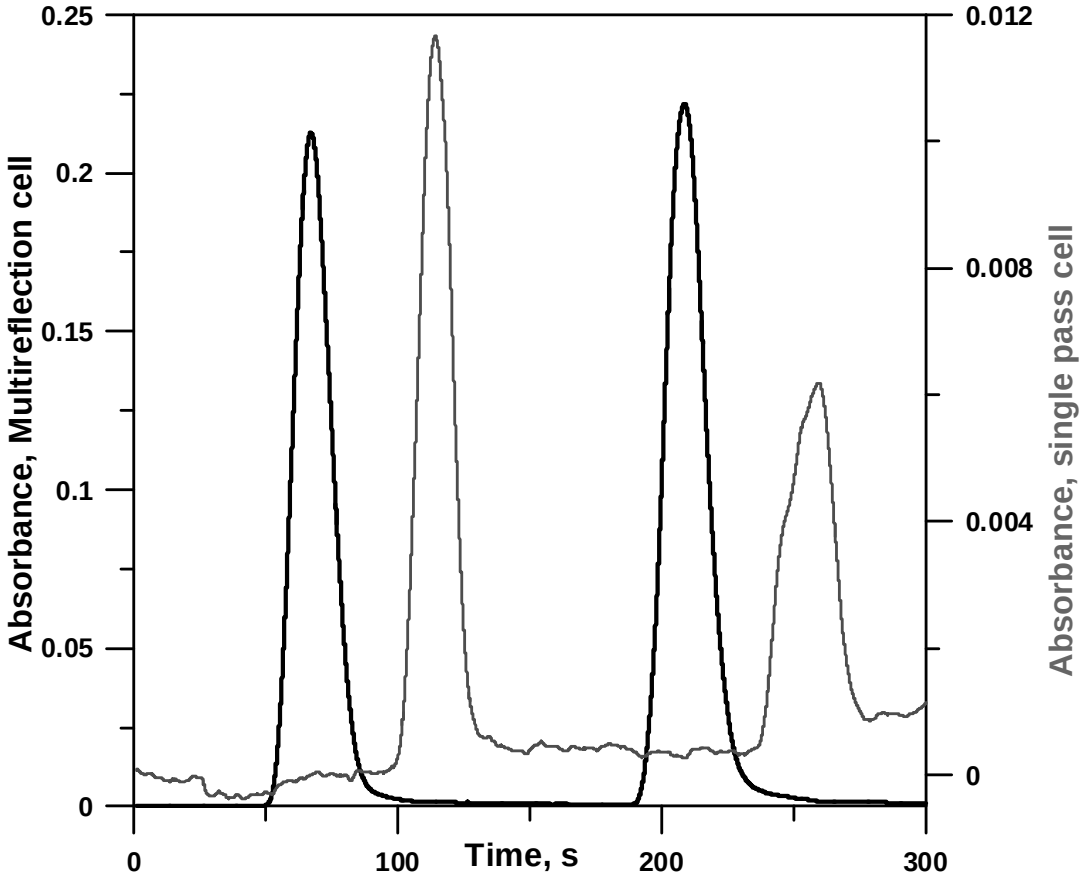

Figure 2.7 Immunity to refractive index effects for a multireflection cell. Heavy trace: multireflection cell; light trace: single radial pass cell. The first injection in each trace is 10 µM alkaline BTB and the second injection is the same analyte in a matrix of 100 ‰ NaCl.

salinity. These results are expected; refractive index effects are maximized when the propagation of light is coaxial with fluid flow such that the light is most directly affected by the lens that develops. This effect is reduced when the direction of light propagation is perpendicular to that of fluid flow and especially when it is reflected back to more or less retrace its path [120,121]. With multiple reflections, this should reduce further.

2.4 Conclusions

We have demonstrated that the multireflection absorbance detectors with noncoherent light sources provide impressive gains in sensitivity and are also remarkably immune to schlieren effects. We demonstrate an LOD of 4.4 fmol for injected BTB dye solution. We have studied the effects of changing the light incidence angle and find that the results do not necessarily agree with a model of simple reflections where the effective path length continues to increase as the launch angle becomes more acute. It appears that such cells really behave as multipath devices where a significant amount of the light might travel through the glass after one or a limited number of reflections and the extent of the latter may depend on the launch angle. Nevertheless, as the demand for sensitive capillary scale optical absorbance detection increases, multireflection cells can play a very significant role.

CHAPTER 3

CAPILLARY SCALE LIQUID CORE WAVEGUIDE BASED FLUORESCENCE DETECTORS FOR LIQUID CHROMATOGRAPHY AND FLOW ANALYSIS

3.1 Introduction

Since the past decade, there has been a significant interest in capillary scale separation and detection techniques [88,126]. The capillary format allows for high efficiency rapid separations with low sample and reagent consumption. In favorable cases, it allows for very low pressure, even gravity-flow separations [127-129]. However, the measurement of trace amounts of analytes in ≤1 μL injected sample volumes demand a lot from detection techniques.

Fluorometry is among the most sensitive of analytical techniques. A focused laser beam offers an ideal way to provide small volume intense excitation. Although laser induced fluorescence (LIF) has been most often used in capillary electrophoresis (CE) and reviewed in that context [130,131], it is applicable for non-electrophoretic capillary scale applications as well. Nevertheless, commercial LIF instrumentation is still too complex and expensive to allow wide, especially pedagogic, use. Further, many laser sources are intrinsically noisy, degrading LODs from what would be predicted on the basis of illumination flux alone. More importantly, the limited number of wavelengths that laser sources can presently conveniently and affordably address require the proverbial changing of the foot to fit the shoes; a whole host of derivatization agents and methods have been developed to fit available LIF instruments. The recent availability of violet laser diode (VLD) sources in digital video disc (DVD) players and recorders, complete with focusing optics, does offer, however, inexpensive opportunities to build fluorescence detectors with such sources and optics.

The attractive performance of liquid core waveguides (LCWs) for transverse/radial excitation fluorescence detection was demonstrated a decade ago [132]. We have since

reviewed the general use of LCWs for optical detection [133]. Recently Okada has reviewed LCW- based absorbance and fluorescence detection (with either axial or radial illumination) [134]. The following developments in LCW- based fluorescence detection are noteworthy: imaging the capillary lumen on a CCD detector and being able to discriminate against the scattered light that primarily propagates along the wall [135], using a similar detector with a multicapillary separation system to perform multiplexed detection [136], imaging the whole column with either axial [137,138] or scanning transverse [139] illumination, detecting ammonia at the low nM level with a photodiode detector [140], utilizing the scheme with CCD based detectors in CE [141] and in flow injection coupled miniature CE systems [142], using multiwavelength array excitation coupled to a CCD spectrometer [143], separating and detecting DNA fragments in microfluidic systems [144] with LODs comparable to LIF detection (aided by modulation, lock-in detection and second wavelength referencing techniques) [145]. In our laboratories, we have extensively used light emitting diode (LED) excited LCW-based fluorescence detection for the determination of atmospheric H_2O_2 [146], HCHO [147] and H_2S [148], developed a flash lamp-excited gated fluorescence detection system for anthrax spores [149], a multiplexed, pulsed-LED detection system for hematin-differentiated [150] measurement system for H_2O_2 and organic peroxides [151] and methods for coating glass and silicon microchannels to render them into waveguides [152,153].

In LCW fluorescence detectors described to date, coupling the emitted light to the detector has generally been accomplished by a distally located optical fiber coupled detector; the convenience unfortunately leads to significant light loss. Preserving the lumen image [135,136] requires an involved optical arrangement where the fluid exit end remains in a liquid reservoir and the termini are imaged by a lens, filter, prism and camera objective before coupling to a CCD detector. Direct coupling to the detector window has only been achieved by allowing the liquid to leak past an exit window in an uncontained manner [144] precluding the possibility of using a subsequent serial detector. To perform affordable multi-dimensional

detection in capillary scale analyzers, it is our objective to develop absorbance [88], conductance [154] and fluorescence detectors in a concerted manner. These detectors should be capable of being deployed singly or serially with a high performance/cost ratio.

In the present chapter, we describe generic designs for inexpensive capillary scale flow through fluorescence detectors and demonstrate attractive performance in flow systems.

3.2 Experimental

3.2.1 Reagents

Sulfoxine, 8-hydroxyquinoline-5-sulfonic acid (HQS), was twice recrystallized (as the monohydrate) from large volumes of hot water. Aluminum sulfate (reagent grade), Coumarin 30 (3- (2-N-methylbenzimidazolyl)-7-N,N-diethylaminocoumarin), Good buffering agents [155] 3-(N-Morpholino)-ethane sulfonic acid (MES), 3-(N-Morpholino)-propane sulfonic acid (MOPS) and 2-(cyclohexylamino)-ethane sulfonic acid (CHES) were used as received (all of the above from www.sial.com). For the present experiments, the stock solutions of the Al salts were diluted serially by the carrier used in the flow analysis system. Coumarin 30 was dissolved in 50% (v/v) methanol and injected for detection in the same solvent. All other solutions were made in distilled deionized water.

3.2.2 Fluorescence detector cell design

Only the HPLED–mPMT detector is described here in detail; the other two designs are discussed here briefly; greater details appear in Appendix B.

3.2.2.1 Light emitting diode: photodiode design

The simplest and least expensive (total electronics cost <$20) scheme uses a modest power UV LED (NSHU550B, www.nichia.com, 5.4 mm dia. metal can) that is estimated to put out ~1.5 mW @ 365 nm at the operative drive current of 15 mA. Refer to Figure B1 in Appendix B and attendant description. The detector is a miniature “light-to-voltage converter”, a photodiode with an integral operational amplifier (TSL250R, www.TAOsinc.com) a square-shaped (4.8 mm × 4.8 mm) clear epoxy bodied 3-pin (power, ground, signal) device that is

1.8mm thick. A centrally placed integrally molded hemispherical lens (Ø0.90 mm) completely covers the photosensitive area (sensitivity 100 mV/W per cm^2 @ 500 nm). We drilled a perpendicular hole (1/32 in., Ø 0.79 mm) directly through/atop the lens terminating just atop the photosensitive surface. A second aperture (0.014 in., 0.37 mm) is drilled parallel to the plane of the device and joins the first aperture atop the photosensitive area to form an L-shaped passage. After cleaning out the debris and polishing the bottom of the vertically drilled aperture as best as possible, a thin coat of clear epoxy was applied to the bottom to restore transparency. The LCW capillary (TSU100375, www.polymicro.com, the same LCW capillary was used in all designs) is inserted in a opaque PEEK sleeve 0.015 in. i.d., 1/32 in. o.d., F-385x, www.upchurch.com)—this is inserted through the vertical aperture. The exit capillary, 180 μm i.d., 350 μm o.d. (TSP180350) is inserted through the horizontal aperture. The assembly is covered over with epoxy adhesive intimately mixed with activated charcoal to prevent ambient light from reaching the detector. The assembly was put into an opaque Delrin fixture with provisions for illuminating the LCW capillary radially by the LED approximately 10 mm above where it enters the detector.

3.2.2.2 Laser diode: miniature photomultiplier tube design

A “Blu-Ray” DVD reader (Pioneer model BDC-2202b) was dis- assembled to gain access to the read/write laser sources. This particular model uses three different discrete laser diode (LD) sources at different wavelengths. The VLD is believed to have an output of 5–7 mW and is used for read functions only. Connections to the VLD leads were made directly on the board and these were then connected to external circuitry to apply power. LD’s are static and surge sensitive. As shown in Figure B3 in Appendix B, a switch keeps the VLD disconnected both before power was applied and before power was shut off. The drive current is read by a digital panel meter via the voltage drop across a 10 ohm resistor in series that connects the VLD to ground. A 10-turn 1 kilo-ohm potentiometer allows control of the drive current (monitored and displayed continuously) via circuitry based on a LM317 (www.nsc.com) based

regulator. The fluorescence cell itself was identical to that described for the HPLED–mPMT design below, except that fluid exit connection was made here via a tee for convenience. The manner in which the LCW was illuminated was as follows. The optical lens element (Ø□1.5 mm) through which the laser beam emerges is located centrally between two horizontal highly magnetized bars (ca. 10 mm long, 2 mm wide, spaced 11 mm apart). The optics is spring-loaded and can be pushed down. At its maximum elevation, the top of the lens is flush at the same level as the magnetized bars. This enables a very simple and effective means of affixing the LCW capillary to the top of the optics. The general arrangement is shown in Figures B4 and B5 in Appendix B. A 0.020 in. wide wedge-shaped groove is machined onto the middle of the short side of a 7.5 mm×15 mm opaque Acetal (Delrin) sheet (1 mm thick), intended to function as the capillary cradle. A 0.79 mm bore aperture is drilled about the center of the groove (the intended location of the optics) and a low sensitivity light to voltage converter (TSL252R, www.TAOSinc.com, for referencing the laser intensity) is cemented on the hole on the obverse side of the groove. Two thin steel pieces (2.5 mm × 7 mm) are cemented with epoxy adhesive on the short edges of the capillary cradle, on the same side as the groove. As the cradle, with the capillary in the groove, is lowered on to the LD optics, the capillary is held in place atop the optics by the magnetic force. It is important to use only thin pieces of steel (we used small portions scored off a razor blade). Else, the permanent magnets are so strong, once the cradle is bought near the optics, it is impossible to control the position and the cradle may be drawn with such force so as to crush the capillary. In our particular arrangement, the illumination point was □5 cm from the mPMT tip of the capillary.

The optical output from the lens element was measured with a calibrated laser power meter (type 840011, www.sperscientific.com). This sensor is calibrated for 632.8 nm and a correction factor of 9.62× was applied for measurement at 405 nm according to manufacturer's instructions. Note that there are significant losses in the optical system and the output power at

the exit of the optical element must be significantly smaller than the power generated by the VLD itself.

3.2.2.3 High power light emitting diode: miniature photomultiplier tube design

Referring to Figure 3.1 (the drawing is not to scale), the light source used is a surface-mount type UV LED L (λ_{max} 365nm, NCSU003A, Nichia Corp). This is a very high brightness excitation source (emitting typically 210 mW continuous at 500 mA, with a maximum permissible continuous current of 700 mA, [156]). It is mounted on a finned heat sink HS with heat sink compound. A pair of screws S sandwich the LED between aluminum block B and HS. A (1/4)-28 threaded male nut N holds down the 1mm core jacketed optical fiber OF (ESKA optical grade fiber, NT02-536, www.edmundoptics.com) on the surface of the LED. The emitting chip dimension is 0.9 mm × 0.9 mm square and the fiber captures most of the emitted light. For a flat-faced LED, previous experience shows that direct interfacing of a fiber with polished termini leads to the best light coupling [115]. In the present experiments, the HPLED was operated at a current of 500 mA.

The cell holder AL is machined from aluminum, the general arrangement is schematically shown in the bottom panel of Figure 3.1. A photograph and dimensional drawing is given in Figure B6 in Appendix B. The holder AL terminates in a flange that has screw holes for directly mounting holder AL on the face of the mPMT (H5784, www.hamamatsu.com) with a set of four M2-threaded screws S. This is a relatively low-cost miniature photosensor module [157] with its own built in high voltage supply. The mPMT has an 8 mm dia. photoactive area, contained in a 10 mm diameter window W that is recessed 1 mm inside the metallic sensor housing. One or more layers of plastic optical filters F were cut as 10 mm circles and put on the PMT window as desired. The holder AL has a central 1/16 in. diameter straight through axial hole which snugly accommodates 1/16 in. o.d. 0.75 mm i.d. PEEK tubing PT (~45 mm long). Tube PT is provided first with one inserted spacer SS (3 mm long, 457 μm i.d./635 μm o.d., PEEK, type PK018-025-BLK, www.upchurch.com). The spacer segment SS is coated thinly with

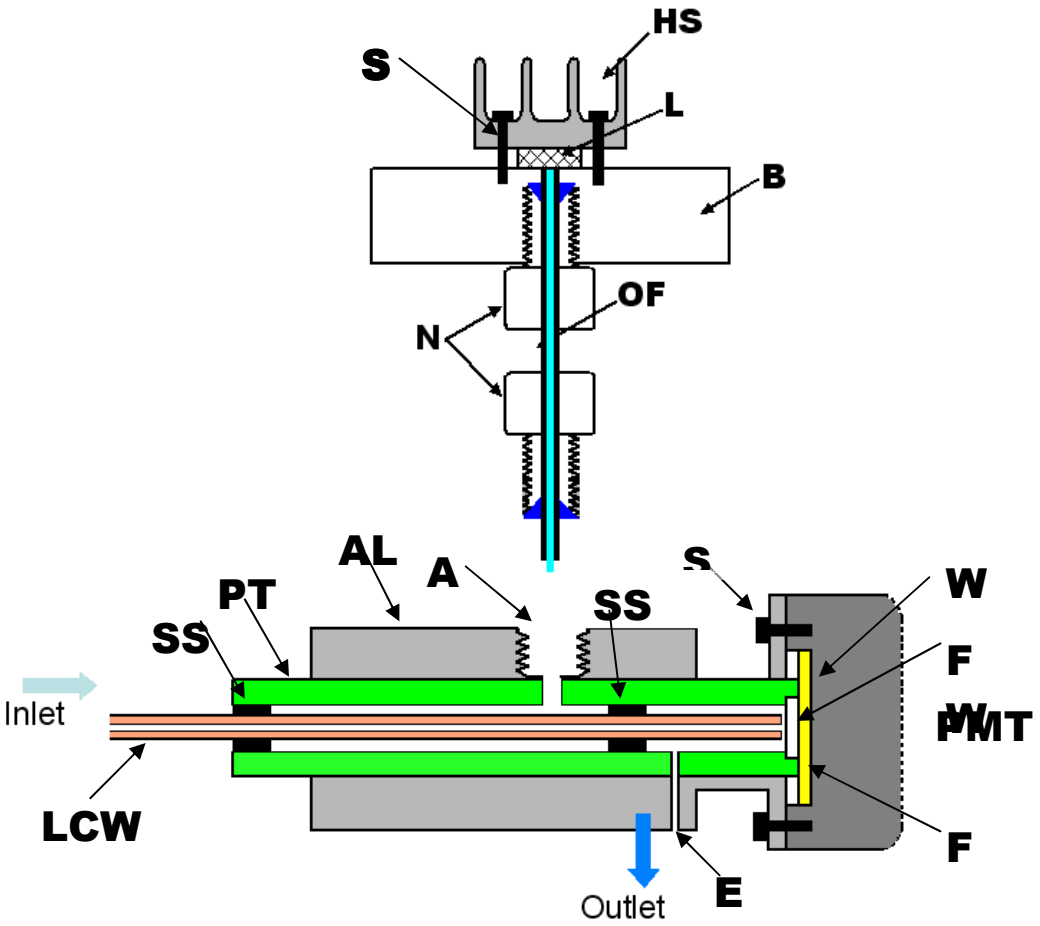

Figure 3.1 Top: high power LED L is sandwiched between heatsink HS and aluminum block B by screws S. 1 mm core acrylate optical fiber OF is coupled to the LED and the fluorescence cell (bottom) with reverse-ferrule equipped ¼-threaded nuts N. The cell is built of an aluminum block AL provided with a ¼-28 threaded flat-bottomed aperture A for the fiber optic to illuminate the 100 μm bore Teflon AF coated fused silica capillary LCW help in a PEEK jacket tubing PT with the help of sealers and spacers SS. PT terminates in a 1 mm long face-polished acrylate optical fiber segment FW functioning as the window against which the LCW butts up. The front flange of the cell attaches directly to the PMT face and FW rests directly on the PNT window W. Optional thin plastic optical filter(s) F can be put on the PMT window W. Liquid enters through the LCW leaks at the tip in the gap between it and FW and exits through aperture E. The drawing is not to scale.

epoxy adhesive on the outside and pushed inside tube PT from one end to a depth of ~15 mm and the epoxy is allowed to cure. The spacer serves to hold the inserted LCW capillary (vide infra) concentric. Tube PT is then provided with a terminal optical window FW at the same end, close to the spacer. We have variously used (vide infra) (a) a 1mm long segment of an acrylate optical fiber (1 mm core, P/N 02-536, www.edmundoptics.com). The fiber is polished at both ends by micro-mesh sandpaper (grades 1500–12,000, www.micro-surface.com) and forcibly inserted into the end of the green PEEK tubing widened at the tip with a 0.040 in. drill bit to a depth of 1 mm, this seals tightly enough that in our experience no leakage occurs. (b) A spherical glass ball lens of 1 mm diameter (NT43-708, www.edmundoptics.com). The ball is forcibly put in at the PEEK tube tip after enlarging the tube tip i.d., in much the same way as the optical fiber segment. (c) A 125 μm thick clear polyester window (Mylar, K-Mac plastics, KS6361, Wyoming, MI). The tip perimeter of tube PT was roughened by sanding, a thin layer of epoxy adhesive was applied and a small piece of the Mylar sheet was then affixed.

With PT inserted in its place in AL, AL is fixed with screws on the top of the mPMT; PT is pushed in until it rests on the mPMT window (with any optical filters already thereon). PT is now fixed in place at its entrance point in AL with a 10–32 nut and ferrule (not shown in Figure 3.1, see Figure B6 in Appendix B for this detail). The (1/4)-28 threaded entrance A in AL ends in a 1 mm aperture. Tubing PT is drilled through at this aperture to allow the 1mm fiber optic to come into PT. On the opposite side of A, a 0.64mm dia. hole is present in AL, this too is now drilled through in PT to serve as fluid exit. PT is now thoroughly washed with methanol using all entry/exit combinations to remove any debris. The capillary LCW (the length chosen ~55 mm, results in ~1 cm protruding from PT at the entrance end) is pushed in from the open end of PT until it rests on window FW. The LCW is not effectively sealed against FW. Rather, liquid entering into the LCW flows past the tip and back around the LCW in the annular space to exit at aperture E where a stainless steel exit tube (0.017 in. i.d./0.025 in. o.d., HTX-23T, www.smallparts.com) is push fit and epoxied in place. Fluorescent light originating from the

excited analytes in the lumen is guided by the LCW to its tip by total internal reflection and is transmitted to the PMT via FW. A second exit sleeve SS is put in and sealed and epoxied in place where LCW enters PT. Connections to the LCW inlet to other 375 μm o.d. capillaries that constitute upstream components of the system are made with a butt-joint using a short polyvinyl chloride pump tubing segment (0.19 mm-i.d., 2.03 mm-o.d.) as a sleeve.

While the data presented comes solely from the above design, for applications where another detector is serially connected, a similar design with a smaller inner diameter for PT (0.5 mm i.d.) was used, without any spacers. The annular gap in this case is ≤60 μm. About 10 mm from the PMT end of the tube PT, a 0.015 in. diameter hole is drilled as the fluid exit aperture. After completion of the assembly, a silica capillary of desired inner diameter is inserted here and epoxied in place.

3.2.3 Electronics

It has been shown elsewhere [115] that short of carefully matched thermistor–resistor combinations, a stable constant voltage power supply and a low value resistor offer the best compromise to obtain a stable light output from an LED as minor variations in ambient temperature occur. Following this maxim, we used a 10-ohm, 10W power resistor in series with the HPLED and powered it with a high current variable voltage power supply. □8.8 V was needed to attain the desired drive current of 500 mA. For the VLD–mPMT experiments, the PMT control voltage was set at 0.9 and no further secondary signal processing was used. For the HPLED experiments, unless otherwise stated, the mPMT gain control voltage was set at 0.7, the primary mPMT output was offset and amplified 10× by a dual JFET-input operational amplifier (TL082CP, www.ti.com), the first stage providing unity gain and variable offset and the second stage providing 10× gain with a time constant of 1 s. Both stages were operated in the inverting amplifier configuration. The circuit diagram is given in Appendix B in Figure B7. In all cases, the detector signal was acquired at 1 Hz by a 12-bit PCM-DAS16D/12 data acquisition card (www.measurementcomputing.com) housed in a mini-notebook personal computer.

Some experiments were conducted where the light source was modulated with an N-channel MOSFET switch (IRLI530N, www.irf.com) with a function generator at □100Hz to address the gate of the logic-level MOSFET switch. The detector output was processed via a balanced demodulator chip (AD630, www.analogdevices.com) using the gate signal for reference. In no case were the results better than dc operation. Hence they are not reported. There are some inherent limitations of this circuitry, better lock-in detection approaches will be discussed in a future paper.

3.2.4 Experimental arrangement

Most experiments were conducted in the flow injection mode, using a single line system. Fluid flow was provided by a 48K step syringe pump (V6, P/N 54022, equipped with a high pressure syringe header valve (P/N 26098) and a 1-mL capacity high pressure syringe (P/N 23994), all from www.kloehn.com. Test solutions were injected with an in-line 1 μL loop injector (070-0134H, www.vici.com). Except as stated, the carrier solution or eluent for chromatography (vide infra) was composed of 1 mM HQS and 1 mM MES, adjusted to pH 5.56 with NaOH and filtered through a 0.22 μm pore size nylon membrane filter and pumped at a flow rate of 4 μL/min. The injector was connected to the detector by a 5 cm long 0.25 mm i.d. fused silica capillary. For most experiments, the detector was simply covered with a cardboard box to provide immunity from ambient light.

3.3 Results and discussion

3.3.1 Basic detector design and performance of the simplest design

Early work on LCW-based capillary scale fluorescence detector clearly indicated the feasibility of such detectors [132]. Presently we first explored the performance of a LCW-based fluorescence detector in which a low power UV LED was used to radially illuminate the LCW capillary directly and the fluorescence was detected with a photodiode-operational amplifier integrated package, sold as a light-to-voltage converter. The response of this very simple detection system to 1 μL of 200□μM $Al(HQS)_3$ exhibited an S/N of 350. While we intended such

a detector to be used primarily for pedagogic purposes and therefore made no further optimization efforts, it is worthwhile to note that an essentially identical detector with approximately 15× greater sensitivity (TSL257R, 1460 mV/W per cm^2 @ 500 nm) is available at the same cost from the same manufacturer. Also it is worthwhile to note that even for HQS chelates, the Al-chelate is not the most fluorescent [158].

3.3.2 The "Blu-ray" laser based detector

This source is misnamed: at 405 nm, it is violet, rather than blue. VLD's have been available for some time; since their availability till now they continue to cost approximately >US$ 2000 as scientific equipment. Lucy and coworkers were the first to use such VLDs for capillary scale fluorescence detection. They observed that at most approximately 30–50% of the power is coupled to a 100μm core fiber optic (FO) when the unmodified LD is coupled to the FO [159]. While they recognized that focusing through additional optics such as a microscope objective is a superior alternative for capillary systems [160,161], they have mostly continued to use the FO coupled configuration [162-164] presumably for the simple reason that incorporating additional optics that necessarily require precise, stable positioning, is cumbersome. Availability of laser based optical drives as a consumer product removes this difficulty. Although the results described in the present work utilizes a different device which uses three different discretely packaged laser sources, based on further experience, we would recommend others to begin with a Sony Playstation 3 (PS3) reader assembly which contains three different laser sources (780, 640 and 405 nm) and a photodiode (that monitors the source output) in a single package. At 20 mW rated output for the 405 nm source, this VLD is also more powerful than the one presently used. Note that although 20 mW VLDs are being produced in quantity (approximately 2 million /month in mid-2007) inexpensively (estimated production cost: US$ 8) [165], they are not available as discrete devices. To our knowledge, there are also no publicly accessible specification sheets. A PS3 reader assembly is however, readily available as a replacement part for <$60 (see Figure B8 in Appendix B) and VLD aficionados have web-accessible

instructions on how to extract the VLD out of the assembly in detailed written [166] and even video [167,168] forms. However, no matter which precise source is used for the VLD, the reader assembly should not be disassembled and the LD extracted for constructing a fluorescence detector. The optics that focuses the beam down to a very small spot is integral to the read (write) assembly and makes it very convenient to simply put the capillary on the top of the lens, aided by the magnetic rails that provide a convenient means to hold the capillary down (all presently available optical drives use magnetic force to keep the disk spinning just away from the lens element without physical contact) and finally, any necessary heat sink is integrally present in an intact assembly. For the more ambitious, the rail and the stepper motor assembly provides a ready means to translate the source along the capillary and thus generate a “whole column” image (albeit the maximum translation length, <40 mm, is rather limited). In the case of the PS3 reader referred to above, any of the three laser sources (the respective pin outs, complete with magnified photos, are available in Refs. [166,168]) are available through the same optics.

In the absence of available specifications, one must necessarily be careful about the maximum current the source can be operated at to avoid irreversible damage. We had no information on the specific Pioneer VLD used here and to err conservatively, assumed it to be a 5 mW device, the lowest power VLDs used in Blu-ray readers. The device shows a weak diffuse output at low currents (similar to that of an LED driven at a low current). As the drive current is increased, the lasing threshold is eventually reached; past this point the light output increases dramatically. Figure 3.2 shows the light output through the lens element vs. drive current. The lasing threshold is computed by extrapolation to be 36.5 mA. It has been suggested that the VLD should not be driven at currents much greater than I_{th} + 10 mA (i.e., ~47 mA in the present case) to avoid irreversible damage [166]. We operated the present VLD up to 54.4 mA for few seconds at a time with a measured power of 3.7 mW at the lens exit, which would probably be close to its maximum operating current (if it is a 5 mW device), accounting for optical losses. To

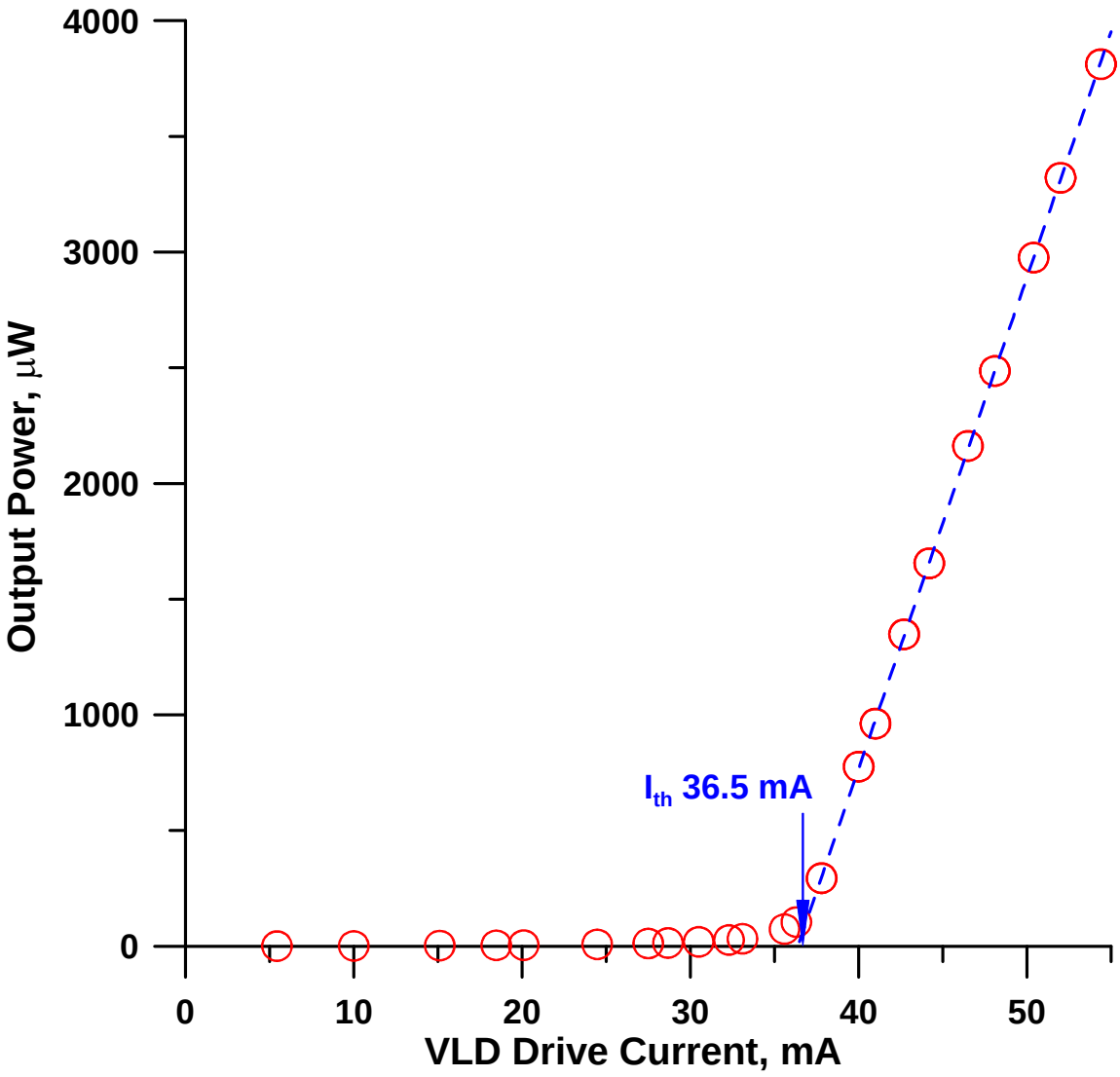

Figure 3.2 Violet laser diode optical output vs. VLD drive current.

be conservative and safe, we initially did most of the work at a drive current of 37 mA, just above the lasing threshold. These results are discussed as operation at this power level will permit essentially indefinite life. Subsequently, the VLD was operated at 47 mA to characterize ultimately attainable LODs from this source. A cooling fan was put on externally to prevent source drift and a smaller aperture was used with the photodiode to prevent saturation.

Although a VLD can be used to detect $Al(HQS)_3$, it is not optimally excited at this wavelength. Vos et al. indicated an LOD of 3 μM for example in a CE configuration [162], this LOD can in essence be reached by our simple LED-PD combination (Section 3.1). In addition, the excitation maximum of $Al(HQS)_3$ is listed as 395 nm [158], this is not strictly correct (vide infra). We chose to explore detection limits with Coumarin 30, which has a □max of 407 nm (in ethanol, for other photophysical data on Coumarin 30 see [169], we used 50:50 methanol water in flow injection experiments both as carrier and as the analyte matrix; absorption and fluorescence spectra obtained in such a matrix was nearly identical to those published for a ethanol medium [169] and are not separately given here). Coumarin dyes are also of particular interest in enzyme-linked immunosorbent assays that most commonly rely on an alkaline phosphatase enzyme utilizing 4-nitrophenylphosphate as substrate. Instead of absorbance detection of the 4-nitrophenol formed at 405 nm, the decrease in fluorescence of concurrently present Coumarin provides a much more sensitive assay [170].

In LCW-based fluorescence detection, we have generally used some form of an optical filter atop the photodetector to filter out excitation light. This unwanted background largely originates from scattering—while the optical quality of the LCW is obviously important, how tightly the excitation beam is focused also greatly governs the extent of scattering. The optics integral to present optical disk drives provide focused spot diameters of 2.11, 1.32 and 0.58□m respectively for the 780, 640, and 405 nm lasers [171]. To our pleasant surprise, the background scattering in the present setup was small enough that even without any filter, the mPMT background signal was easily manageable (<0.2V) (at a PMT gain of 0.9 this

corresponds to within 2× of the maximum gain for this particular device) and VLD drive current of 37 mA. Without any filter, the results for 1 micro-liter of 1 micro-molar Coumarin 30 injection are shown in Figure 3.3. The VLD output as measured by the TSL252 R photodiode on the other side of the capillary is very stable as seen in the upper horizontal line. A 133× magnified view of the VLD output is also shown. This indicates a very small but slow downward drift over time, likely due to heating and temperature equilibration. Note that the more major baseline disturbances (that are discernible both in the mPMT and the PD traces) come from injection valve actuations. Referring to the mPMT trace, switching the valve from inject to load and back to inject cause the mPMT signal to go low while the valve is in the load position. If we try to correlate the mPMT baseline signal to the TSL252R baseline signal in a region where there is no valve actuation artifacts, it is readily revealed that there is no correlation ($r < 0.02$). Predictably the S/N observed in the mPMT trace (~30, noise being defined as peak-to-peak noise, leading to an LOD of ~100 nM) is not improved by ratioing the signal to the laser output. Also predictably, running a 5-s moving average filter significantly improved the S/N, leading to an LOD <40 nM. Of course the LOD is directly dependent on the laser intensity. The above results were all obtained with a drive current of 37 mA.

As the laser output is an order of magnitude greater at a drive current of 47 mA (Figure 3.2), the LODs are much better. Figure 3.4 shows results for the injection of 50 and 100 nM (solution preparation and surface adsorption losses for Coumarin 30, a very hydrophobic dye, preclude reproducible results at lower levels) injections. In the laser induced fluorescence literature, limit of detection has been defined in many different ways. Here, if we assume the raw data at 5 Hz and peak-to-peak noise, the S/N = 3 LOD is 7.7 nM (these and following data are based on the 50 nM injections, the LODs are more than 1.5× lower when calculated for the 100 nM injections—but this degree of change in short term noise is not unusual). Based on the p–p noise of the 5-s averaged data, the S/N = 3 LOD is 2.8 nM. Finally if noise is defined as the standard deviation of the drift corrected baseline in the 1250–1350 s region where no injections

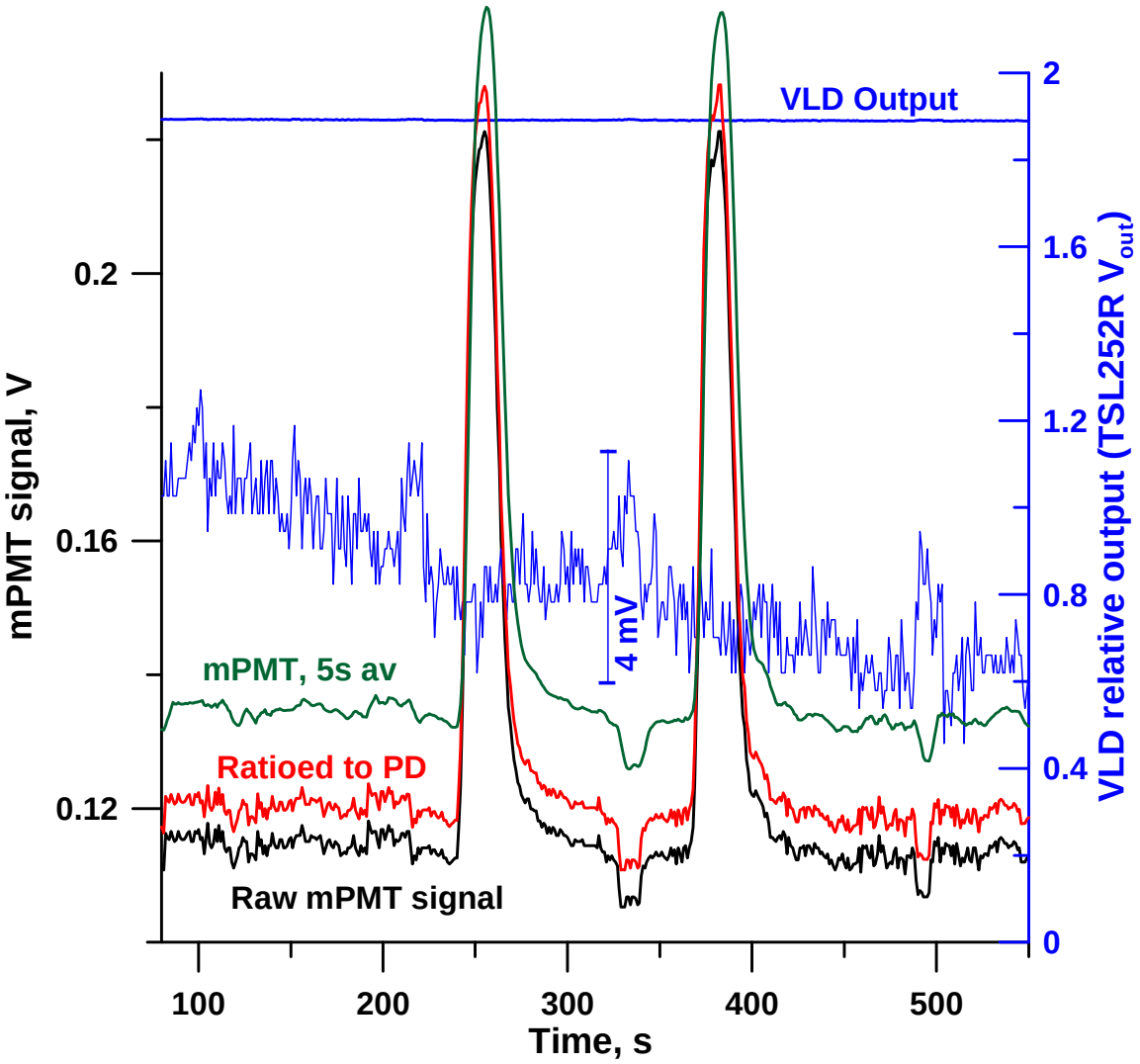

Figure 3.3 Detection of 1 μL of 1 μM Coumarin 30 in 50:50 Methanol:water injected in the same solvent flowing at 4 μL/min. The laser output (VLD drive current 37 mA) is shown as the top horizontal line (right ordinate); it is also shown magnified 133x. The S/N of the fluorescence signal does not significantly change upon ratioing to the laser output but does predictably improve with a moving average filter.

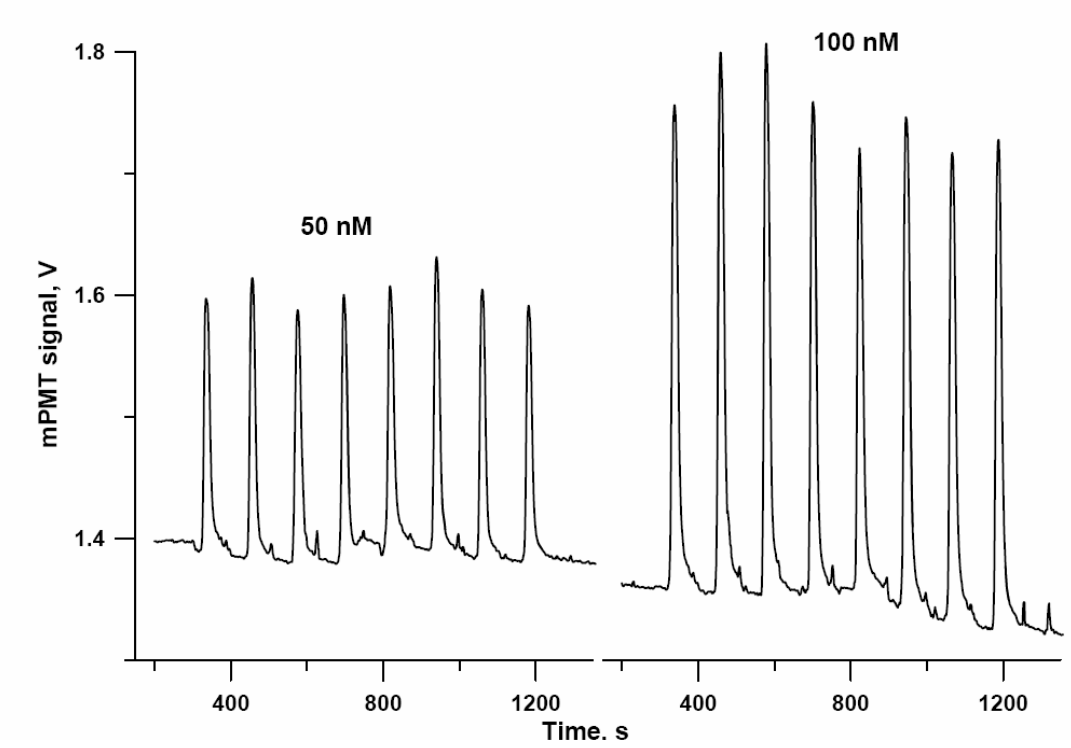

Figure 3.4 Injection of 50 and 100 nM Coumarin 30 with the VLD driven at 47 mA. The data were acquired at 5 Hz and a 5-s moving average filter applied, Note that there is no secondary electronics to the mPMT output and the background signal represents the true mPMT background. No optical emission filter was used.

are made, the S/N = 3 LOD will correspond to 0.4 nM. If we assume that the probe volume is equivalent to a 100 µm (i.d. of LCW) long cylinder with 1 µm diameter, the probe volume is ~80 fL. For a 2.8 nM LOD, there are ~140 analyte molecules in that volume.

3.3.3 The HPLED based detector

3.3.3.1 Optimum wavelength to excite metal-sulfoxine complexes

One principal reason we are interested in capillary scale fluorescence detectors is to utilize them in metal ion chromatography. HQS forms a large number of fluorescent metal complexes, most have an excitation maximum around 390 nm with a large Stokes shift, several other derivatives of HQ with attractive fluorescence properties have been more recently synthesized as well [172-174]. The potential of HQS either in the eluent or as a postcolumn reagent in conventional scale metal ion chromatography has long been demonstrated, with or without micellar sensitization [158,175,176]. We chose to explore performance for Al-HQS detection, the fluorescent Al-chelate is often regarded as the archetypal HQS chelate [177].

The excitation maximum of $Al(HQS)_3$ at its optimum pH is reported as 395 nm [158]. Of LED sources we examined for exciting $Al(HQS)_3$, the primary candidates were two devices with center wavelengths of at 365 and 385 nm with comparable half bandwidths (10–12 nm), respectively emitting 210 and 290 mW @ 500 mA (Nichia NCSU033A and NCSU034A). The obvious expectation was that the 385 nm emitter will provide significantly better performance. To our surprise, the results were substantially the opposite (Figure 3.5). We then reexamined the fluorescence characteristics of $Al(HQS)_3$; the data are shown in Figure 3.6. These data show that the excitation maximum actually red shifts with increasing concentration. Near the LOD, at low concentration, excitation at 365 nm is actually superior to that at 385 nm. The 365 nm HPLED was used henceforth.

3.3.3.2 Cell terminal window material and light throughput

The terminal window sits directly on the PMT and conducts the light to the detector. It must also be chemically inert for the given application and withstand some modest backpressure. Aside

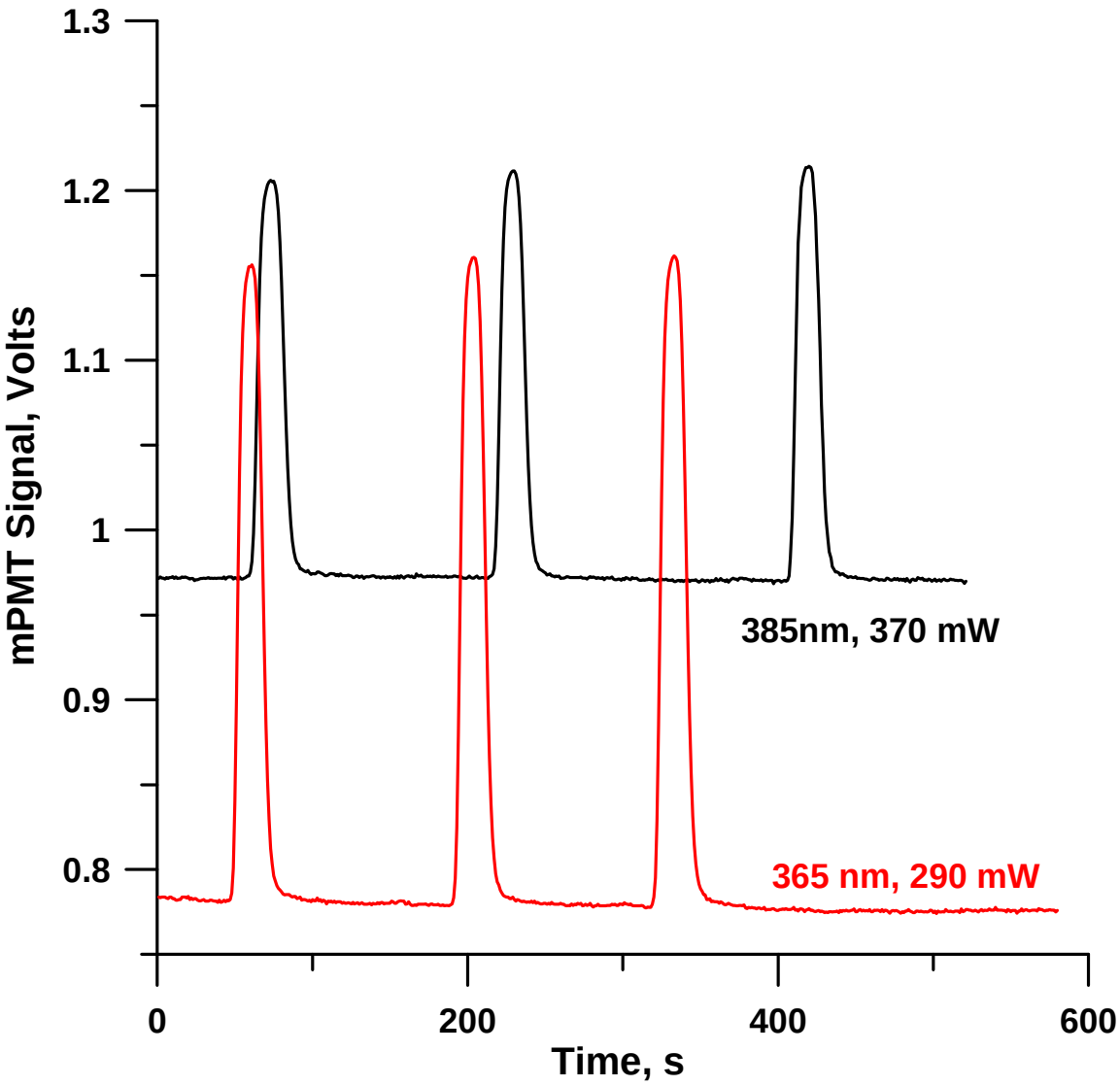

Figure 3.5 Response elicited by an injection of 1 μL of 2 μM $Al(HQS)_3$, mPMT gain 0.7, secondary amplification 100x. Top trace: 385 nm emitter; bottom trace 365 nm emitter. A double layer of Roscolux #369 green plastic filters was placed on the mPMT.

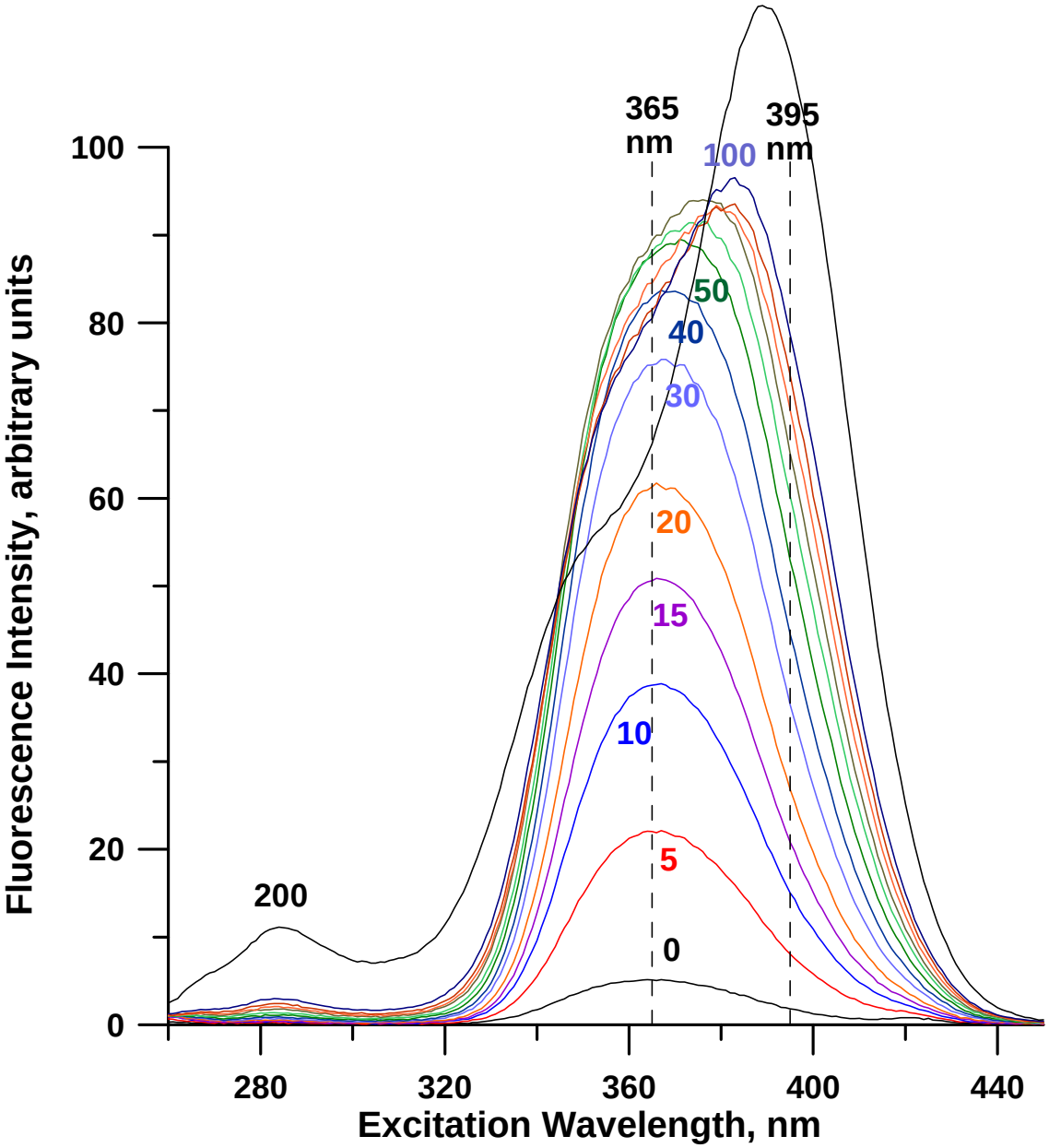

Figure 3.6 Excitation spectrum of the indicated concentrations of Al^{3+} (in μM) in 1 mM HQS, pH 6. The excitation maximum red shifts with concentration.

from the optical fiber segment already mentioned in the experimental section, based on initial experiments we investigated two other window types. One involved a spherical glass ball lens of 1 mm diameter (NT43-708, Edmund Industrial Optics, Barrington, NJ) that was forcibly put in at the PEEK tube tip after enlarging the tube tip i.d., in much the same way as the optical fiber segment. The other involved a 125 μm thick clear polyester window (Mylar, K-Mac plastics, KS6361, Wyoming, MI). The tip area of the PEEK tube was roughened by sanding, a thin layer of epoxy adhesive was applied and a small piece of the Mylar sheet was then affixed. Rather than measuring fluorescence emission, we simply measured the light transmission efficiency of the water-filled cell assembly. A miniature tee was put in the LCW tube entrance and an optical fiber was butted against the LCW tip. The other end of the optical fiber was connected to a LED emitting at 450 nm powered at a constant current of 10 mA. Water was pumped during the experiment through the perpendicular arm of the tee. The relative light intensities registered on the detector (adjusted to operate at a low sensitivity) were 0.376 ± 0.021, 0.340 ± 0.029 and 0.402 ± 0.012 for the polyester window, glass ball and the optical fiber, respectively. Considering that the cell tip has to be disassembled and reassembled for each test arrangement, the overall difference between the three is probably within experimental uncertainty. Nevertheless, we chose to do further experiments with the putative best, the cell with the optical fiber window.

3.3.3.3 Performance

Relative to coupling with a fiber optic, Melanson and Lucy [160] have shown that a pinhole and a microscope objective can provide a better focused arrangement for fluorescence excitation, leading to less scattered light and thus a better S/N. In the present case, even discounting interfacial losses, geometric considerations (HPLED emitting area vs. fiber optic cross section and far more importantly, fiber optic cross section vs. LCW bore) will dictate that maximally approximately 7–8% of the emitted light serves to illuminate the analyte over an estimated volume of 8 nL. Despite all this, we chose the fiber optic coupled arrangement rationalizing that

the very large emitted power of the HPLED will provide enough light and counting on optical filters to filter out the scattered light; the simplicity and cost constituted a big plus. We examined three filters: Roscolux 369 (NT39-418), thin film UV filter sheet (NT39-426) and Wratten 44A (NT54-465, all from www.edmundoptics.com). The first two performed essentially equally well and the third one produced approximately 2× lower S/N; the emission spectra of the LED, the emission spectra of $Al(HQS)_3$ and the transmission spectra of two sheets of the Roscolux 369 joined by a thin layer of optical grade epoxy are shown in Figure 3.7. The spectra of the two other optical filters tested are provided in Figure B10 of Appendix B.

The performance of this detector is shown in the flow injection mode for a calibration set of samples containing 10–100 nM Al^{3+}. Data where a reference detector was used to reduce drift and then smoothed (5-s moving average filter) are shown for the low concentration data in the inset. (Figure 3.8) In this case, the smoothing actually has very little effect on the S/N. The primary noise in the baseline comes from frequent back and forth switching of the injector, as would be apparent from the trace after the last 100 nM sample, when no further injections were made. If we take the conservative approach and consider the baseline disturbances from the injector as part of noise, the S/N=3 LOD will be 4 nM for either the raw 1 Hz data or the smoothed one. On the other hand, with noise defined as the standard deviation of the drift corrected baseline, the S/N = 3 LOD is in fact calculated to be approximately 0.8 nM. The signal is linear for at least two orders of magnitude (0.01–2.0 μM, linear r^2 0.9991). The relative standard deviation at the 20 nM level was 1.5% (n = 10).

3.4 Conclusions

Recent advances in solid state light emitting sources, in conjunction with liquid core waveguides make possible attractive capillary scale fluorescence detectors that are both highly commercial products is a boon to an experimentalist and can be harnessed to make very high performance very small volume detectors. Dedicated monochromatic source based fluorescence detectors do have the disadvantage that the extant source wavelength may be

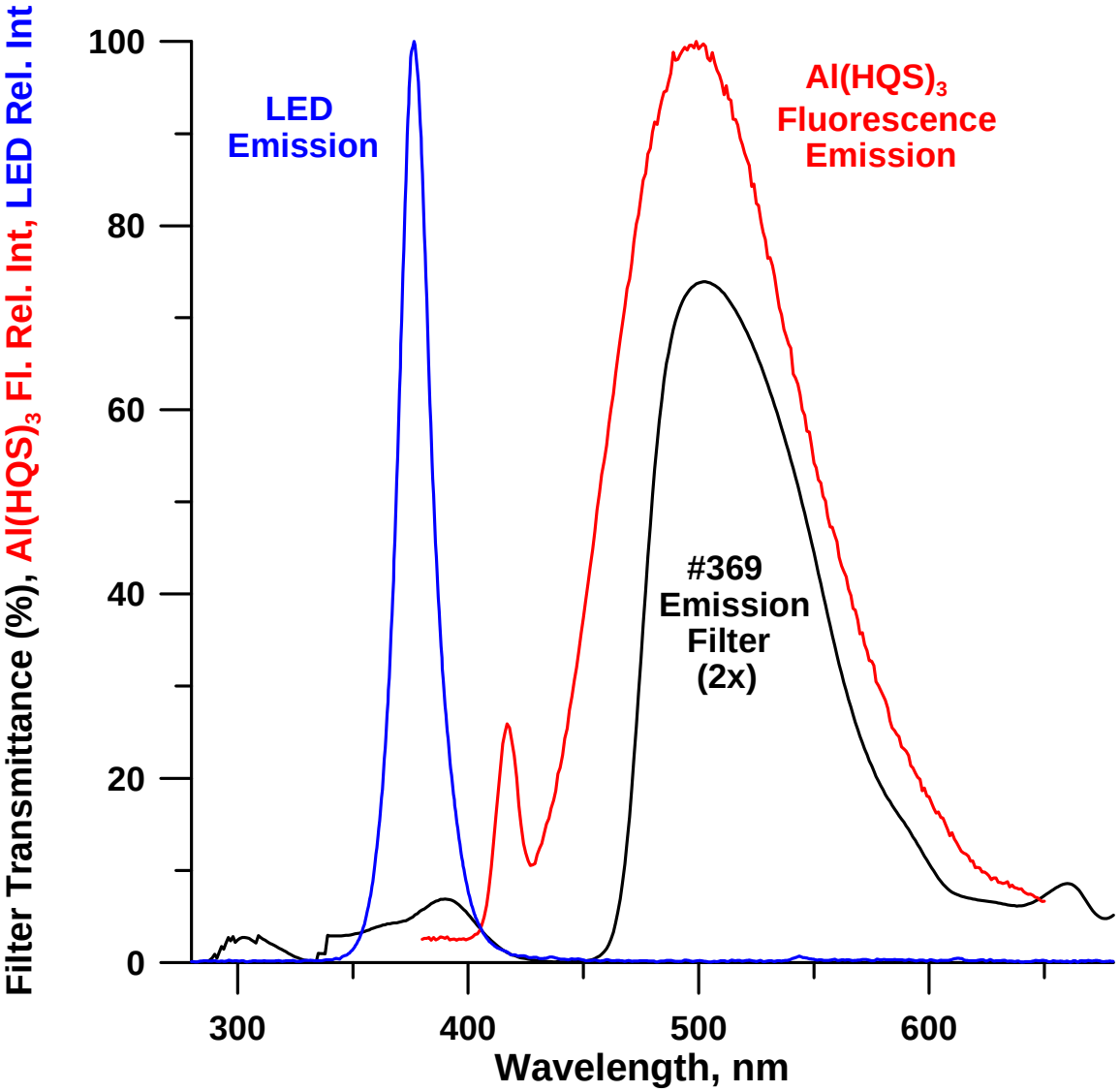

Figure 3.7 Spectral characteristics of the excitation source, the fluorescence emission and two sheets of the #369 filter used for emission filtering.

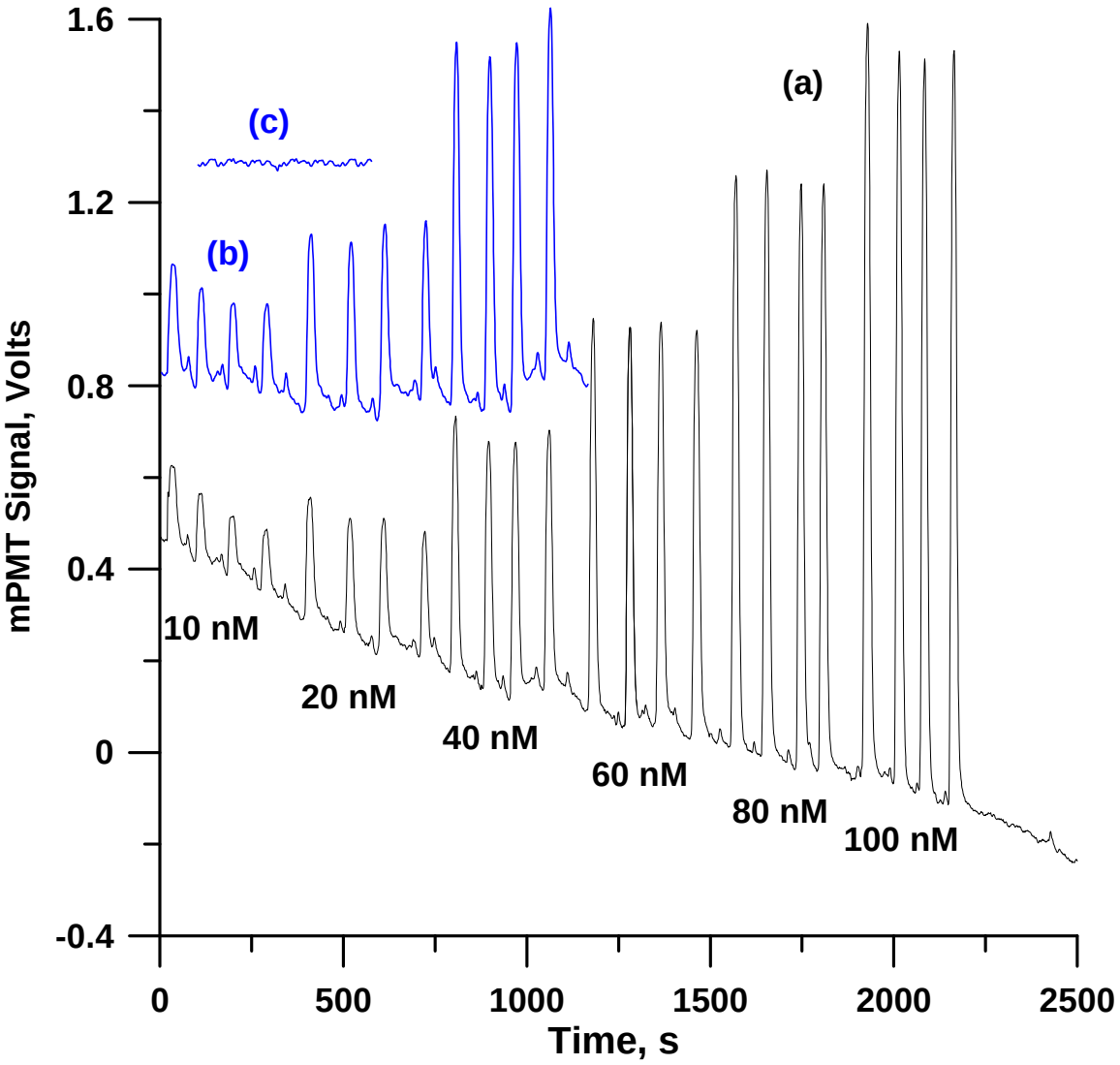

Figure 3.8 (a) Typical output for Al^{3+} determination. The Al^{3+} concentration of the sample in μM is indicated. At low levels, the drift, which mostly appear to arise from thermal changes causing a difference in source output can be significant, (b) shows drift corrected magnified traces for the 10-40 nM injections and (c) shows the corresponding drift corrected baseline trace when no injections are made.

affordable and highly sensitive. We have provided here generic designs for LCW-based flow through detectors that can be used in series with other detectors. It is rare that a new device is made for analytical use—the advent of short wavelength laser diodes in inexpensive unsuitable for a particular application. Ref. [115] provides a discussion of many vendors and the wavelengths in which LEDs and LDs can be obtained. This is a dynamic marketplace and the corresponding websites should be visited for up to date information, however.

CHAPTER 4

ELECTRODIALYTIC REAGENT INTRODUCTION IN FLOW SYSTEMS

4.1 Introduction

Postcolumn reagent introduction is one of the oldest techniques used in liquid/ion chromatography. The first amino acid analyzers utilized postcolumn reaction detection with ninhydrin [178,179]. Detection sensitivity and selectivity in many flow techniques can be dramatically increased by introduction of a derivatization reagent. Assuming postcolumn reaction kinetics is not a limiting factor, reagent introduction into a flow stream has two basic issues. These are (a) volumetric dilution by the reagent and (b) extent and speed of mixing. To achieve rapid mixing, different geometries, including T-, Y-, arrow, miniature cyclones, etc., were studied [180]. For reagent introduction we had ourselves worked with screen-tee mixers and continuously or intermittently pressurized porous membranes [181,182]. Any pulsation associated with reagent introduction impairs detection limits, especially where the unreacted reagent optically absorbs at the monitoring wavelength [181].

One can introduce acids or bases in the gas phase. This is possible for reagents with sufficient vapor pressure (e.g., HCl or NH_3); they can permeate/diffuse through appropriate membranes without volumetric dilution [183]. Teflon AF has a uniquely low refractive index and is useful as a liquid core waveguide [133]. It is also uniquely gas permeable [184], and acid or ammonia vapors can permeate through it, rendering it a “chemically active” waveguide [185]. It is possible to introduce other reagents in vapor phase through suitable membranes [186]. However, reagents that have sufficient vapor pressure and membranes that will permit sufficient transmembrane flux and still be robust enough for flow through applications are few. Electrodialysis is widely used in a large scale, mostly for removal of ions [187]. It is not typically used to introduce ions. We have examined dilutionless electrodialytic reagent introduction in the

past. It is possible to introduce acids or bases by deploying one electrode in the flow channel and another isolated by an ion exchange membrane [188-190]. However, gas bubbles are generated in the detected stream and contribute to the noise; systems relying on Donnan-forbidden leakage were found to have lower baseline noise [191]. The latter approach has serious limitations, however. It is not possible to introduce a significant flux of a reagent where the reagent is strongly retained by the membrane. Also, any approach that relies solely on a concentration gradient to move material across is not easily controlled. One can control the flux only by changing the feed reagent concentration, requiring significant equilibration time. In addition, none of these approaches promotes mixing.

A dual membrane device recently solved the in-stream gas generation problem in electrodialysis. Electrodes are placed outside the membranes, and there is no gas evolution in the central channel [128]. Ion exchange resin beads are used for high pressure applications and acid, base, or salt can be generated [192]. Doubtless, these substances can be introduced as reagents into a flow stream as well. Imagine that a desired reagent anion X^- is placed as NaX on the anion exchanger side that also contains the negative electrode. Some indifferent electrolyte, e.g., KNO_3 is placed on the cation exchanger side where the positive electrode is placed. As current flows, X^- and K^+ are drawn into the central channel. An important aspect is that each ion electromigrates all the way to the opposite membrane (that it cannot penetrate due to Donnan exclusion). The bulk fluid flows perpendicular to the electrical transport. The electrical transport from the entry membrane to the Donnan-forbidden membrane drives transverse mixing.

In this laboratory, we have a long-term goal of characterizing atmospheric aerosols [193-194]. One ongoing effort is to collect aerosols in a cyclone collector, periodically digest it online, and then comprehensively analyze the digest (including for heavy metals) by capillary chromatography. To this end, we have developed inexpensive capillary scale absorbance, fluorescence, and capacitance detectors [88-154]. The most common way to perform chro-

matographic metal ion analysis is to use 4-(2-pyridyl(azo) resorcinol) (PAR) as a postcolumn reagent [195-197].

Herein we show how to achieve PAR introduction without dilution with unfunctionalized or anion exchange functionalized cellulose membranes. The introduction is achieved under current control. Capillary scale postcolumn reactions remain challenging. They range the gamut from reaction in bulk volume [198] to laser drilled capillaries [199]; some of these systems are quite complex [200]. We accomplish here capillary scale reagent introduction; the technique will be generically applicable in many situations.

4.2 Experimental

4.2.1 Device

The capillary electrodialytic reagent introduction system (cEDRIs) is shown in Figure 4.1. The central disk (5 mm diameter) is punched out from a 380 μm thick poly(vinylchloride) sheet. A 300 μm wide 3000 μm long slot is machined on this disk and 150 μm diameter holes connect to the slot through opposing sides (see Figure C1 in the Appendix C). Silica capillaries (75 μm i.d,,150 μm o.d.) glued therein address this central flowstream. Atop the central slotted chamber is a cation exchange membrane disk (125 μm thick, radiation grafted Teflon, ion exchange capacity 1.2-2 mequiv/g, www.dionex.com). A 250 μm diameter platinum wire that functions as the positive electrode is placed atop the cation exchanger disk. A 2 M KNO_3 solution is flushed at 200 μL/min by a peristaltic pump through this top chamber. The membrane on the bottom of the central slotted chamber was one of the following: (a) a thin anion exchange membrane similar to the cation exchange membrane above, (b) a regenerated cellulose dialysis membrane (wet thickness approximately 30 μm, 12-14 kD molecular weight cutoff, www.spectrapor.com/dialysis/BiotechTubing.html), or (c) the dialysis membrane in part b functionalized into a methacrylate skeleton methyldiethanolamine functionality anion exchanger (capacity 0.11 mequiv/g, see details in the Supporting Information). The bottom compartment contained the negative electrode and peristaltically pumped or recirculated 1.0-28.0 mM PAR

solution (pH adjusted to 10.0 with NH_4OH). The 1/4-28-threaded male nuts held the membranes inside a standard chromatographic union. The union had two 0.3 mm wide slots cut to half the height of the union to accommodate the central disk with capillaries. The central channel has an internal volume of 340 nL. See Figure C2 in the Appendix C for electrode arrangement. A constant current source powered the electrodes.

4.2.2 Flow injection setup

A syringe pump (model V6, www.Kloehn.com) with a 1 mL glass syringe pumped carrier deionized water (Milli-Q, acidified with HCl to pH 4) at 7.5 µL/ min to a 525 nm light-emitting-diode (LED) based on-capillary absorbance detector via a loop injector. The injector was six-port type and electrically actuated (www.vici.com, 1.0 or 5.0 µL loop, nonmetallic flow path). The detector was built in-house and utilizes multireflection [88]. The detector output was acquired by a laptop personal computer using a USB-based 16-bit data acquisition card (http://www.mccdaq.com/usb-data-acquisition/USB- 1608FS.aspx). The raw transmittance data was software converted to absorbance. Experiments were conducted at laboratory temperature (22 degree C). The detector was calibrated with 0-250 µM PAR solutions so that the observed absorbance can be related to the PAR concentration introduced (Figure C3 in Appendix C).

4.3 Results and discussion

4.3.1 Electrodialytic introduction of PAR: PAR concentration

The PAR solution must be alkaline to maintain PAR in the anionic form, typically as the dianion ($pK_{a1} \approx 3$, $pK_{a2} \approx 5.5$) [202], and to neutralize the originally acidic carrier/eluent stream after mixing. Typically, the PAR solution contains ammonia or an amine as an auxiliary weak ligand that helps prevent metal precipitation. The PAR dianion and OH^- are the two principal anionic current carriers in the feed. The latter has a far greater mobility than the former. Consequently, transport of PAR is not particularly current-efficient.

Excess PAR leads to greater background absorbance (see Figure C3 in Appendix C for quantitative data) and thus increased the baseline noise. However, too little PAR limits the

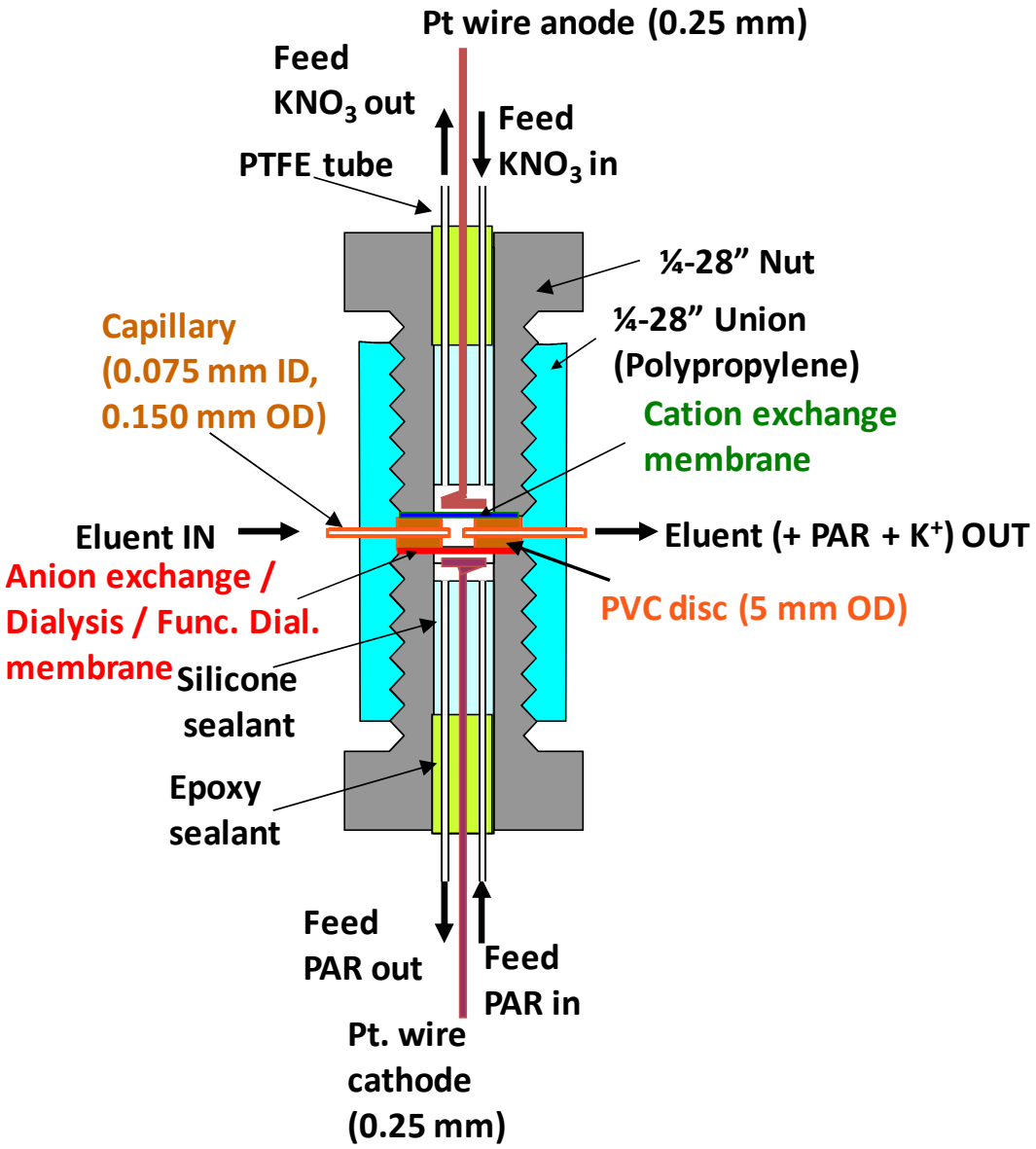

Figure 4.1 Dual membrane capillary electrodialytic reagent generator schematic.

applicable measurement range. The exact PAR concentration is therefore of importance. In a recent benchmark example, Barron *et al.* [195] uses a final PAR concentration in the mixed stream of approximately 40 μM; in an Application Note from a manufacturer [203], the suggested value is approximately 90 μM.

4.3.2 Bead and membrane-based devices

In initial experiments we used a dual ion-exchange resin bead based device [128] with an ammoniacal PAR solution (pH 10, 1 mM PAR) on the anion exchanger bead, negative electrode side. There was no significant PAR introduction. Subsequently, the present membrane-based cEDRIs were tested with anion exchange membranes as thin as 25 μm (prepared by radiation grafting PTFE with vinylbenzyl chloride, approximately 10% cross-linked, and then quaternized). We attained current flow with no gas evolution in the central channel but observed little or no PAR introduction (Figure 4.2); what was introduced was current-independent.

In contrast, PAR was readily electrodialytically introduced through both the native and functionalized dialysis membrane (Figure 4.2). Seemingly, the native membrane permits a greater range, but actually the drift and noise tend to be substantially greater compared to the functionalized membrane. Figure C4 in the Appendix C shows this more clearly.

4.3.3 Current and feed concentration based control of reagent introduction

As Figure 4.2 shows, current can control the electrodialytically introduced PAR concentration. Increasing the feed PAR concentration increases the amount of PAR introduced and increases the range of current control because this changes the PAR/hydroxide ratio and hence the relative importance of PAR as the current carrier. We depict this in Figure 4.3, which also shows the baseline noise at -30, -10, 0, +10, and +30 μA levels of drive current (PAR_{feed} = 7 mM). The baseline noise (that ultimately controls the LOD) does not markedly vary, and active current controlled introduction leads to lower noise than open circuit (0 μA) penetration even when the PAR_{feed} is much lower.

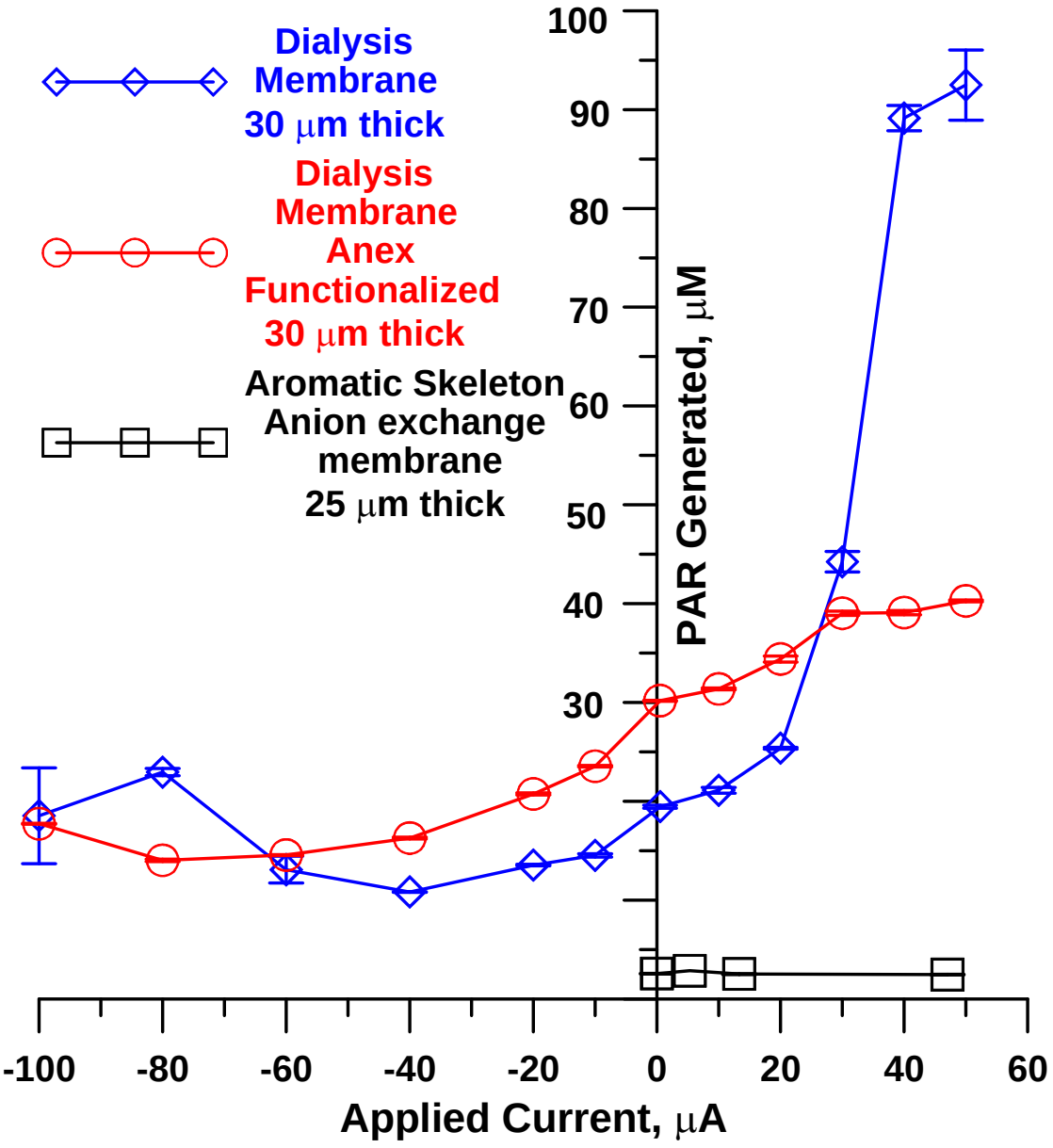

Figure 4.2 Performance comparison of different membranes towards electrodialytic generation of PAR.

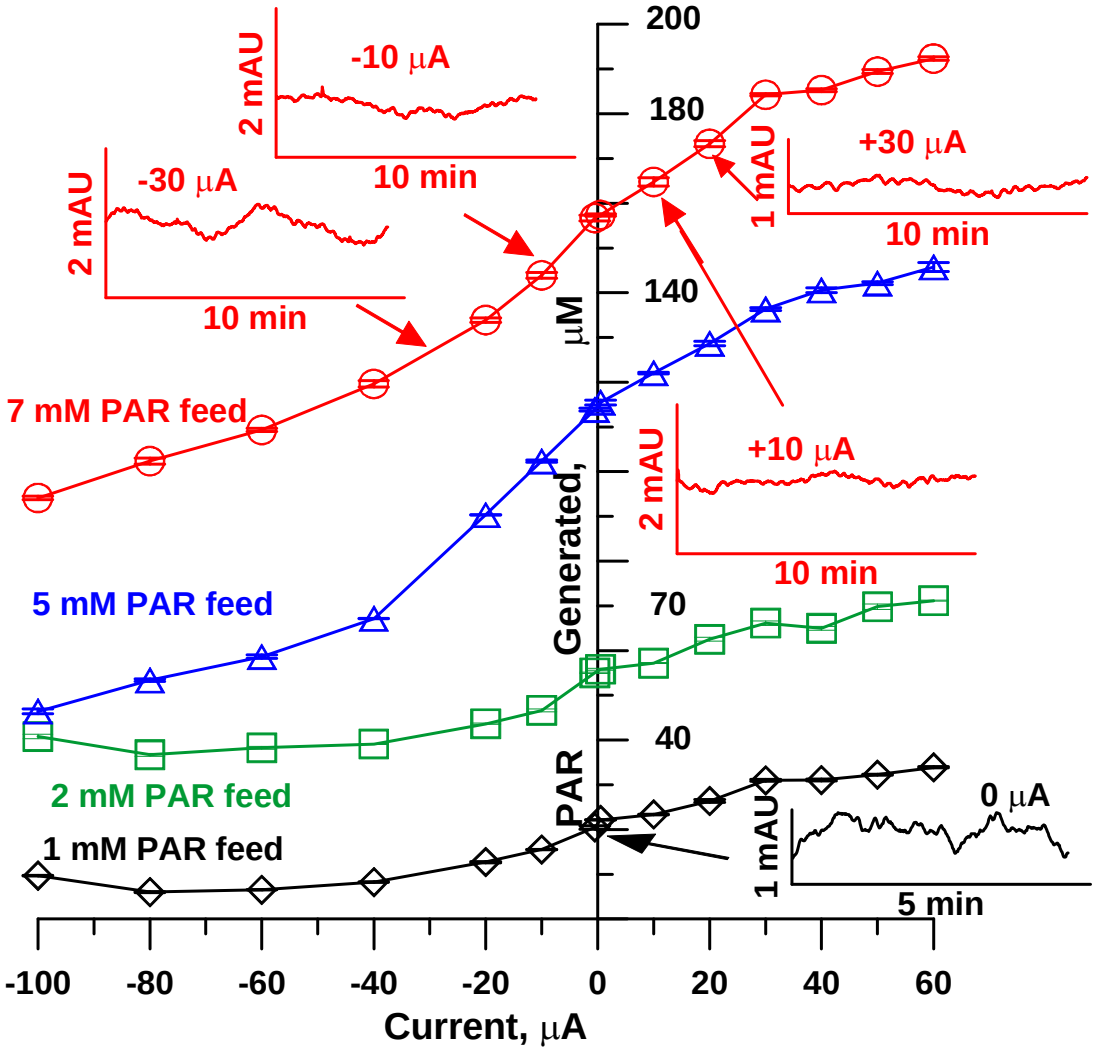

Figure 4.3 Electrodialytic PAR generation with anion exchange functionalized dialysis membrane at different PAR feed concentrations. Inset shows baseline noise (ordinate scaling same in all 5 cases) at indicated feed concentrations and drive current.

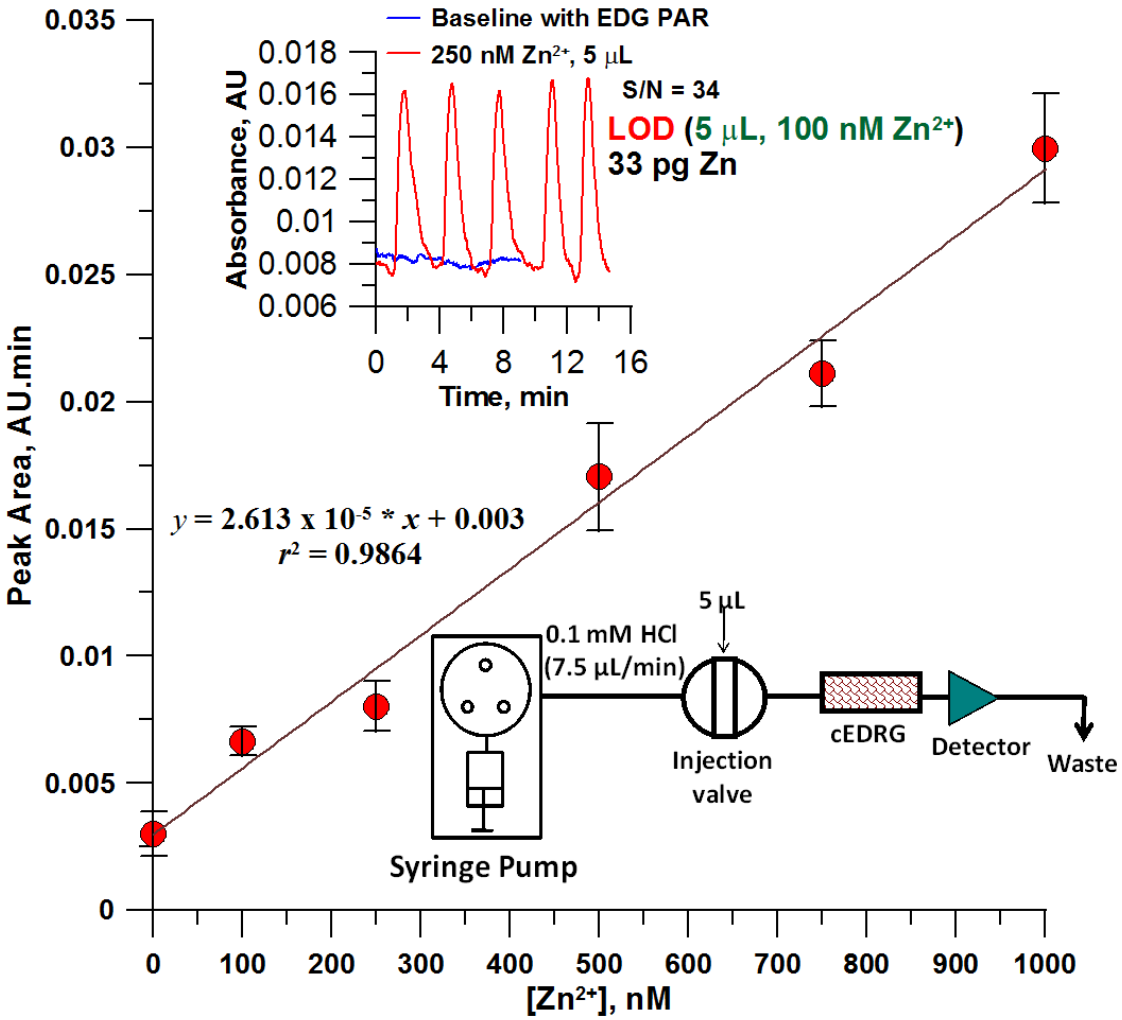

Figure 4.4 Test system: single line capillary scale flow injection system 5 µL loop 6-port nonmetallic injector, cEDRG and multi-reflection absorbance detector. Inset FIAgram shows the baseline and the absorbance peak due to the injection of 5 µL of 250 nM Zn^{2+}. Over a broader range (0.1-50 µM) the linear r^2 value was slightly worse at 0.98.

4.3.4 Performance

The reaction between Zn^{2+} and PAR are depicted in Figure C5 in the Appendix C. Figure 4.4 shows the basic system performance. On the basis of the signal from the 250 nM Zn^{2+} and blank traces, we conservatively estimate the LOD to be ~100 nM (33 pg). This compares with LODs of 180-220 nM (600-700 pg) Zn on 2 mm benchmark chromatographic systems [195]. PAR generation is reasonably reproducible day-to-day, as shown in Figure C6 in Appendix C for three consecutive days with 7 mM PAR as the feed.

Potential analyte loss with the native membrane was also of interest. A positively charged metal ion can be lost to the negative electrode through the dialysis membrane unless PAR chelation is rapid. For most metals, PAR chelation appears to be rapid (we will present detailed kinetic data elsewhere): we observed no difference in analyte response for the two membranes (Figure C7 in Appendix C).

4.3.5 Potentials and limitations

The maximum current used with the present device was 96 μA at 2.65 V for an active membrane area of 0.9 mm^2; this amounts to a current density of 0.11 kA/m^2. For a flow of 7.5 μL/min, we estimate a steady-state temperature rise of 0.5 ℃ under adiabatic conditions. In comparison, commercial suppressors with active membrane areas of 14 cm^2 on each side operate at currents up to 0.5 A at 3.75 V (flow rate 2 mL/min). This translates to a current density up to 0.36 kA/m^2 with an adiabatic temperature rise of ~13 ℃. In r eality, the actual temperature rise is likely to be a small fraction of the adiabatic estimate in both cases. The fluids in the exterior channels flow at an equal or greater rate and carry much of the heat away. In terms of total power dissipation, the present devices can likely be pushed to much higher limits. Electrolytic gas evolution is generally not a problem; electrical breakdown is prevented by a large flow/recirculation rate in the outer chambers and maintaining a large exit aperture. While the present membranes will not be particularly tolerant of pressure, it has already been shown that ion exchange beads can be used to build much higher pressure devices [128,192]. This

concept can be used to potentially to carry out precolumn derivatization. In summary, the gasless electrodialytic reagent introduction concept has been successfully demonstrated for PAR, an important application, and should be applicable for a variety of other uses.

CHAPTER 5

CONCLUSIONS AND FUTURE WORK

Aerosols, relatively stable suspensions of solid or liquid particles in gas (commonly air), occur naturally and are also anthropogenic. Ambient aerosols span the inhalable size range and can be hazardous to human health because of their composition. Various metals have been detected in ambient aerosols. To measure metals in ambient aerosols, the sample must be collected for an extended period and the process operates necessarily in a discrete batch mode. It has long been realized that ambient aerosol composition changes rapidly with time. There is presently no instrumentation that can provide real time or near-real time information about concentrations of metals in atmospheric aerosols. It is therefore necessary to develop an instrument that can provide qualitative and quantitative analysis of metals in atmospheric aerosols in a real time, or near real time basis. In case of on-line or real-time analysis, sampling, sample preparation and analysis must be integrated in an automated manner. This will reduce contamination, minimize human error, labor costs and costs of analysis per sample and improve the data quality, system reliability and sample throughput. Thus, to preserve sample integrity and to deliver accurate qualitative and quantitative information about metal concentrations in atmospheric ambient aerosols for source identification and source apportionment purposes, on-line analysis is essential.

The primary objective of this dissertation research was to develop automated instrumentation for the continuous on-line measurement of atmospheric metals by capillary ion chromatography towards source identification and source apportionment studies. To achieve this objective, capillary scale detectors were developed that had very high mass sensitivity so trace levels of metals could be detected. Also, a capillary scale reagent introduction device was

developed to enhance the applicability of the detector so that it can measure a wide variety of metals.

There are several advantages of using a capillary ion chromatography system for the detection of metal ions. These include (1) low reagent consumption, (2) small sample requirement, (3) high mass sensitivity, (4) more efficient separations and (5) facile coupling to mass spectrometers and flame/plasma based detectors that can work with low flow rates. Capillary scale ion chromatography separation has several challenges. These include preparation of packed capillary columns of small dimensions, preparation and efficient use of narrow bore open tubular capillary columns, reliable pumping of extremely small flow rates, reproducible injection of minuscule amount of sample (to avoid overloading of column as well as prevent band broadening), and detection in a very small volume without loss of sensitivity to measure very small amounts of analyte.

Optical detection is the most common mode of detection in analytical chemistry. Among all the available optical detections methods, absorbance detection is used most frequently. With an objective to develop a capillary ion chromatography system equipped with an optical detector, we fabricated a simple, versatile, economical, light-emitting-diode based capillary scale multi-reflection absorbance detector with very high detection sensitivity. The details of construction, parametric optimization, operation and applications have been described in Chapter 2. The total internal reflection property was provided to the detector cell by externally silver coating the walls of commercially available 180 μm i.d. fused silica capillary after removing the protective polyimide coating of the capillary. Parameters like capillary cross-section, angle of light incidence and length of silver coating on the wall were optimized and the detection volume of this novel capillary absorbance detector was 500 nL. Under pneumatic flow conditions in a flow injection analysis set up this device could detect 4.4 fmol (2.6 pg) of Bromothymol Blue. This detection sensitivity prompted us to explore this multi-reflection absorbance detector for the detection of metal ions.

Fluorescence detection is often much more sensitive than absorbance detection. This motivated us to develop a capillary scale fluorescence detector that could detect metal ions through the formation of fluorescent metal complexes. Our effort in developing a liquid core waveguide based capillary scale fluorescence detector that could be coupled to capillary ion chromatography system equipped with a post column reagent addition device centered on Teflon® AF coated fused silica capillaries. Teflon® AF has a refractive index lower than that of water and hence when light is launched into a water-filled Teflon AF tube, the light is essentially is trapped in the aqueous core as it prefers to remain in an optically denser medium. A Teflon® AF coated capillary was transversely illuminated to excite the analyte flowing through it using an LED or a laser diode as the light source. The fluorescence was detected using either an inexpensive light-to-voltage converter or a miniature photomultiplier tube. The best S/N=3 limit of detection of the capillary scale fluorescence detector was observed with a high power LED source and a miniature PMT detector; this was 3.8 fmol of Aluminum. Hence, this detector can be conveniently utilized in the capillary ion chromatography system for the detection of metal ions.

In general, metal ions by themselves are neither intensely absorbing nor fluorescent. They cannot be detected sensitively in native form and must be complexed with a chromogenic agent or fluorogenic agent to form a metal complex that can be detected by an absorbance or fluorescence detector. To facilitate the introduction of chromogenic or fluorogenic agent inside a flowstream that will carry the metal ions, a reagent introduction device is necessary. To achieve this objective, we fabricated different types of capillary scale reagent introduction devices wherein the complexing agent solution was physically introduced on-line (using an additional pump) into the flowing analyte stream. This led to dilution of the analyte as the volume increased due to the addition of the reagent. Also the pump typically introduced significant additional baseline noise. These factors together impaired the detection sensitivity. Chapter 4 discussed my efforts towards the development of a capillary scale electrodialytic reagent

introduction device wherein only the reagent ions were introduced into the flowing analyte stream in a current-controlled manner, as opposed to a pump in conventional reagent introduction devices. This device displayed the dual advantage of dilution-less addition of reagent and elimination of a reagent introduction pump. It was then used in the flow-injection analysis mode towards the detection of trace level of transition metals and as little as 68 pg of Zn^{2+} could be measured as the intensely colored chelate with electrodialytically generated 4-(2-pyridylazo)resorcinol (PAR).

The studies described in Chapters 2-4 represent an advance in the detection of trace levels of metals. However, the initial goal of the dissertation research was only partially achieved. The research on integrated automated measurement metal ions in ambient aerosols is currently underway. This is being carried out in online or continuous mode wherein the air sampling, digestion of particulate matter for the extraction of metal ions and subsequent detection of metal ions is combined. In an attempt to determine metals in atmospheric aerosols, the sampling is carried out continuously (at the rate of 30 liters/minute) and the aerosol particulate matter is collected at the bottom of a commercial mini-cyclone sample collector. The collected air particles are continuously washed out from the bottom of the mini-cyclone into a tee where the sample stream is mixed with another stream of high concentration of nitric acid flowing at the same rate as that of sample stream. The mixed stream is then passed through a quartz coil, which is wound on a miniature UV lamp tube. The UV light facilitates the digestion of the sample and assists in the dissolution of metals with the help of nitric acid. This digested sample is then aspirated/pumped directly into the analyzer, presently an inductively coupled plasma mass spectrometer. Preliminary experiments indicate the presence of about 26 metals detectable in the atmospheric aerosol samples in Arlington, TX. These include Beryllium, Sodium, Aluminum, Potassium, Calcium, Titanium, Vanadium, Chromium, Manganese, Cobalt, Nickel, Copper, Zinc, Gallium, Rubidium, Zirconium, Niobium, Molybdenum, Silver, Cadmium, Cesium, Tantalum, Tungsten, Thallium, Lead and Uranium. Further experiments have to be

carried out in future to completely understand the roles of nitric acid and UV lamp in the digestion process. Additionally a method validation experiment has to be performed using a certified standard reference material of particulate matter. When the digestion parameters have been optimized and method has been validated, then ICPMS detector could be replaced by capillary ion chromatography system with components discussed in chapters 2-4 of this dissertation.

Preliminary experiments have been carried out for the separation of metal ions using LED-based, capillary scale multi-reflection absorbance detector and commercially available nano-Tee mixer. Results indicated that the multi-reflection absorbance detector constructed with 0.18 mm i.d. fused silica capillary resulted in excessive band broadening and the resultant chromatogram had poor efficiency. Further research work is needed to decrease the volume of the multi-reflection absorbance detector. The design of the new multi-reflection absorbance detector could be identical to the detector mentioned in Chapter 2, except for a much lower bore fused silica capillary.

The electrodialytic reagent introduction device, mentioned in Chapter 4, has an internal volume of 0.3 µL. Depending on the results of preliminary chromatography experiments, its volume need to be further lowered in the future. This can be performed by fabricating the central channel in the disc to be narrower than current width of 0.5 mm. with a channel width of $\leq$ 0.1 mm, the internal volume of the electrodialytic reagent introduction device could be reduced proportionally. This modification will greatly improve the efficiency of the observed separation and will ultimately lead to better measurement of metal ions.

APPENDIX A

CAPILLARY SCALE LIGHT EMITTING DIODE BASED MULTI-REFLECTION ABSORBANCE DETECTOR

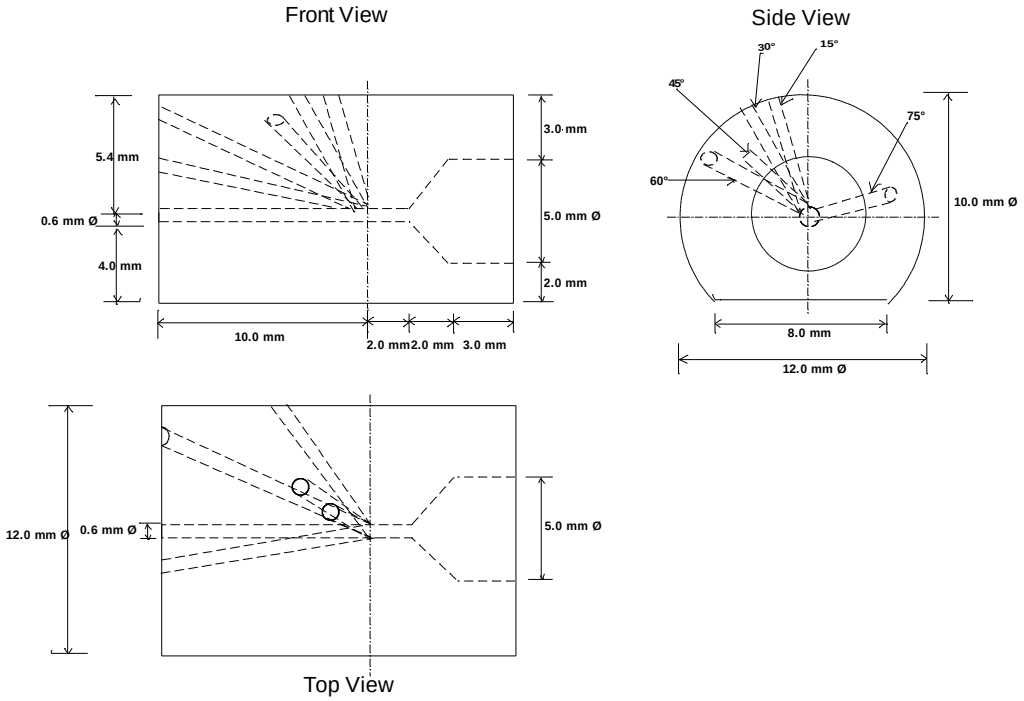

A1(a)

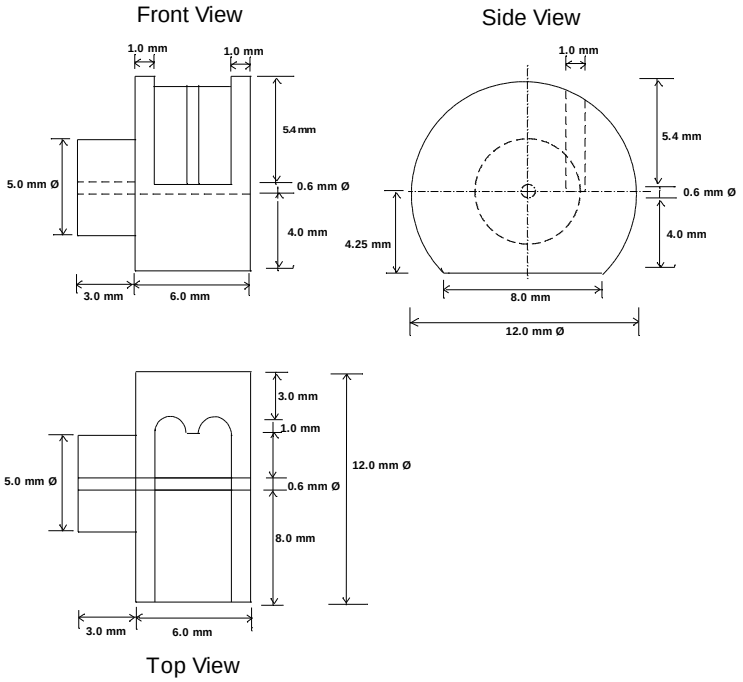

A1(b)

Figure A1: Machinist's drawing for multi-reflection capillary detector: (a) Capillary and optical fiber holder, (b) Capillary and photo-detector holder

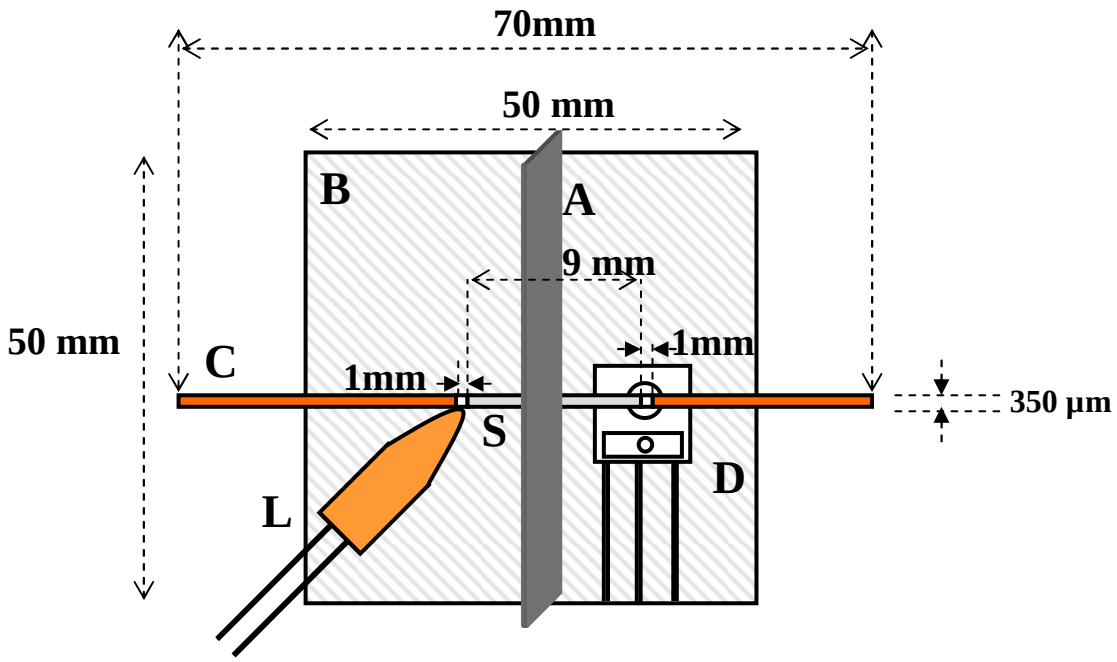

Fig A2 Multi-reflection detection cell on a breadboard. A: Aluminum foil barrier, B: Aluminum block, C: Capillary, D: Photodector, L: LED, S: Silvered portion of capillary.

Description of fixed angle fixed pathlength cell Figure A2

Figure A2 shows the schematic layout of the fixed-pathlength (dimensions below pertain to a 10-mm cell), fixed launch-angle multireflection cell. Approximately 7 cm section of the polyimide-coated fused silica capillary was taken and 11 mm of the polyimide coating was removed by hot conc. H_2SO_4 from approximately the center portion. One millimeter of the clear region at each end was covered with clear adhesive tape as a mask to allow for light entrance and exit windows and then the tube was silvered. The entire window and silvered region was then painted with a thin coating of epoxy adhesive for both mechanical and chemical protection.

Much of the epoxy molding of the same type of LED as described in the main text was removed to result in a tip approximately 0.5 mm in diameter. The tip was re-polished to ensure good light throughput. The capillary was taped to a styrofoam block with the edge of the block placed midway through the silvered region. The LED tip was now glued to the entrance window of the capillary resting on the block with optical grade epoxy adhesive at the desired angle (we generally used 45°with respect to the cylindrical axis of the capillary). A 2.5 cm square piece of Al foil was taken and a hole made in the center of the foil using a piece of capillary as a drilling tool. This foil was then slipped on to the free end of the detection cell capillary resting on the styrofoam block to serve as a partition to prevent scattered light from the LED source reaching the detector. A second styrofoam block was then placed under the free end of the capillary. At the light exit window, a TSL250R sensor, which contains a 1.5 mm dia. hemispherical lens over the 1.1 mm dia. Photodetector, is slipped under the light exit region of the capillary and affixed there with epoxy adhesive. The cell assembly was then put in a light tight enclosure.

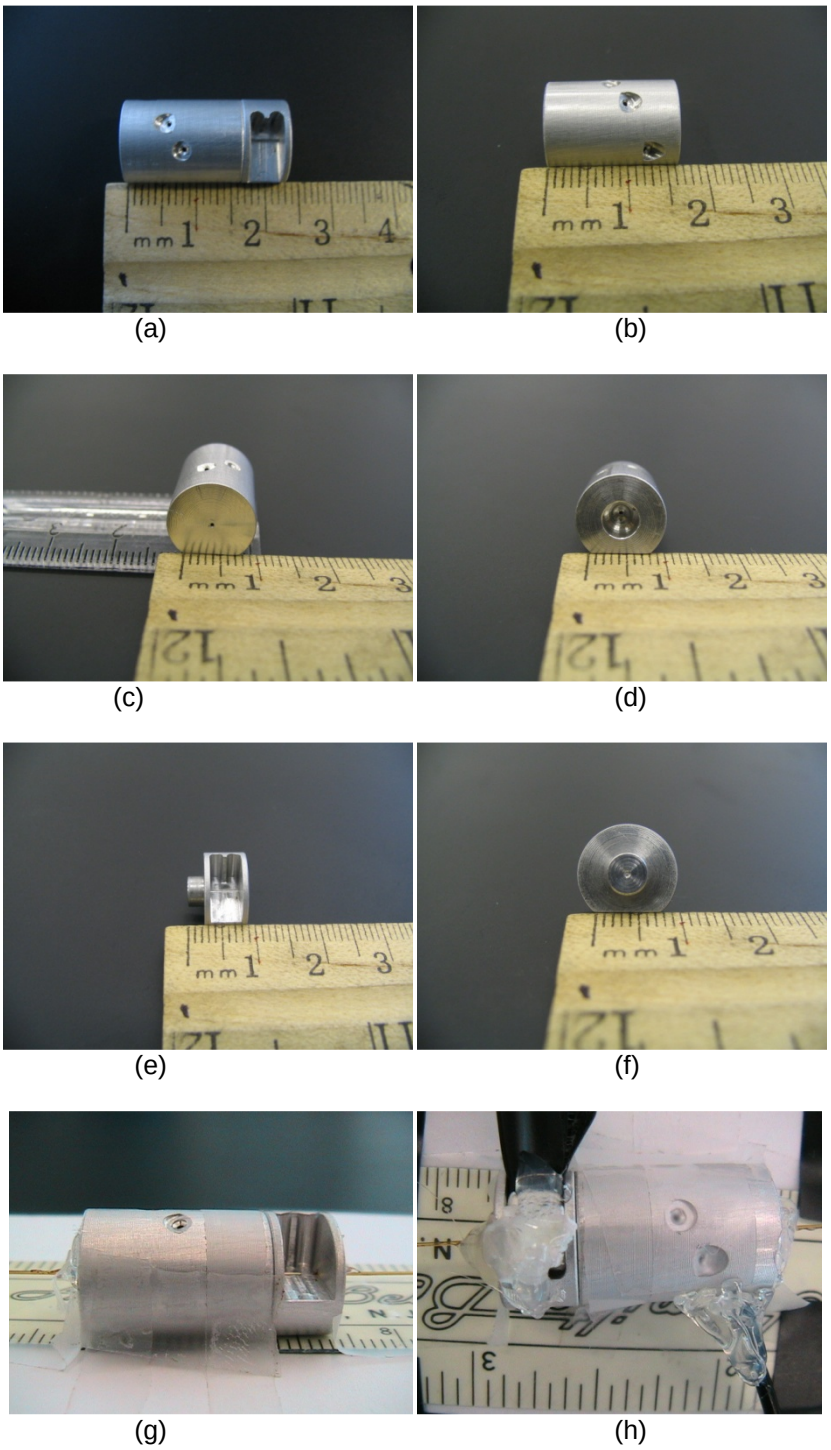

Figure A3 Photographic details of the multi-reflection capillary cell holder. (a) Part A & Part B combined, (b) Part A (front view), (c) Part A (side view), (d) Part A (side view), (e) Part B (front view), (f) Part B (side view), (g) Part A + Part B + Capillary cell, (h) Part A + Part B + Capillary cell + PD + Optical fiber

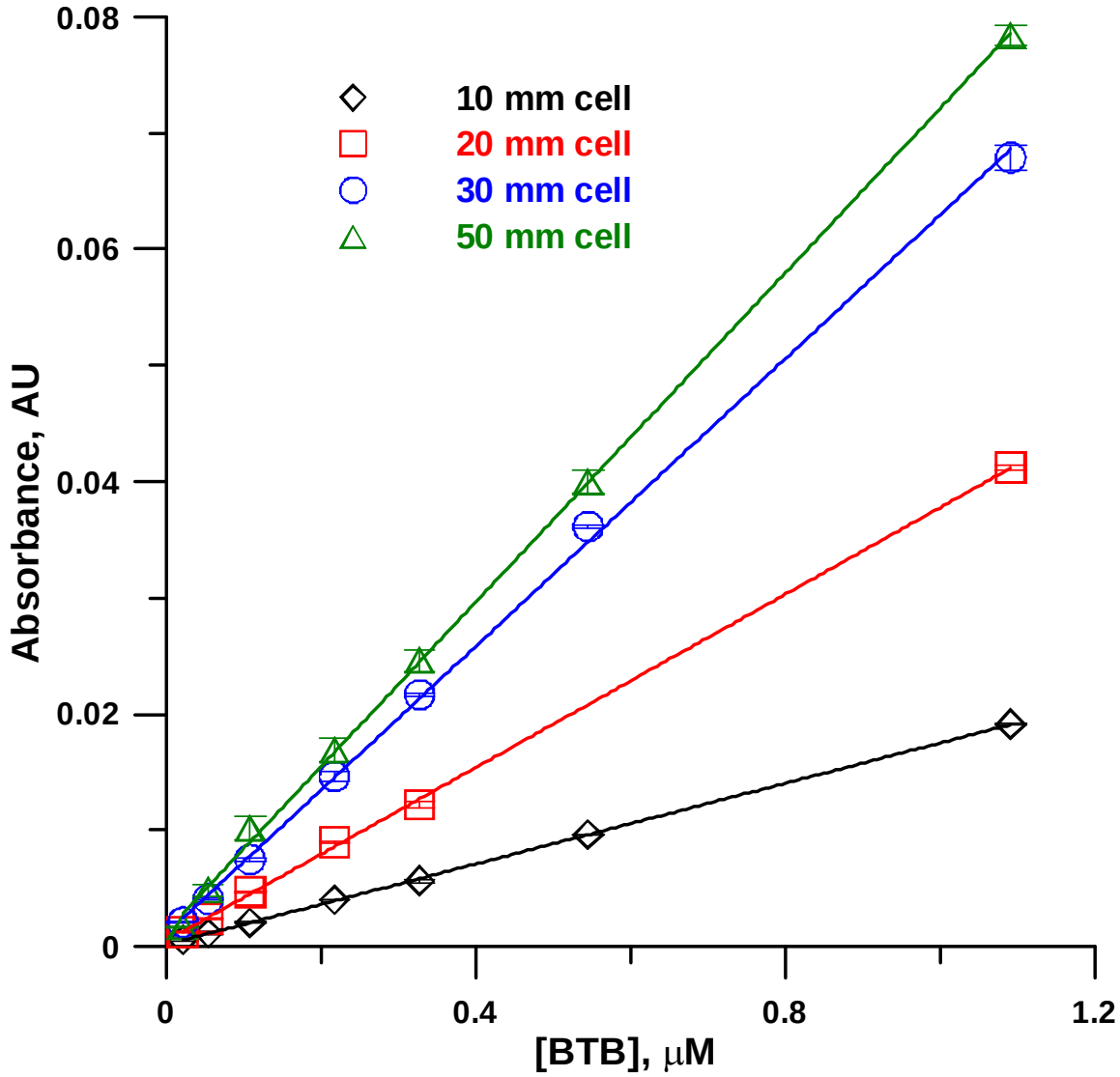

Figure A4 Length dependence study.

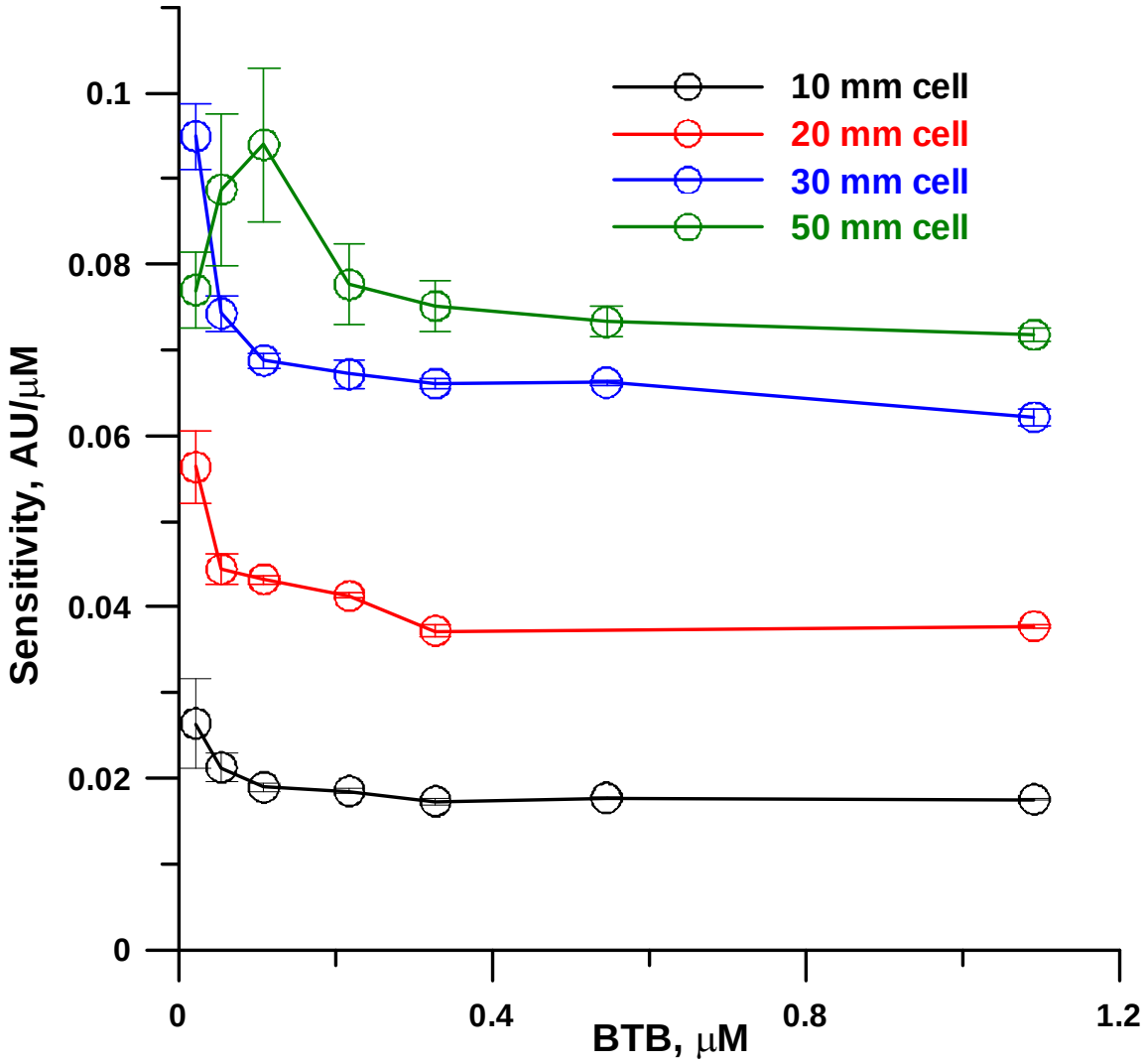

Figure A5 Length dependence study (Cassidy plot).

APPENDIX B

CAPILLARY SCALE LIQUID CORE WAVEGUIDE BASED FLUORESCENCE DETECTORS FOR LIQUID CHROMATOGRAPHY AND FLOW ANALYSIS

B1. LED-photodiode detector design

B1.1 Construction

The detector was based on light-to-voltage optical sensor (TSL250R, www.taosinc.com) and utilized Teflon® AF coated silica capillary (TSU100375, www.polymicro.com, the LCW capillary) for the flow through cell. Figure B1 shows the cross-sectional schematic diagram of TSL250R based LCW fluorescence detector. Two orthogonal holes were drilled on the hemispherical epoxy lens of TSL250R optical sensor with miniature drill bits of sizes 0.014 in. (or 368μm) and 1/32 in (or 787 μm). The holes drilled were initially rough which were smoothened with very fine coat of commercial grade epoxy. The 508 μm hole was drilled perpendicular to the body to fit a thin PEEK sleeve (F-385X, www.upchurch.com) which could incorporate the TSU100375 capillary, while the 368 μm hole was drilled parallel to the body so as to fit the TSP180350 capillary. The TSU and the TSP capillaries were in close contact to each other in 'L-shape' so that the solution flowing in through the TSU capillary could exit through TSP capillary.

The fluorescence detector set up was then covered with black epoxy resin (1:1 mixture of epoxy resin and activated charcoal) so as to exclude ambient and stray excitation light. The output of the TSL optical sensor was connected to a two-stage FET-input amplifier (TL082CP, www.ti.com) which was provided a two-stage gain of 200. The TSU capillary was pushed inside the TSL250R optical sensor so as that the tip could be brought closest to the photodiode active area. A 365 nm LED (NSHU550B, www.nichia.com) was used to illuminate the LCW capillary. The LED was serially connected with a 100 Ω resistor and was powered by 5 V, this resulted in a current of 15 mA. A 5 x 5 mm area was machined 2 mm deep at the center of one face of a 30 mm Black Delrin cube. A 1/32 in. hole was drilled straight through the centre of the machined area to the opposite side so as to allow the passage of the LCW capillary along with its protective PEEK sleeve. Also, at a distance of approximately 12 mm from the bottom, a ¼-28 threaded aperture was made perpendicular to the vertical passage to accommodate the LED and a ¼-28" threaded male nut held the LED in place.

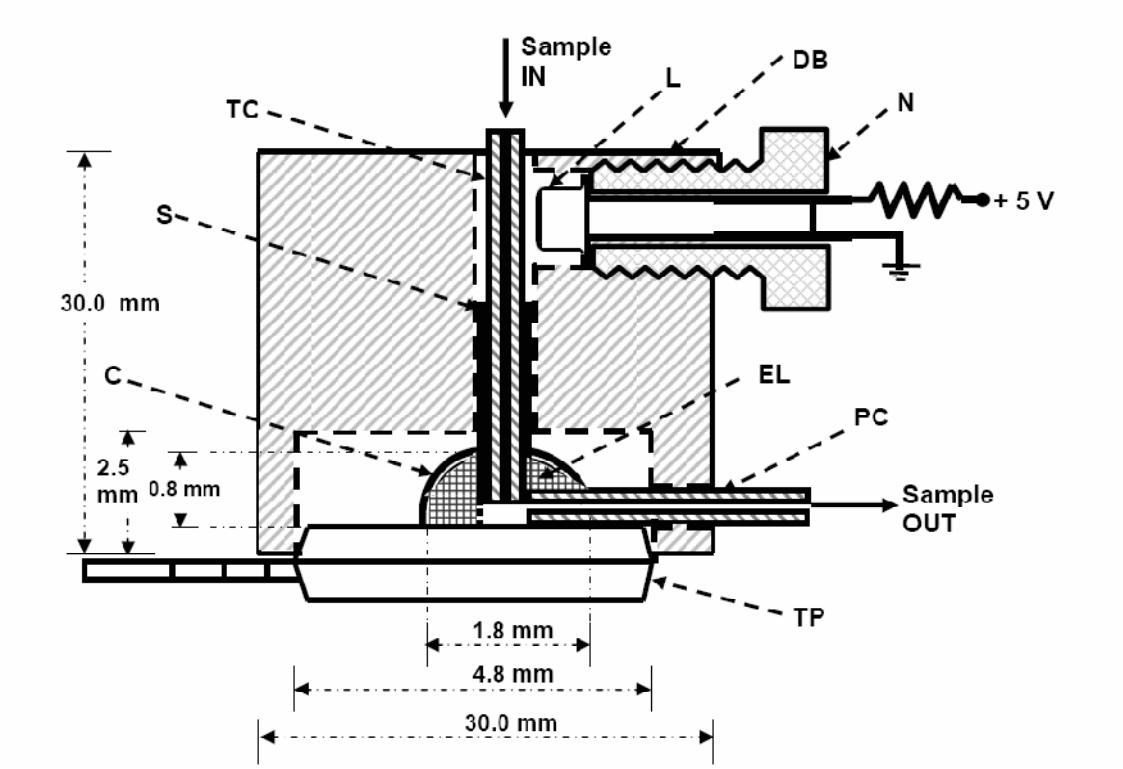

Figure B1 Schematic cross-sectional view (not to scale) of LCW fluorescence dxetector: TP, TSL250R light-to-voltage optical sensor; PC, polyimide coated TSP180350 fused silica capillary; EL, hemispherical epoxy lens of TSL250R; N, ¼-28” male nut; DB, Delrin cube (30mm x 30mm x 30mm); L, 365 nm LED (NSHU550B); TC, Teflon AF coated TSU100375 fused silica capillary; S, black plastic sleeve tubing; C, coating of epoxy-charcoal mixture on the hemispherical lens of TSL250R.

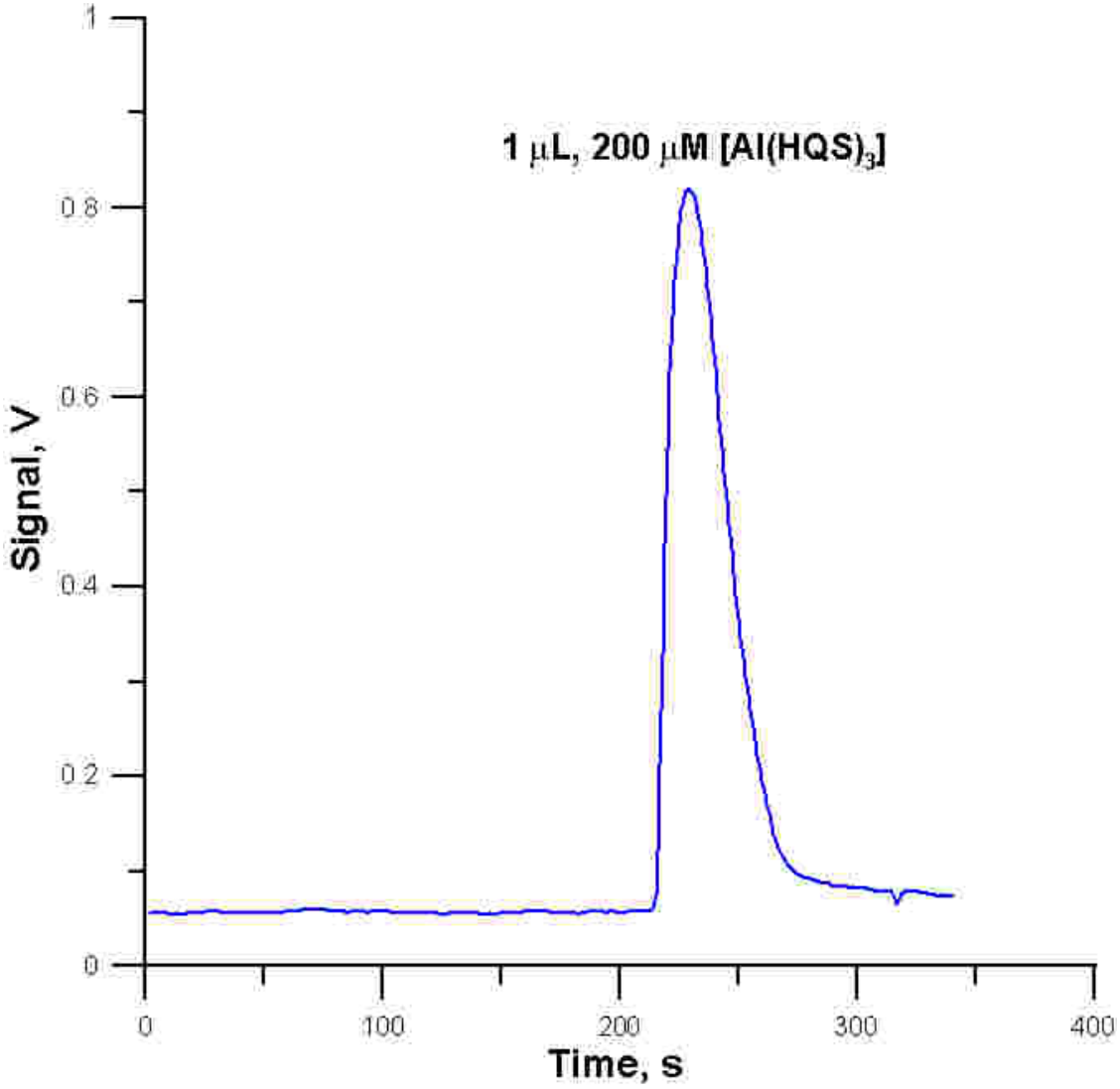

Figure B2 Response of the LED-PD detection system for 1 μL of injected 200 μM Al^{3+}. The S/N is 350.

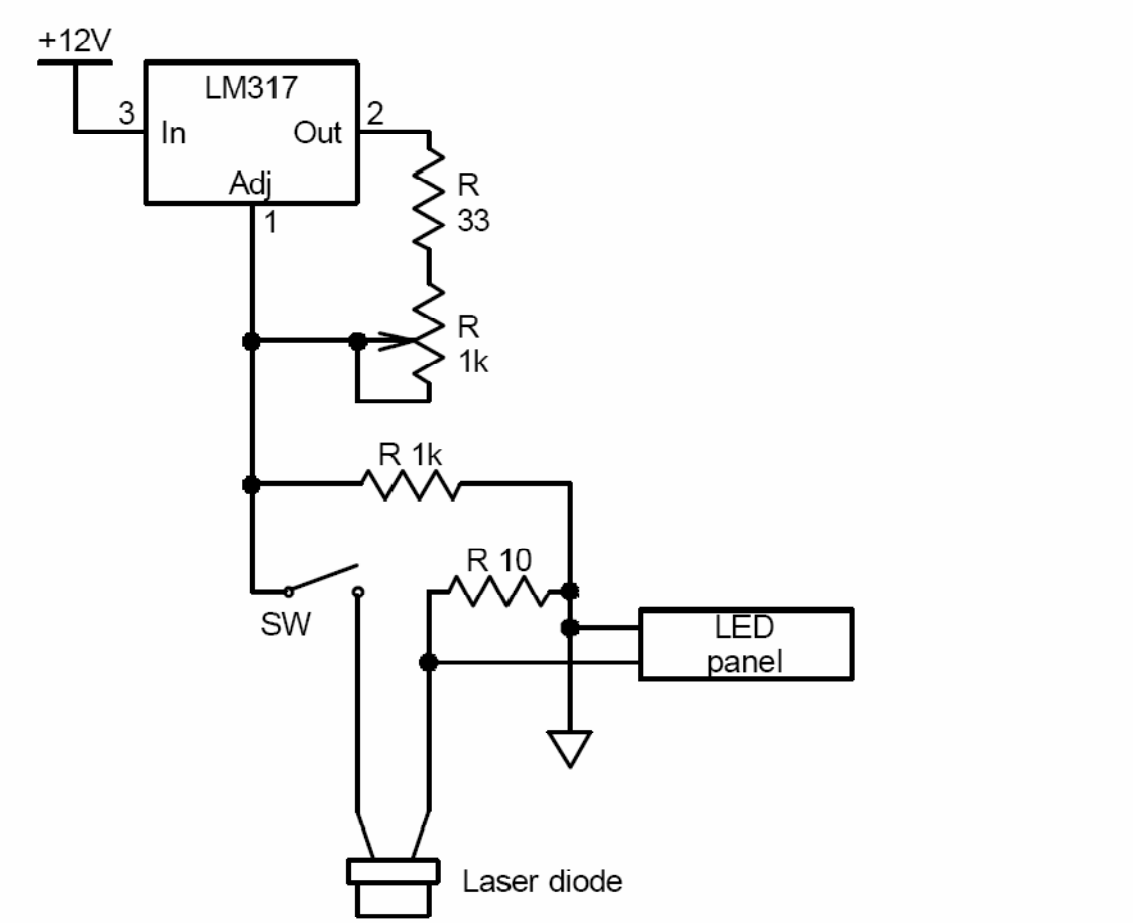

Figure B3 LM317 based circuit to power the LD. Power is initially applied to the circuit with SW open and the 1 K potentiometer adjusted to produce the minimum voltage output. The switch SW is then closed. The current flowing through the LD is measured by measuring the voltage across the 10 Ω serial resistor. The 1K potentiometer is adjusted until the desired LD drive current level is reached.

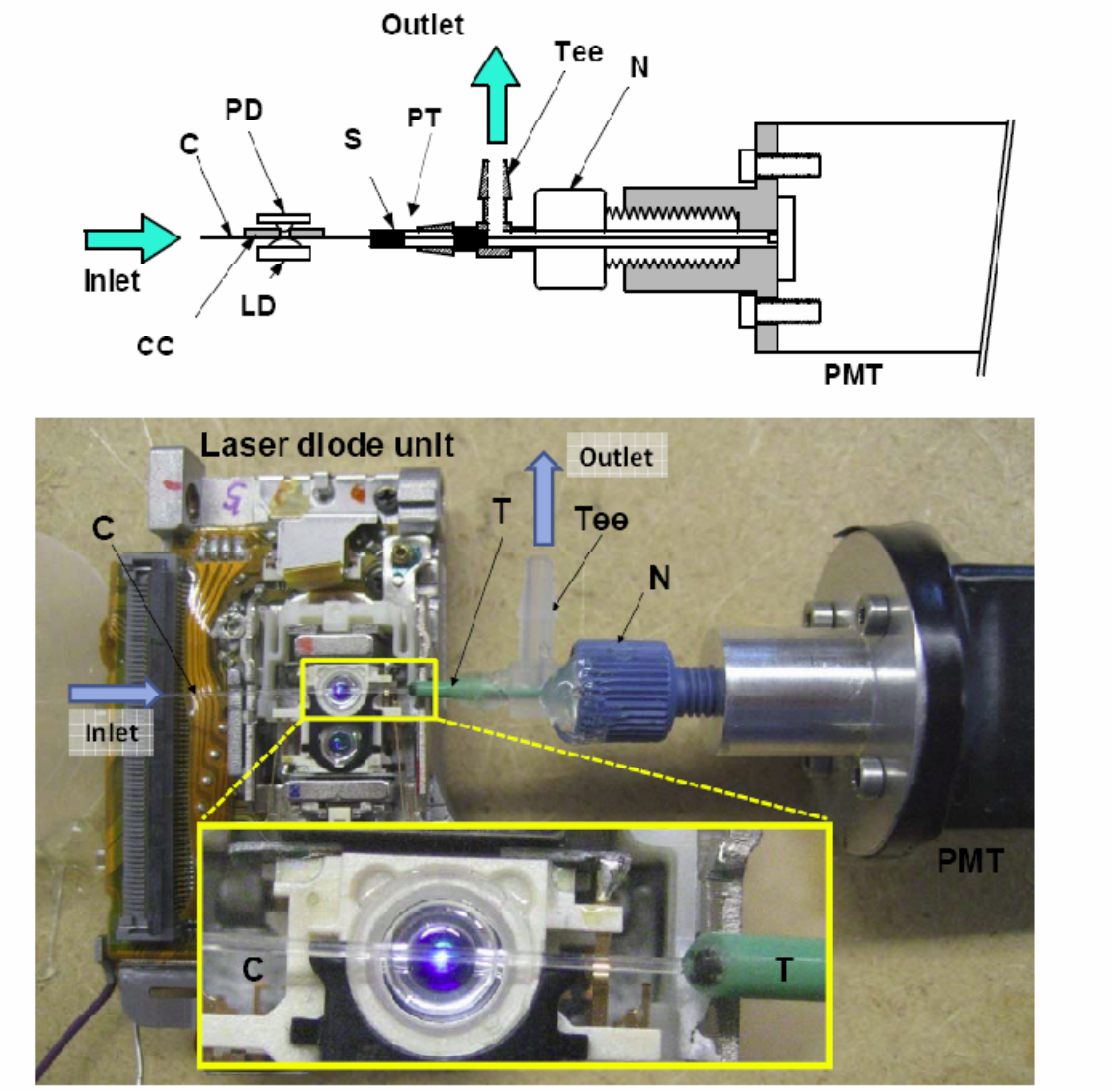

Figure B4 LD-mPMT detector shown without the capillary cradle in place. C: LCW capillary; CC: Capillary Cradle, PD:Photodiode TSL252. The LCW rests on the Laser diode LD, held in place by the capillary cradle (not shown in the photo. The capillary goes into a 0.75 mm i.d. green PEEK tubing PT via a large tee. For details at the PMT end see Figure 1 in main text. The space where capillary C enters PT is sealed with the help of an inner sleep tubing and adhesive (see Figure 1).

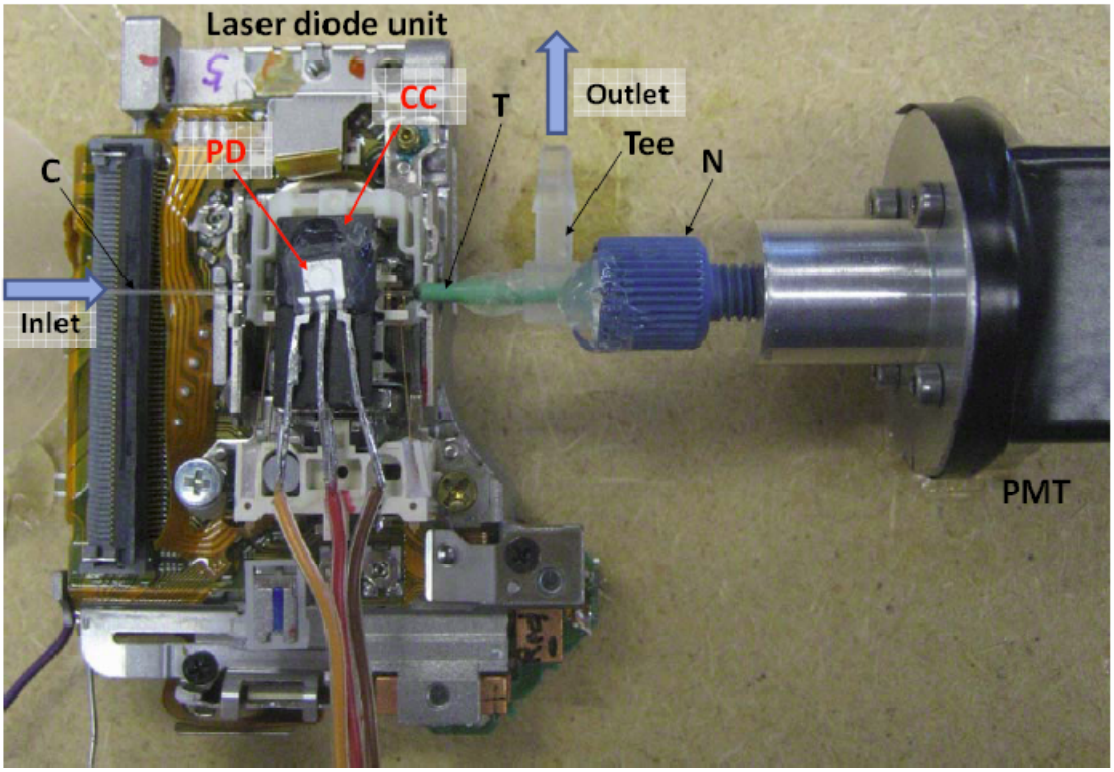

Figure B5 Arrangement shown with the capillary cradle and photodiode detector for transmitted light in place.

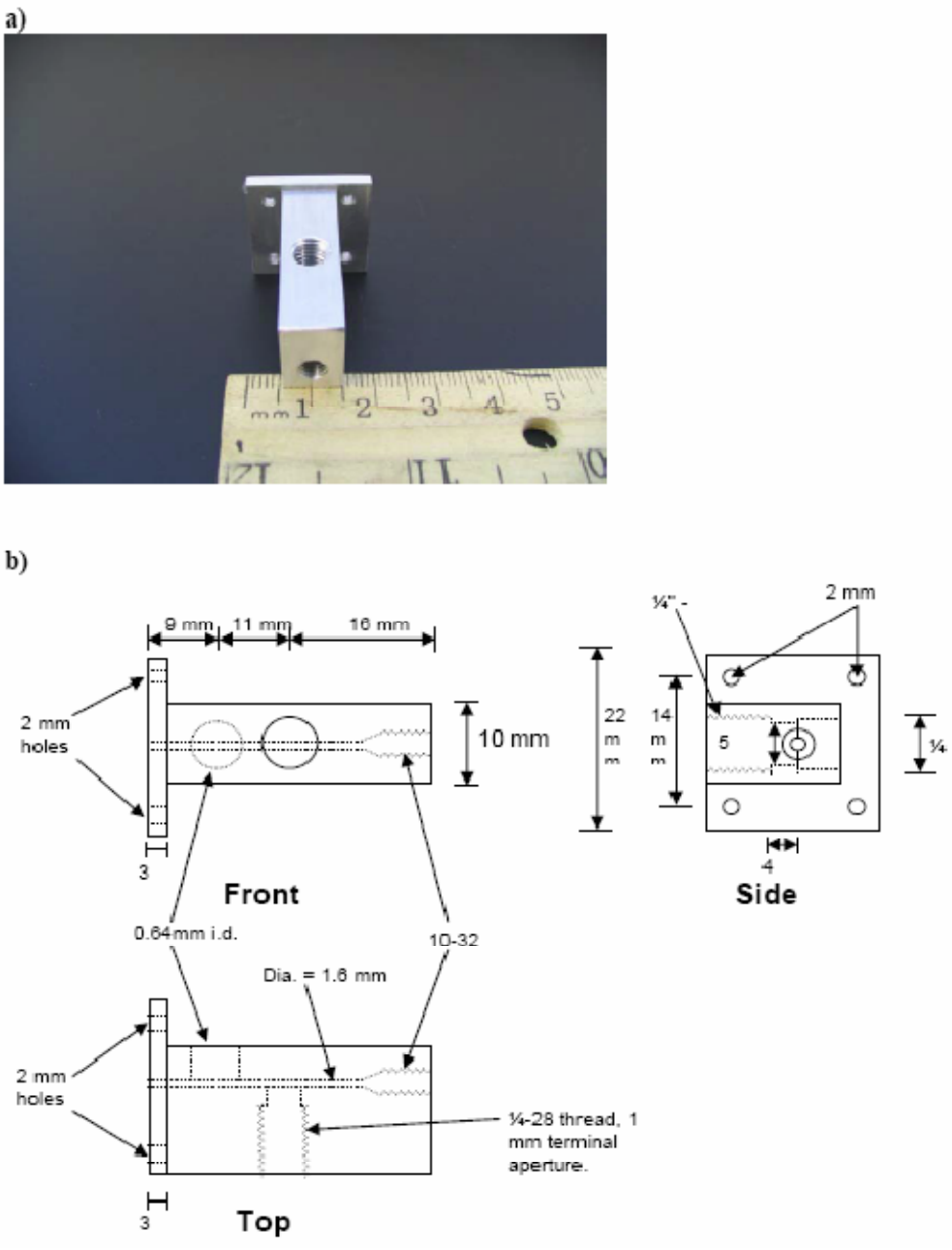

Figure B6 (a) Capillary detection cell holder, photographically shown; (b) Schematic representation

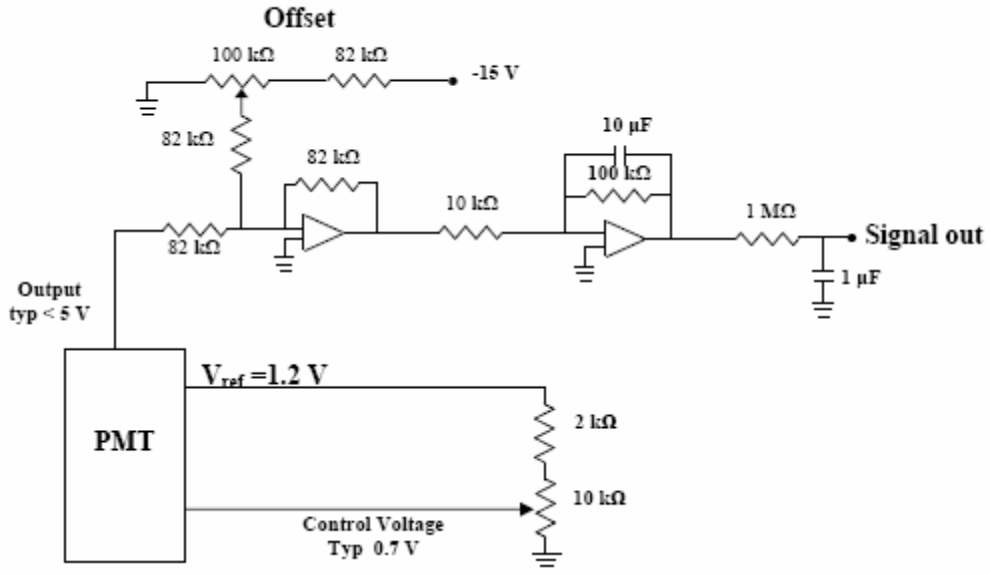

Figure B7 mPMT signal processing schematic for HPLED experiments.

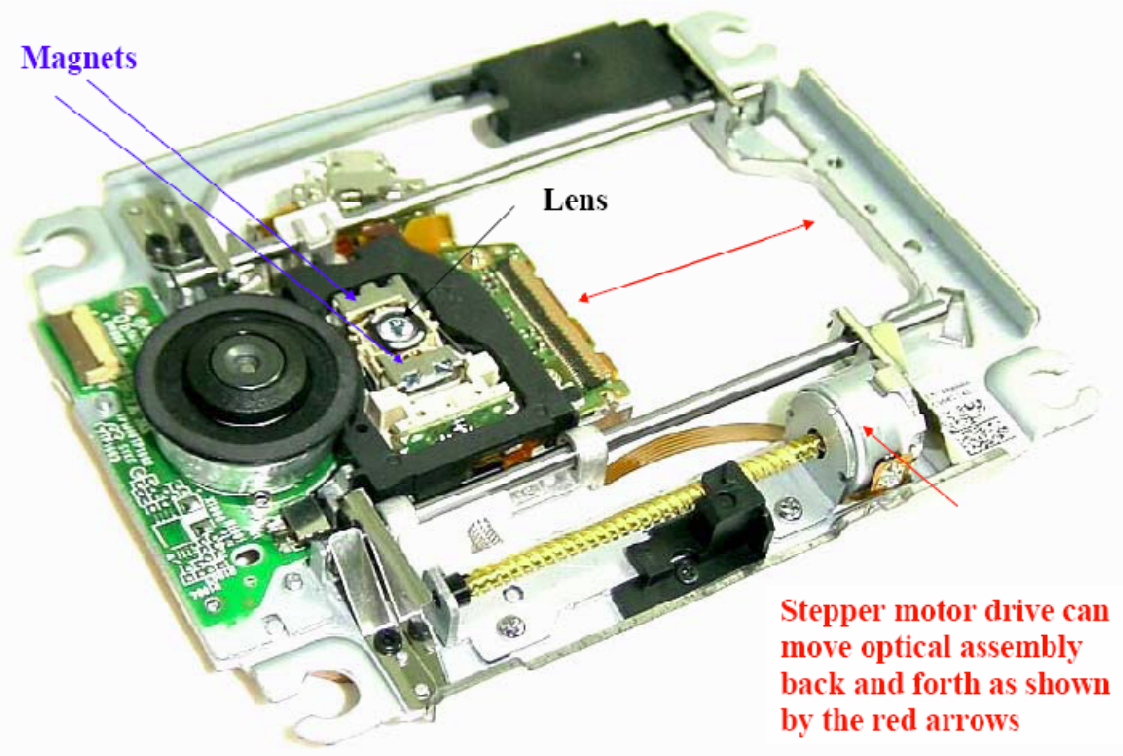

Figure B8 SONY playstation 3 PS3 KES-400AAA reader assembly. The laser source is on the bottom portion of the movable reader assembly, with readily accessible 5 pins for ground, + power inputs for violet, infrared, red lasers and photodiode output.

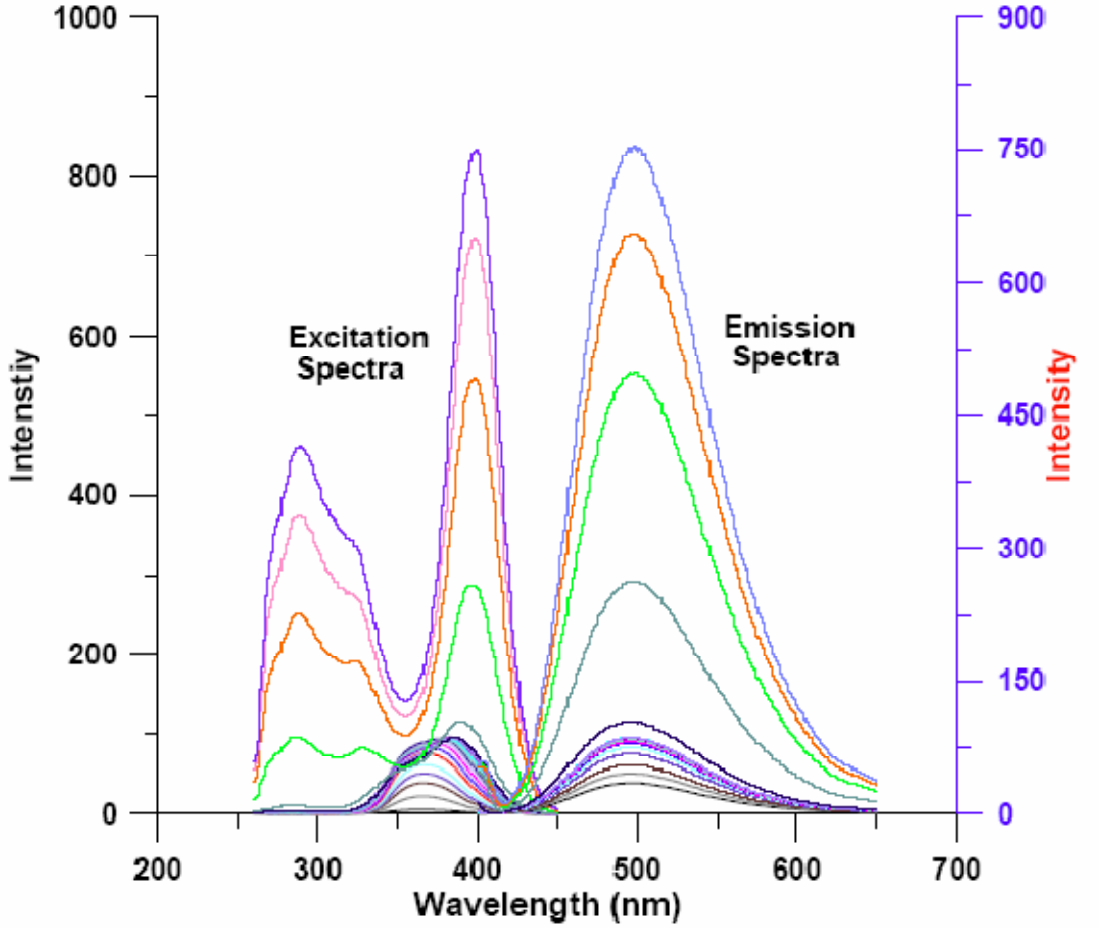

Figure B9 Excitation and emission spectra obtained on a Shimadzu RF 540 spectrofluorometer. Experimental conditions: Scanning Speed: Fast, Response time 0.1 s, Sampling interval 1.0 nm, Excitation and Emission Slit Widths 10 nm, Sensivity low, pH 6, Total [HQS] = 1 mM; Al concentration: 5, 10, 15, 20, 30, 40, 50, 60, 70, 80, 90, 100, 110, 120, 200, 400, 600, 800 and 1000 μM.

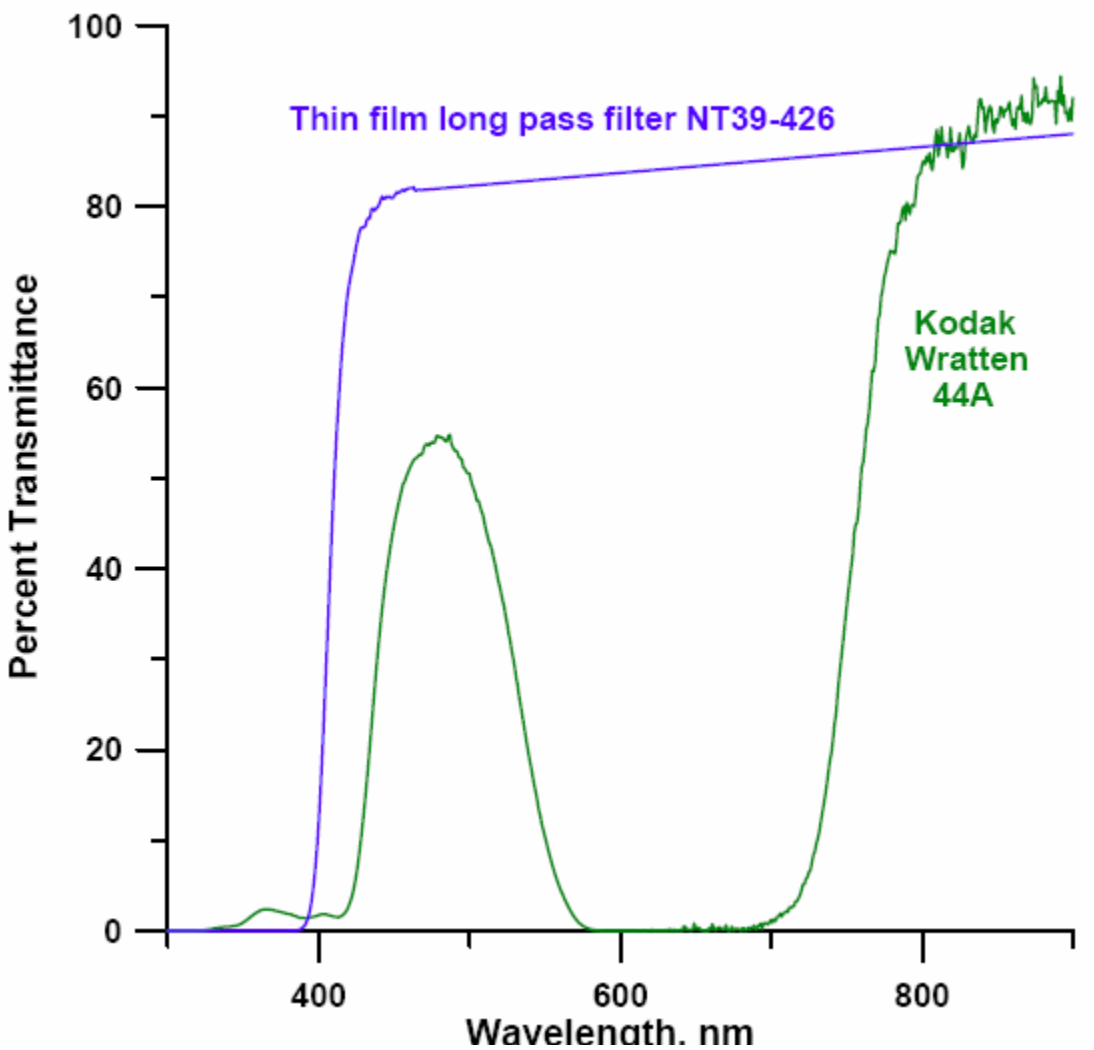

Figure B10 Transmittance spectra of other emission filters examined.

APPENDIX C

ELECTRODIALYTIC REAGENT INTRODUCTION IN FLOW SYSTEMS

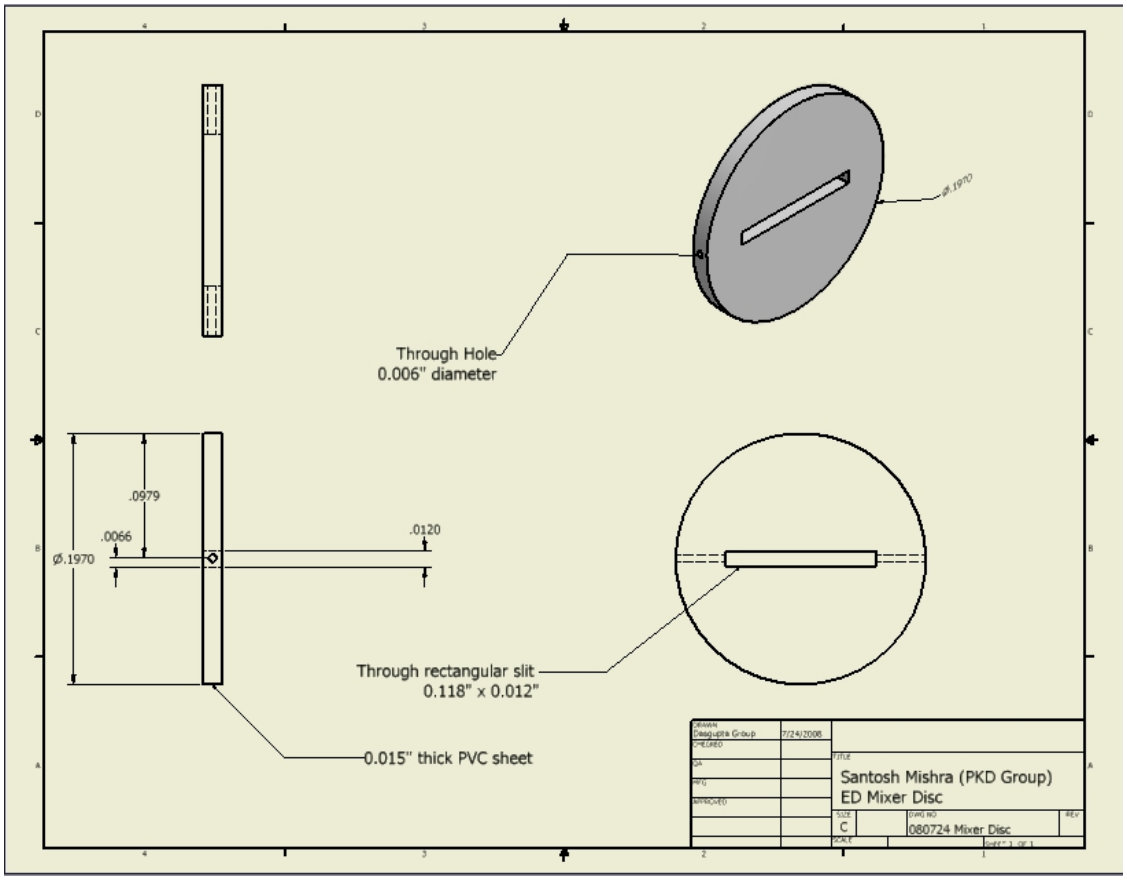

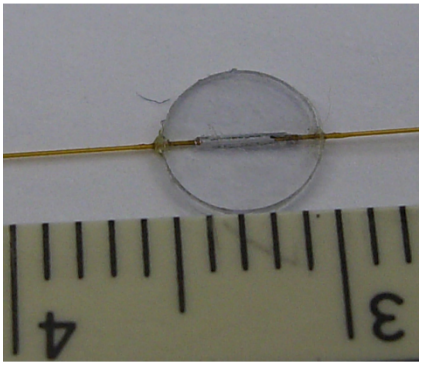

Figure C1 Machine diagram and photograph of polyvinylchloride disc spacer (0.38 mm thick, 5.0 mm diameter) having 3.0 mm x 0.30 mm hollow rectangular through section (total active surface area is 0.9 mm^2/membrane and total volume of rectangular through section is 0.34 µL).

Dialysis membrane functionalization

Note: All the containers were thoroughly cleaned before use.

1. The dialysis membrane tubing (2.3 cm diameter, 5 cm length) was immersed in milli-Q water so that the tubing could be opened easily. The edges were cut in order to achieve two single layers of dialysis membrane (2.0 cm x 5 cm). The wet membranes were then hung up in a closed wide mouth bottle in an inert atmosphere of Nitrogen gas and dried. (The cap of the wide mouth bottle was equipped with four holes. Two holes were used for the inlet and the outlet of the N2 gas while the remaining two holes were used for inserting a wire which could hold on to the dialysis membrane with the help of a U-pin paper clip. The bottle was placed in Shimadzu GC heater).

2. Polymer solution was prepared by mixing Glycidyl methacrylate (75% v/v) and Ethyleneglycol dimethacrylate (25% v/v) by purging N2 gas. Then 2,2'-Azobis-isobutyronitrile initiator (12 mg) was put into the solution and N2, purging was continued until the mixture turned clear from turbid.

3. The previously dried membrane is rinsed with the polymer solution rapidly by spraying the polymer solution on the hanging dialysis membranes.

4. After spraying the polymer solution, the cap is placed on the bottle and N2 gas is purged for 3 minutes so as to remove the air efficiently.

5. The membrane with the polymer coat was then heated at 60º C for 24 hours under inert atmosphere.

6. After 24 hours, the polymerized membrane (dialysis membrane with GMA-EDMA polymer backbone) was then taken out of the wide mouth bottle and functionalized by treating it with 50% (v/v) N-methyldiethanolamine at 75º C for 12 hours.

7. Finally, the membrane was washed with water and dried.

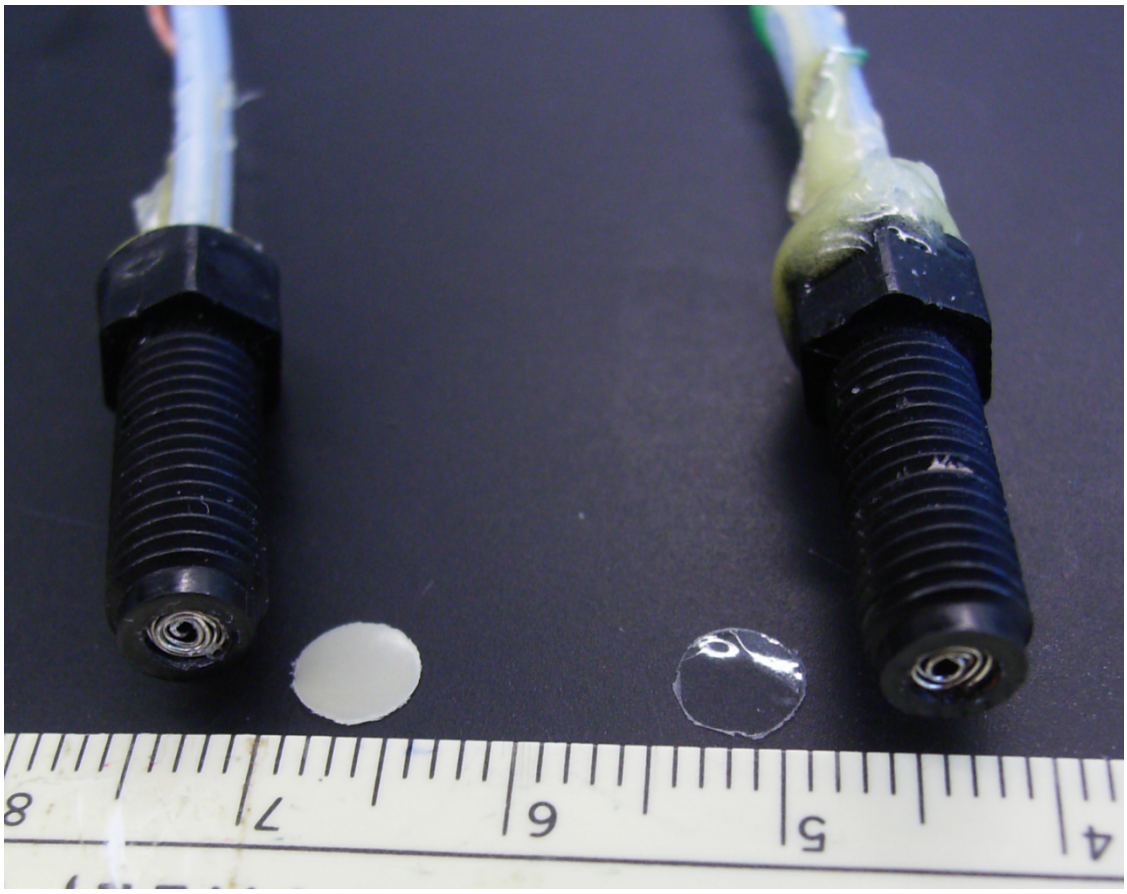

Figure C2 Platinum wire electrodes, made with 250 µm diameter platinum wires, closely coiled (in a plane) so that it could fit in the bore of ¼-28 nut.

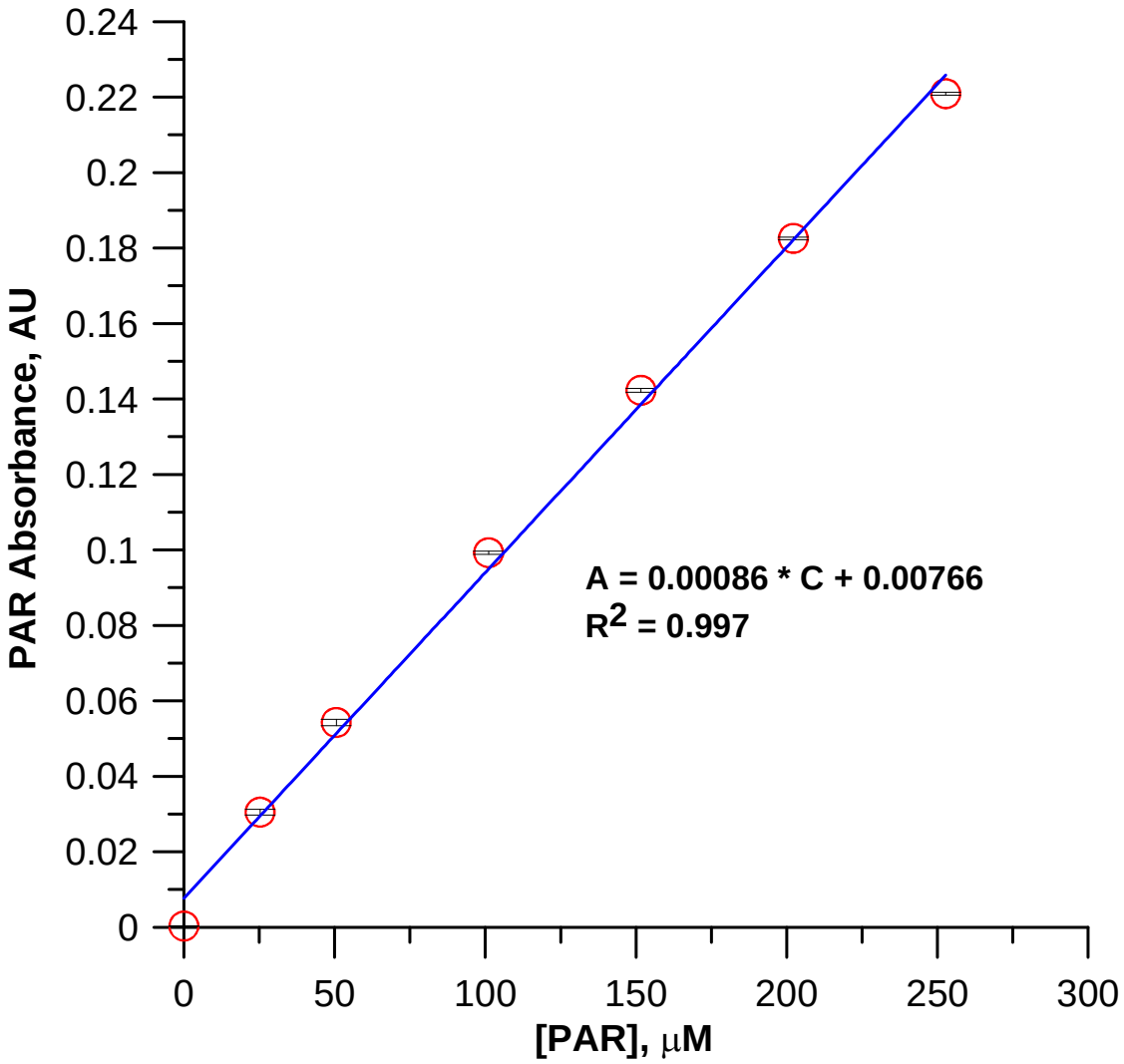

Figure C3 PAR concentration vs. absorbance relationship for the LED-multireflection detector used.

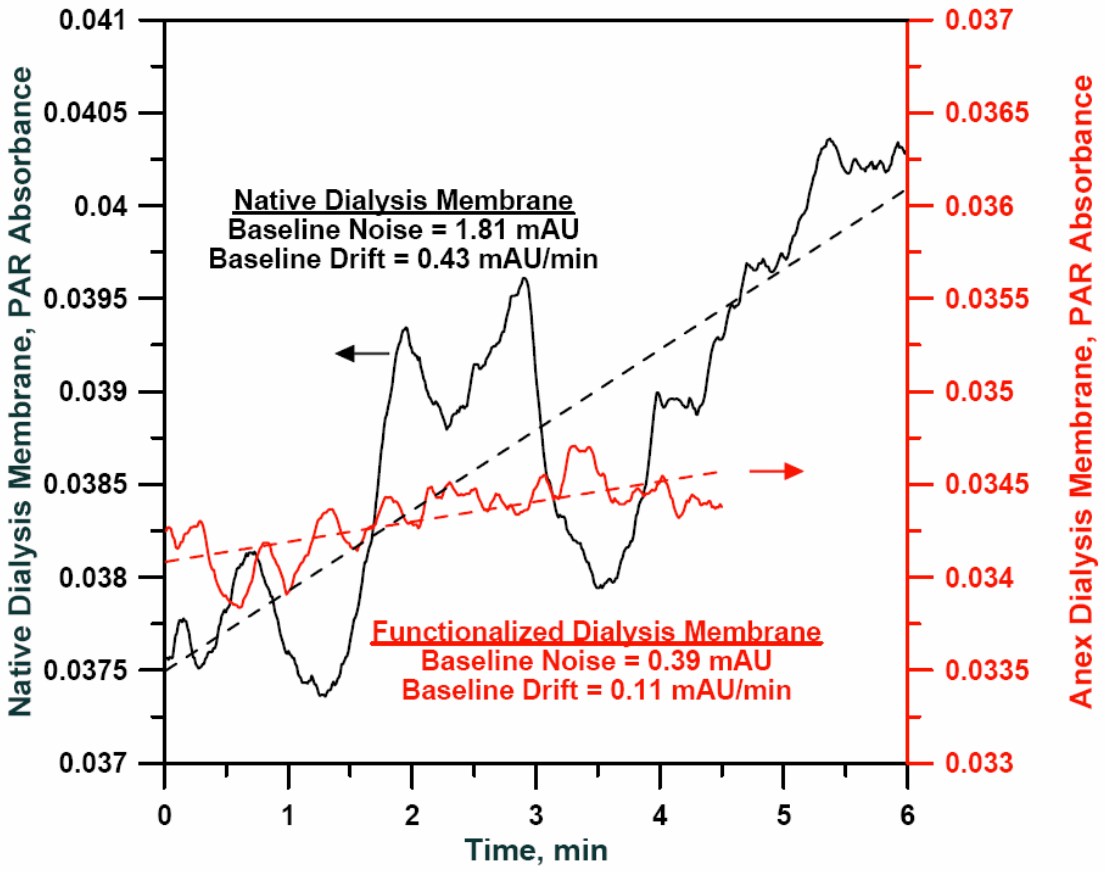

Figure C4 Comparison of baseline drift and noise in electrodialytic generation of PAR with both native and anion exchange-functionalized dialysis membrane with approximately the same level of PAR introduced.

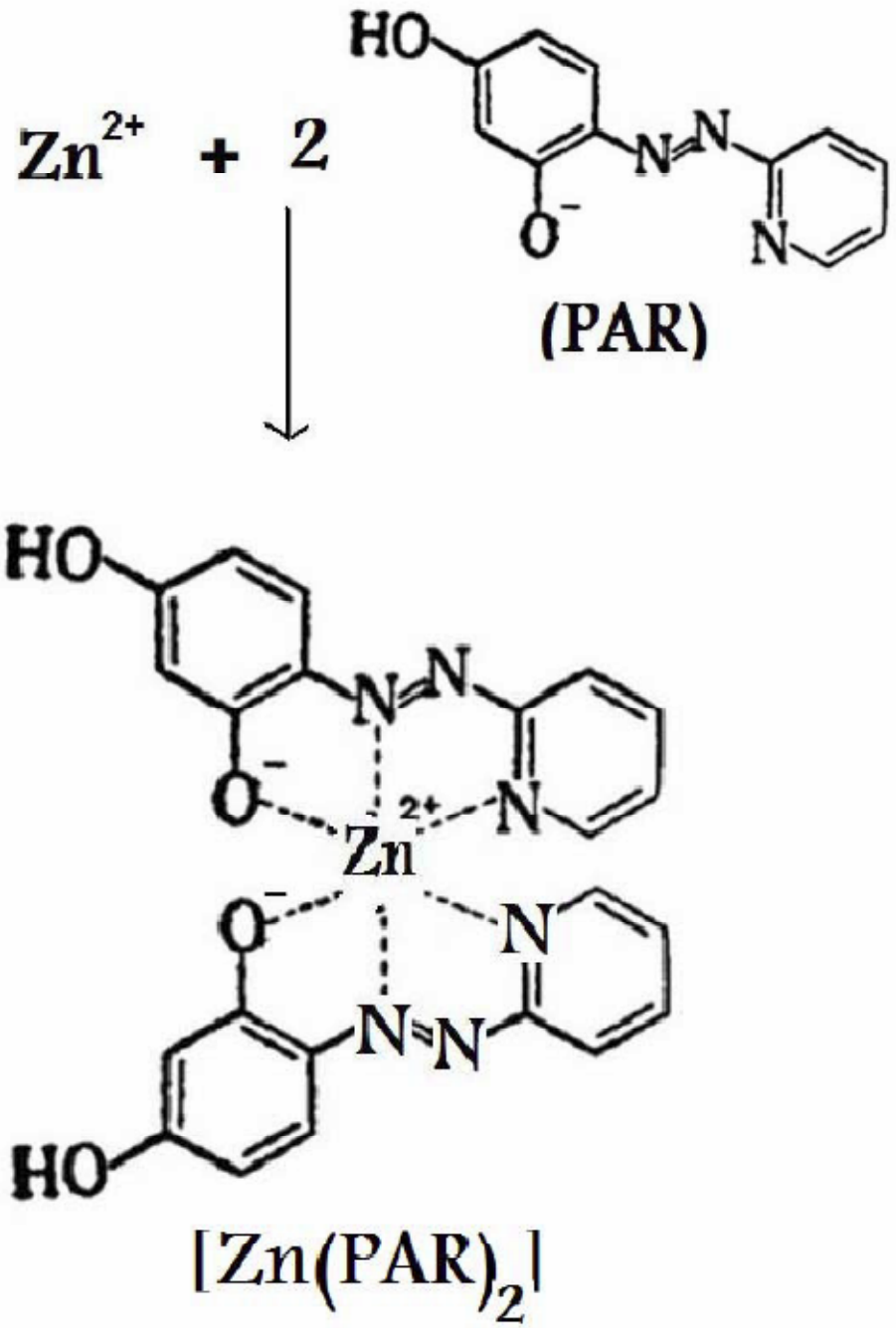

Figure C5 The reaction between Zn^{2+} and PAR.

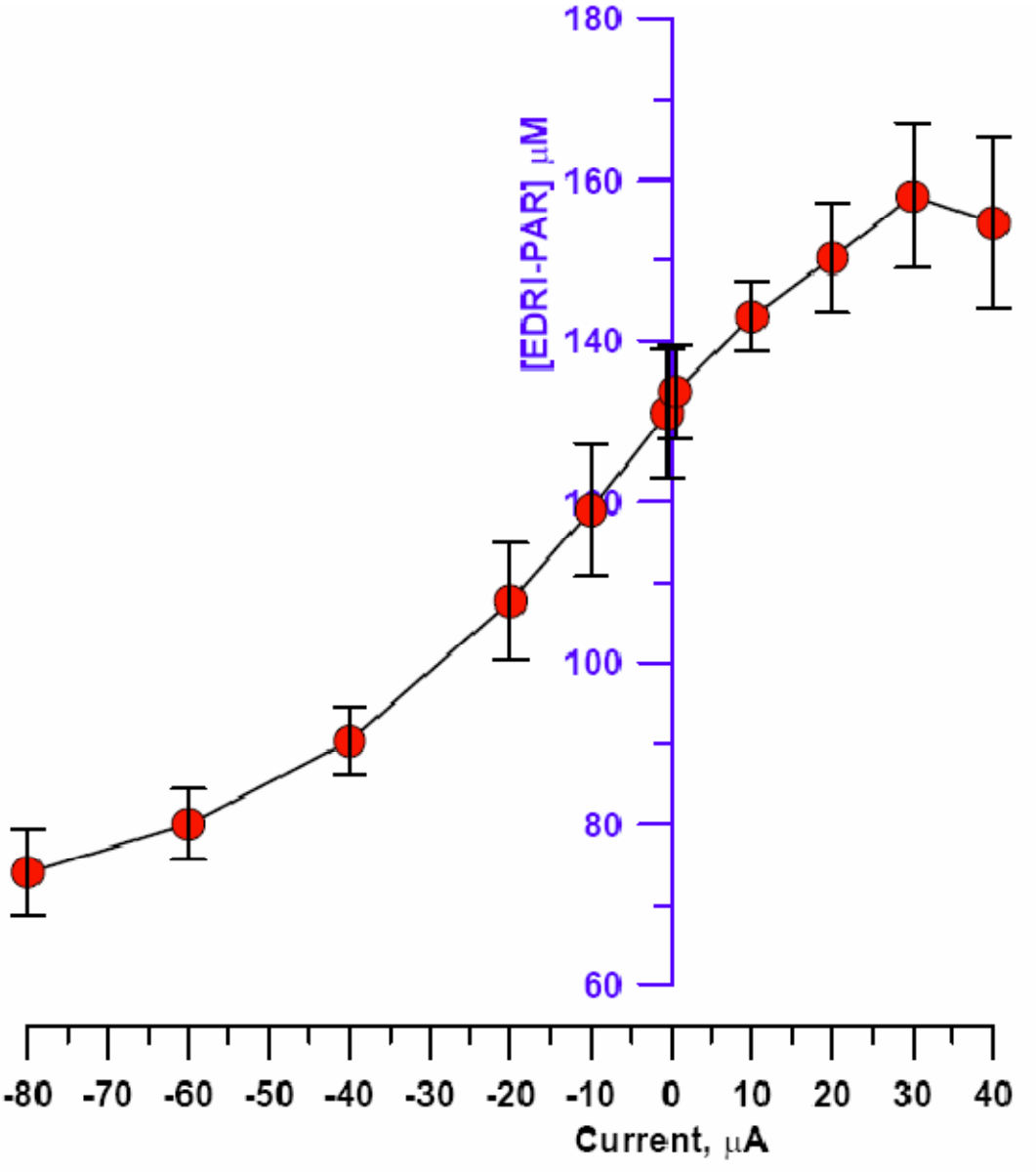

Figure C6 Day-to-day variation in the generation of PAR (for 3 days) under the same experimental conditions (7 mM PAR feed solution). The full range of the experiment was repeated for three successive days, making fresh PAR feed solution each day. The error bar represents ±1 standard deviation for the entire three-day data set.

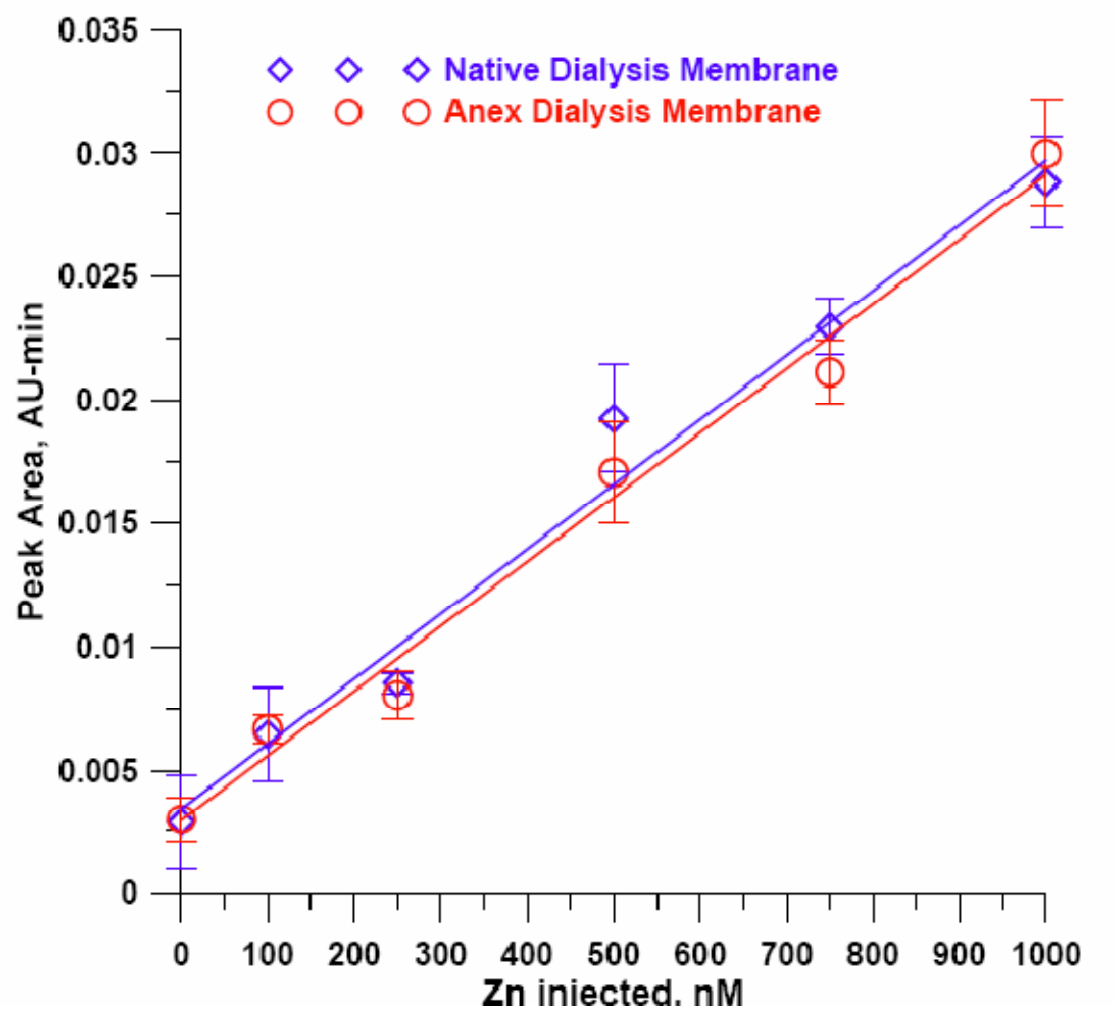

Figure C7 Analyte loss comparison study for non-functionalized and functionalized dialysis membrane in cEDRI.

REFERENCES

1. Hinds, W.C. *Aerosol Technology*, 2nd Edition, Wiley-Interscience, 1982; pp 1-9
2. Pandis, S.N.; Seinfeld H.J. *Atmospheric Chemistry and Physics,* Wiley-Interscience, 2006; pp 350
3. Dasgupta, P.K.; Poruthoor, S.K. *Comprehensive Analytical Chemistry* XXXVII, Ed. J Pawliszyn, 2002 Elsevier Science
4. Pandis, S.N.; Seinfeld H.J. *Atmospheric Chemistry and Physics,* 2nd Edition Wiley-Interscience, 2006; pp 381-385
5. Hinds, W.C. *Aerosol Technology*, 2nd Edition, Wiley-Interscience, 1982; pp 49-51
6. Colbeck. I. *Environmental Chemistry of Aerosols,* Blackwell Publishing, 2008, pp1
7. Nazaroff, W.W.; Singer, B.C. Inhalation of hazardous air pollutants from environmental tobacco smoke in US residences. *Journal of Exposure Analysis and Environmental Epidemiology*, **2004**, 14, S71–S77
8. Analysis and Environmental Epidemiology (2004) 14, S71–S77 Humbert, S. Marshall, J. D. Shaked, S. Spadaro, J. V Nishioka, Y. Preiss, P. McKone, T. E. Horvath, A. Jolliet, O. Intake Fraction for Particulate Matter: Recommendations for Life Cycle Impact Assessment. *Environmental Science & Technology* **2011**, *45*. 4808-4816.
9. http://www.epa.gov/air/particlepollution/
10. Valavanidis, A.; Fiotakis, K.; Vlachogianni, T. Airborne Particulate Matter and Human Health: Toxicological Assessment and Importance of Size and Composition of Particles for Oxidative Damage and Carcinogenic Mechanisms. *Journal of Environmental Science and Health* **2008**, 26, 339-362.

11. Cheng, M. T.; Chou, W. C.; Chio, C. P.; Hsu, S. C.; Su, Y. R. Kuo, P. H. Tsuang, B. J. Lin, S. H. C. Chou, C. K. Compositions and source apportionments of atmospheric aerosol during Asian dust storm and local pollution in central Taiwan. *Journal of Atmospheric Chemistry* **2008**, *61*, 155-173.
12. Ghio, J.; Stonehuerner, J.; Dailey, L. A.; Carter, J. D. Metals associated with both the water-soluble and insoluble fractions of an ambient air pollution particle catalyze an oxidative stress. *Inhalation Toxicology* **1999**, *11*. 37-49.
13. Ravindra, K.; Stranger, M.; Van Grieken, R. Chemical characterization and multivariate analysis of atmospheric PM2.5 particles. *Journal of Atmospheric Chemistry* **2008**, *59*. 199-218,
14. Cizmecioglu, S. C.; Muezzinoglu, A. Solubility of deposited airborne heavy metals. *Atmospheric Research* **2008**, *89*. 396-404.
15. Hu, S.; Herner, J.D.; Shafer, M.; Robertson, W.; Schauer, J.J.; Dwyer, H.; Collins, J.; Huai, T.; Ayala, A. Metals emitted from heavy-duty diesel vehicles equipped with advanced PM and NOX emission controls . *Atmospheric Environment* **2009**, 43, 2950–2959
16. Birmili, W.; Allen, A.G.; Bary, F.; Harrison, R. M. Trace metal concentrations and water solubility in size-fractionated atmospheric particles and influence of road traffic. *Environmental Science & Technology* **2006**, *40*, 1144-1153,
17. Bonetta, S.; Gianotti, V.; Gosetti, F.; Oddone, M.; Gennaro, M. C.; Carraro, E. DNA damage in A549 cells exposed to different extracts of PM2.5 from industrial, urban and highway sites. *Chemosphere* **2009**, *77*, 1030-1034,
18. Mukhtar, A.; Limbeck, A. On-line determination of water-soluble zinc in airborne particulate matter using a dynamic extraction procedure coupled to flame atomic absorption spectrometry. *Journal of Analytical Atomic Spectrometry* **2010**, *25*, 1056-1062.
19. Sangani, R. G.; Soukup, J. M.; Ghio, A. J. Metals in air pollution particles decrease

whole-blood coagulation time. *Inhalation Toxicology* **2010**, *22*, 621-626.

20. Darrow, L. A.; Klein, M.; Strickland, M. J.; Mulholland, J. A.; Tolbert, P. E. Ambient Air Pollution and Birth Weight in Full-Term Infants in Atlanta, 1994-2004. *Environmental Health Perspectives* **2011**, *119*, 731-737.
21. Roubicek, D. A. Gutierrez-Castillo, M. E. Sordo, M. Cebrian-Garcia, M. E. Ostrosky-Wegman, P. Micronuclei induced by airborne particulate matter from Mexico City. *Mutation Research-Genetic Toxicology and Environmental Mutagenesis* **2007**, *631*, 9-15.
22. http://www.epa.gov/ies/pdf/india/iesfinal_0405.pdf
23. Ginevan, M.E.; *Introduction to Environmental Forensic,* 2nd Edition, Elsevier Academic Press, 2007; chapter 6
24. Egan, B.A. Murphy, L.; *Introduction to Environmental Forensic,* 2nd Edition, Elsevier Academic Press, 2007; chapter 12
25. Wait, D. Ramsey, C.; *Introduction to Environmental Forensic,* 2nd Edition, Elsevier Academic Press, 2007; chapter 4
26. Gauthier, T.D. Hawley, M.E.; *Introduction to Environmental Forensic,* 2nd Edition, Elsevier Academic Press, 2007; chapter 5
27. Vasconcellos, P. C.; Balasubramanian, R.; Bruns, R. E.; Sanchez-Ccoyllo, O.; Andrade, M. F.; Flues, M. Water-soluble ions and trace metals in airborne particles over urban areas of the state of sauo paulo, Brazil: Influences of local sources and long range transport. *Water Air and Soil Pollution* **2007**, *186*, 63-73.
28. Okuda, T.; Nakao, S.; Katsuno, M.; Tanaka, S. Source identification of nickel in TSP and PM2.5 in Tokyo, Japan. *Atmospheric Environment* **2007**, *41*, 7642-7648.
29. Garcia, R.; Ma, C. T.; Padilla, H.; Belmont, R.; Azpra, E.; Arcega-Cabrera, F.; Baez, A. Measurement of chemical elements in rain from Rancho Viejo, a rural wooded area in the State of Mexico, Mexico. *Atmospheric Environment* **2006**, *40*, 6088-6100.
30. Theodosi, C.; Im, U.; Bougiatioti, A.; Zarmpas, P.; Yenigun, O.; Mihalopoulos, N.

Aerosol chemical composition over Istanbul. *Science of the Total Environment* **2010**, *408*, 2482-2491.

31. Canepari, S.; Astolfi, M. L.; Moretti, S.; Curini, R. Comparison of extracting solutions for elemental fractionation in airborne particulate matter. *Talanta* **2010**, *82*, 834-844.
32. Cheung, K.; Daher, N.; Kam, W.; Shafer, M. M.; Ning, Z.; Schauer, J. J.; Sioutas, C. Spatial and temporal variation of chemical composition and mass closure of ambient coarse particulate matter (PM10-2.5) in the Los Angeles area. *Atmospheric Environment* **2011**, *45*, 2651-2662.
33. Watson, J.G. Chow, J.C.; *Introduction to Environmental Forensic,* 2nd Edition, Elsevier Academic Press, 2007; chapter 8
34. Johnson, G.W. Ehrlich, R. Full, W. Ramos, S.*; Introduction to Environmental Forensic,* 2nd Edition, Elsevier Academic Press, 2007; chapter 7
35. Shukla, S. P.; Sharma, M. Source apportionment of atmospheric PM10 in Kanpur, India. *Environmental Engineering Science* **2008**, *25*, 849-861.
36. Cancio, J.L.; Castellano, A.V.; Herna´ndez, M.C.; Bethencourt, R. G.; Ortega, E. M. Metallic species in atmospheric particulate matter in Las Palmas de Gran Canaria. *Journal of Hazardous Materials.* **2008**, 160, 521–528.
37. Godoy, M.; Godoy, J. M.; Roldao, L. A.; Soluri, D. S.; Donagemma, R. A. Coarse and fine aerosol source apportionment in Rio de Janeiro, Brazil. *Atmospheric Environment* **2009**, *43*, 2366-2374.
38. Brinkman, G.L.; Milford, J.B.; Schauer, J.J.; Shafer, M.M.; Hannigan, M.P. Source identification of personal exposure to fine particulate matter using organic tracers, *Atmospheric Environment*, **2009** ,43, 1972–1981.
39. von Schneidemesser, E.; Stone, E. A.; Quraishi, T. A.; Shafer, M. M.; Schauer, J. J. Toxic metals in the atmosphere in Lahore, Pakistan. *Science of the Total Environment* **2010**, *408*, 1640-1648.
40. Cantanho, A.D.A.; Artaxo, P. Wintertime and summertime Sao Paulo aerosol source

apportionment study. *Atmospheric Environment* **2001**, *35,* 4889-4902.

41. Khan, M. F.; Hirano, K.; Masunaga, S. Quantifying the sources of hazardous elements of suspended particulate matter aerosol collected in Yokohama, Japan. *Atmospheric Environment* **2010**, *44*, 2646-2657.
42. Querol, X.; Alastuey, A.; Rodriguez, S.; Plana, F.; Ruiz, C. R.; Cots, N. Massague, G. Puig, O. PM 10 and PM2.5 source apportionment in the Barcelona Metropolitan area, Catalonia, Spain. *Atmospheric Environment* **2001**, *35*, 6407-6419.
43. Chen, S. J.; Cheng, S. Y.; Shue, M. F.; Huang, K. L.; Tsai, P. J.; Lin, C. C. The cytotoxicities induced by PM10 and particle-bound water-soluble species. *Science of the Total Environment* **2006**, *354*, 20-27.
44. Zhang, L.; Masui, M.; Mizukoshi, H.; Ninomiya, Y.; Koketsu, J.; Kanaoka, C. Properties of water-soluble and insoluble particulate matter emitted from dewatered sewage sludge incineration in a pilot-scale ash melting furnace. *Fuel* **2008**, *87*, 964-973.
45. Cheng, M.T.; Chou, W.C;. Chio, C.P.; Hsu, S.C.; Su, Y.R.; Kuo, P.H.; Tsuang, B.J.; Lin, S. H.; Chou, C. C. K. Compositions and source apportionments of atmospheric aerosol during Asian dust storm and local pollution in central Taiwan. *Journal of Atmospheric Chemistry* **2008**, *61*, 155-173.
46. Veli, S.; Kirli, L.; Alyuz, B.; Durmusoglu, E. Characterization of bottom ash, fly ash, and filter cake produced from hazardous waste incineration. *Polish Journal of Environmental Studies* **2008**, *17*,139-145.
47. Vedal, S.; Hannigan, M. P.; Dutton, S. J.; Miller, S. L.; Milford, J. B.; Rabinovitch, N.; Kim, S. Y.; Sheppard, L. The Denver Aerosol Sources and Health (DASH) study: Overview and early findings. *Atmospheric Environment* **2009**, *43*, 1666-1673
48. Dos Santos, M.; Gomez, D.; Dawidowski, L.; Gautier, E.; Smichowski, P. Determination of water-soluble and insoluble compounds in size classified airborne particulate matter. *Microchemical Journal,* **2009**, *91*, 133-139.
49. Terzi, E.; Argyropoulos, G.; Bougatioti, A.; Mihalopoulos, N.; Nikolaou, K.; Samara, C.

Chemical composition and mass closure of ambient PM10 at urban sites. *Atmospheric Environment* **2010**, *44*, 2231-2239.

50. Basak, B.; Alagha, O. Trace metals solubility in rainwater: evaluation of rainwater quality at a watershed area, Istanbul. *Environmental Monitoring and Assessment* **2010**, *167*, 493-503.
51. Kumar, A.; Sarin, M. M. Aerosol iron solubility in a semi-arid region: temporal trend and impact of anthropogenic sources. *Tellus Series B-Chemical and Physical Meteorology* **2010**, *62*, 125-132.
52. Gabor, M.; Mihaly, O.; Istvan, V.; Peter, C.; Roland, D.; Gyula, Z. Chemical characterization of PM10 fractions of urban aerosol. *Microchemical Journal* **2011**, *98*, 1-10.
53. Popovicheva, O.; Kireeva, E.; Shonija, N.; Zubareva, N.; Persiantseva, N.; Tishkova, V.; Demirdjian, B.; Moldanova, J.; Mogilnikov, V. Ship particulate pollutants: Characterization in terms of environmental implication. *Journal of Environmental Monitoring* **2009**, *11*, 2077-2086.
54. Sato, K.; Tamura, T.; Furuta, N. Partitioning between soluble and insoluble fractions of major and trace elements in size-classified airborne particulate matter collected in Tokyo. *Journal of Environmental Monitoring* **2008**, *10*, 211-218.
55. Millette, J.R.; Brown, R.S. *Introduction to Environmental Forensic,* 2nd Edition, Elsevier Academic Press, 2007; chapter 13
56. Ham, W. A.; Ruehl, C. R.; Kleeman, M. J. Seasonal Variation of Airborne Particle Deposition Efficiency in the Human Respiratory System. *Aerosol Science and Technology* **2011**, *45*, 795-804.
57. Lindgren, P. F.; Dasgupta, P. K. Measurement of atmospheric sulfur-dioxide by diffusion scrubber coupled ion chromatography. *Analytical Chemistry* **1989**, *61*, 19-24.
58. Zhang, G.; Dasgupta, P. K.; Dong, S. Measurement of atmospheric ammonia. *Environmental Science & Technology* **1989**, *23*, 1467-1474.

59. Vecera, Z.; Dasgupta, P. K. Measurement of ambient nitrous-acid and a reliable calibration source for gaseous nitrous-acid. *Environmental Science & Technology* **1991**, *25*, 255-260.
60. Vecera, Z.; Dasgupta, P. K. Measurement of atmospheric nitric and nitrous acids with a wet effluent diffusion denuder and low-pressure ion chromatography postcolumn reaction detection. *Analytical Chemistry* **1991**, *63*, 2210-2216.
61. Simon, P. K.; Dasgupta, P. K. Continuous automated measurement of the soluble fraction of atmospheric particulate matter. *Analytical Chemistry* **1995**, *67*, 71-78.
62. Simon, P. K.; Dasgupta, P. K. continuous automated measurement of gaseous nitrous and nitric-acids and particulate nitrite and nitrate. *Environmental Science & Technology* **1995**, *29*, 1534-1541.
63. Poruthoor, S. K.; Dasgupta, P. K. An automated instrument for the measurement of atmospheric aerosol composition. *American Laboratory* **1997**, *29*, 51.
64. Ito, K.; Chasteen, C. C.; Chung, H. K.; Poruthoor, S. K.; Zhang, G. F.; Dasgupta, P. K. A continuous monitoring system for strong acidity in aerosols. *Analytical Chemistry* **1998**, *70*, 2839-2847.
65. Zhang, G. F.; Slanina, S.; Boring, C. B.; Jongejan, P. A. C.; Dasgupta, P. K. Continuous wet denuder measurements of atmospheric nitric and nitrous acids during the 1999 Atlanta Supersite. *Atmospheric Environment* **2003**, *37*, 1351-1364.
66. Toda, K.; Ohira, S.; Tanaka, T.; Nishimura, T.; Dasgupta, P. K. Field instrument for simultaneous large dynamic range measurement of atmospheric hydrogen sulfide, methanethiol, and sulfur dioxide. *Environmental Science & Technology* **2004**, *38*, 1529-1536.
67. Ullah, S. M. R.; Takeuchi, M.; Dasgupta, P. K. Versatile gas/particle ion chromatograph. *Environmental Science & Technology* **2006**, *40*, 962-968.
68. Samanta, G.; Boring, C. B.; Dasgupta, P. K. Continuous automated measurement of hexavalent chromium in airborne particulate matter. *Analytical Chemistry* **2001**, *73*.

2034-2040.

69. http://www.iupac.org/publications/pac/1993/pdf/6504x0819.pdf
70. Takeuchi, T. Modern aspects of micro-bore column HPLC. *Fresenius Zeitschrift Fur Analytische Chemie* **1989**, *334*, 616-616.
71. Horvath, C. G.; Preiss, B. A.; Lipsky, S. R. Fast liquid chromatography - an investigation of operating parameters and separation of nucleotides on pellicular ion exchangers. *Analytical Chemistry* **1967**, *39*, 1422.
72. Ishii,D.; Asai, K.; Hibi, K.; Jonokuchi, T.; Nagaya, M. A study of micro-high-performance liquid chromatography: I. Development of technique for miniaturization of high-performance liquid chromatography, *J. Chromatography.* **1977**, *144*, 157.
73. Vissers, J. P. C.; Claessens, H. A.; Cramers, C. A. Microcolumn liquid chromatography: Instrumentation, detection and applications. *Journal of Chromatography A* **1997**, *779*, 1-28.
74. Legido-Quigley, C.; Marlin, N. D.; Melin, A.; Manz, N.; Smith, W. Advances in capillary electrochromatography and micro-high performance liquid chromatography monolithic columns for separation science. *Electrophoresis* **2003**, *24*, 917-944.
75. Takeuchi, T. Development of capillary liquid chromatography; *Chromatography*, **2005**, 26, 1
76. Small, H.; Stevens, T. S.; Bauman, W. C. Novel ion-exchange chromatographic method using conductimetric detection. *Analytical Chemistry* **1975**, *47*, 1801-1809.
77. Kuban, P.; Dasgupta, P. K. Capillary ion chromatography. *Journal of Separation Science* **2004**, *27*, 1441-1457.
78. Rokushika, S.; Qiu , Z.Y.; Hatano , H. Micro column ion chromatography with a hollow fibre suppressor;; *J. Chromatogr.* **1983**, *260*, 81-8780.
79. Rokushika, S.; Zong, Y.Q.; Zhuo, L.S.; Hatano, H. Microbore packed-column anion chromatography using a Uv detector. *Journal of Chromatography* **1983**, *280*, 69-76.

80. Sjogren, A.; Boring, C. B.; Dasgupta, P. K.; Alexander, J. N. Capillary ion chromatography with on-line high pressure electrodialytic NaOH eluent production and gradient generation. *Analytical Chemistry* **1997**, *69*. 1385-1391.
81. Boring, C. B.; Dasgupta, P. K.; Sjogren, A. Compact, field-portable capillary ion chromatograph. *Journal of Chromatography A* **1998**, *804*, 45-54.
82. Boring, C. B.; Poruthoor, S. K.; Dasgupta, P. K. Wet effluent parallel plate diffusion denuder coupled capillary ion chromatograph for the determination of atmospheric trace gases. *Talanta* **1999**, *48*, 675-684.
83. Takeuchi, T.; Suzuki, E.; Ishii, D. Indirect Photometric Detection of Monovalent Cations via Postsuppressor Ion Replacement in Microcolumn Ion Chromatography. *Chromatographia,* **1988**, *25*, 582.
84. Muller, S. R.; Simon, W.; Widmer, H. M.; Grolimund, K.; Schomburg, G.; Kolla, P. Separation of cations by open-tubular column liquid-chromatography. *Analytical Chemistry* **1989**, *61*, 2747-2750.
85. http://www.dionex.com/en-us/webdocs/35499-ICS3000_Environmental_Brochure_V28_releasedJC030206.pdf
86. Dasgupta, P. K.; Eom, I. Y.; Morris, K. J.; Li, J. Z. Light emitting diode-based detectors absorbance, fluorescence and spectroelectrochemical measurements in a planar flow-through cell. *Analytica Chimica Acta* **2003**, *500*, 337-364.
87. Dasgupta, P. K.; Soroka, K.; Vithanage, R. S. Metal Ion Chromatography with Fluorescence Detection. *J. Liq. Chromatogr.* **1987,** *10*, 3287-3319.
88. Mishra, S. K.; Dasgupta, Purnendu K. Capillary scale light emitting diode based multi-reflection absorbance detector. *Analytica Chimica Acta* **2007**, *605*, 166-174.
89. Song, G. Q.; Villanueva-Fierro, I.; Ohira, S. I.; Mishra, S., Bailiff, H.; Savage, C. R.; Dasgupta, P. K. Capillary scale liquid core waveguide based fluorescence detectors for liquid chromatography and flow analysis. *Talanta* **2008**, *77*, 901-908.
90. Mishra, S.K.; Dasgupta, P.K. Electrodialytic reagent introduction in flow systems.

Analytical Chemistry **2010**, *82*, 3981-3984.

91. Khaledi, M. *High Performance Capillary Electrophoresis*, John Wiley & Sons, 1998, 146, 303.
92. Kitagishi, K.; Sato, Y. Significant improvement of signal-to-noise ratio in capillary electrophoresis through optimization of aperture width for UV absorption detection. *Electrophoresis* **2001,** *22*, 3395-3400.
93. Kahle, V. Fiber optic z-cell for CZE, *Biomed. Chromatogr*. **1999**,*13*, 93.
94. Liu, H. H.; Dasgupta, P. K., Dual-wavelength photometry with light-emitting-diodes - compensation of refractive-index and turbidity effects in flow-injection analysis. *Analytica Chimica Acta* **1994,** *289*, 347-353.
95. Boring, C. B.; Dasgupta, P. K., An affordable high-performance optical absorbance detector for capillary systems. *Analytica Chimica Acta* **1997,** *342*, 123-132.
96. Dasgupta, P.K.; Rhee, J.S.; Loree, E.L. A Simple and Versatile Photodetector System for Peak-width Measurement-Based Flow Injection Analysis. *Spectroscopy,* **1987**, *10*, 39.
97. Dasgupta, P. K., Multipath cells for extending dynamic-range of optical absorbance measurements. *Analytical Chemistry* **1984,** *56*, 1401-1403.
98. Dasgupta, P. K.; Rhee, J. S. Optical-cells with partially reflecting windows as nonlinear absorbency amplifiers. *Analytical Chemistry* **1987,** *59*, 783-786.
99. Tsuda, T.; Sweedler, J. V.; Zare, R. N. Rectangular capillaries for capillary zone electrophoresis. *Analytical Chemistry* **1990,** *62*, 2149-2152.
100. Xue, Y. J.; Yeung, E. S. Characterization of band broadening in capillary electrophoresis due to nonuniform capillary geometries. *Analytical Chemistry* **1994,** *66*, 3575-3580.
101. Xi, X. B.; Yeung, E. S. Axial-beam absorption detection for capillary electrophoresis with a conventional light-source. *Applied Spectroscopy* **1991** *45*, 1199-1203.

102. Wada, A.; Harada, M.; Okada, T. Kinetic monitoring of electrophoretically induced solute reaction by axial absorption detection with liquid-core waveguide. *Analytical Chemistry* **2006,** *78*, 4709-4712.

103. Wang, T. S.; Aiken, J. H.; Huie, C. W.; Hartwick, R. A. Nanoliter-scale multireflection cell for absorption detection in capillary electrophoresis. *Analytical Chemistry* **1991,** *63*, 1372-1376.

104. Wang, T. US Patent 5,273,635, December 28, 1993.

105. J.-P. Chervet, US Patent 5,057,216, October 15, 1991

106. Moring, S. E.; Reel, R. T.; Vansoest, R. E. J. Optical improvements of a z-shaped cell for high-sensitivity uv absorbency detection in capillary electrophoresis. *Analytical Chemistry* **1993,** *65*, 3454-3459.

107. Djordjevic, N. M.; Ryan, K. An easy way to enhance absorbance detection sensitivity of waters Quanta-4000 capillary electrophoresis system. *Journal of Liquid Chromatography & Related Technologies* **1996,** *19*, 201-206.

108. Djordjevic, N. M.; Widder, M.; Kuhn, R. Signal enhancement in capillary electrophoresis by using a sleeve cell arrangement for optical detection *J. High Resolut. Chromatogr.* **1997**, 20, 189.

109. Heiger, D. N.; Kaltenbach, P.; Sievert, H. J. P. Diode-array detection in capillary electrophoresis. *Electrophoresis* **1994,** *15* (10), 1234-1247.

110. Xue, Y. J.; Yeung, E. S., Characterization of band broadening in capillary electrophoresis due to nonuniform capillary geometries. *Analytical Chemistry* **1994,** *66*, 3575-3580.

111. Culbertson, C. T.; Jorgenson, J. W. Lowering the UV absorbance detection limit and increasing the sensitivity of capillary electrophoresis using a dual linear photodiode array detector and signal averaging. *Journal of Microcolumn Separations* **1999,** *11*, 652-662

112. Liu, H. H.; Dasgupta, P. K.; Zheng, H. J. High-performance optical absorbency detectors based on low-noise switched integrators. *Talanta* **1993,** *40*, 1331-1338.

113. Dasgupta, P. K.; Bellamy, H. S.; Liu, H. H.; Lopez, J. L.; Loree, E. L.; Morris, K.; Petersen, K.; Mir, K. A. Light-emitting diode based flow-through optical-absorption detectors. *Talanta* **1993,** *40*, 53-74.

114. Dasgupta, P. K.; Eom, I.-Y.; Morris, K. J.; Li, J. Light emitting diode based detectors. Absorbance, fluorescence and spectroelectrochemical measurements in a planar flow-through cell. *Anal. Chim. Acta*, **2003**, 500, 337-364.

115. Eom, I. Y.; Dasgupta, P. K. Frequency-selective absorbance detection: Refractive index and turbidity compensation with dual-wavelength measurement. *Talanta* **2006,** *69*, 906-913.

116. White, J.U. Long optical paths of large aperture. *Journal Of The Optical Society Of America* , **1942**, 32, 285.

117. Moosavi, H.S.; Jiang, Y.; Lester, L.; McKinnon, G.; Harrison, D.J. A multireflection cell for enhanced absorbance detection in microchip-based capillary electrophoresis devices, *Electrophoresis,* **2000***, 21,* 1291-1299.

118. Ellis, P. S.; Lyddy-Meaney, A. J.; Worsfold, P. J.; McKelvie, I. D., Multi-reflection photometric flow cell for use in flow injection analysis of estuarine waters. *Analytica Chimica Acta* **2003,** *499*, 81-89.

119. Fogg, A. G.; Cipko, E.; Farabella, L.; Tyson, J. F. Shapes of flow-injection signals - effect of refractive-index on spectrophotometric signals obtained for online formation of bromine from bromate, bromide and hydrogen-ion in a single-channel manifold using large-volume time-based injections. *Analyst* **1990,** *115*, 593-597.

120. Dasgupta, P. K.; Bellamy, H. S.; Liu, H. H. Sandwich-type flow-through fiberoptic cells for optical absorbency measurements. *Talanta* **1993,** *40*, 341-345.

121. Jambunathan, S.; Dasgupta, P. K.; Wolcott, D. K.; Marshall, G. D.; Olson, D. C. Optical fiber coupled light emitting diode based absorbance detector with a reflective flow cell. *Talanta* **1999,** *50*, 481-490.

122. Global FIA Inc., XLD Miniphotometer Detector, http://globalfia.com/whatsnew/xld.html.

123. Liu, H. H.; Dasgupta, P. K. Dual-wavelength photometry with light-emitting-diodes - compensation of refractive-index and turbidity effects in flow-injection analysis. *Analytica Chimica Acta* **1994,** *289*, 347-353.

124. Cassidy, R.; Janoski, M. Is your calibration curve linear. *Lc Gc-Magazine of Separation Science* **1992,** *10*, 692.

125. Hauser, P. C.; Rupasinghe, T. W. T.; Cates, N. E., A multiwavelength photometer based on light-emitting-diodes. *Talanta* **1995,** *42* (4), 605-612.

126. Kuban, P.; Dasgupta, P. K. Capillary Ion Chromatography. A Review. *Journal of Separation Science* **2004,** *27,* 1441-1457.

127. Kuban, P.; Dasgupta, P. K.; Pohl, C. A. Open tubular anion exchange chromatography. Controlled layered architecture of stationary phase by successive condensation polymerization. *Analytical Chemistry* **2007,** *79*, 5462-5467.

128. Yang, B. C.; Takeuchi, M.; Dasgupta, P. K. On-line gas-free electrodialytic eluent generator for capillary ion chromatography. *Analytical Chemistry* **2008,** *80*, 40-47.

129. Kubán, P.; Kubán, V.; Klakurková, L.; Dasgupta, P. K. Gravity-flow Open Tubular Cation Chromatography. *J. Sep. Sci.* **2008**, *31*, 2745-2753.

130. Parrot, S.; Bert, L.; Mouly-Badina, L.; Sauvinet, V.; Colussi-Mas, J.; Lambas-Senas, L.; Robert, F.; Bouilloux, J. P.; Suaud-Chagny, M. F.; Denoroy, L.; Renaud, B. Microdialysis monitoring of catecholamines and excitatory amino acids in the rat and mouse brain: Recent developments based on capillary electrophoresis with laser-induced fluorescence detection - A mini-review. *Cellular and Molecular Neurobiology* **2003,** *23*, 793-804.

131. Gonzalez, E.; Laserna, J. J. Laser induced fluorescence detection in capillary electrophoresis. A review of instrumental advances and analytical applications. *Quimica Analitica* **1997,** *16*, 3-15.

132. Dasgupta, P. K.; Zhang, G. F.; Li, J. Z.; Boring, C. B.; Jambunathan, S.; Al-Horr, R. Luminescence detection with a liquid care waveguide. *Analytical Chemistry* **1999,** *71* (7), 1400-1407.

133. Dallas, T.; Dasgupta, P. K. Light at the end of the tunnel: recent analytical applications of liquid-core waveguides. *Trac-Trends in Analytical Chemistry* **2004,** *23*, 385-392.

134. Okada, T. Liquid-core waveguide in CE. *Electrophoresis* **2007,** *28*, 3414-3419.

135. Hanning, A. Lindberg, P. Westberg, J. Roeraade, J. Laser-induced fluorescence detection by liquid core waveguiding applied to dna sequencing by capillary electrophoresis**,** *Analytical Chemistry* **2000**, 72, 3423–3430.

136. Curcio, M.; Stalhandske, P.; Lindberg, P.; Roeraade, J. Multiplex high-throughput solid-phase minisequencing by capillary electrophoresis and liquid core waveguide fluorescence detection. *Electrophoresis* **2002,** *23*, 1467-1472.

137. Liu, Z.; Pawliszyn, J. Capillary isoelectric focusing of proteins with liquid core waveguide laser-induced fluorescence whole column imaging detection. *Analytical Chemistry* **2003,** *75*, 4887-4894.

138. Liu, Z.; Pawliszyn, J. Applications of capillary isoelectric focusing with liquid-core waveguide laser-induced fluorescence whole-column imaging detection. *Analytical Biochemistry* **2005,** *336*, 94-101.

139. Olivares, J. A.; Stark, P. C.; Jackson, P. Liquid core waveguide for full imaging of electrophoretic separations. *Analytical Chemistry* **2002,** *74*, 2008-2013.

140. Li, J. Z.; Dasgupta, P. K.; Genfa, Z. Transversely illuminated liquid core waveguide based fluorescence detection - Fluorometric flow injection determination of aqueous ammonium/ammonia. *Talanta* **1999,** *50*, 617-623.

141. Kostal, V.; Zeisbergerova, M.; Hrotekova, Z.; Slais, K.; Kahle, V. Miniaturized liquid core waveguide-based fluorimetric detection cell for capillary separation methods: Application in CE of amino acids. *Electrophoresis* **2006,** *27*, 4658-4665.

142. Wang, S. L.; Huang, X. J.; Fang, Z. L.; Dasgupta, P. K. A miniaturized liquid core waveguide-capillary electrophoresis system with flow injection sample introduction and fluorometric detection using light-emitting diodes. *Analytical Chemistry* **2001,** *73*, 4545-4549.

143. Li, Q. Y.; Morris, K. J.; Dasgupta, P. K.; Raimundo, I. M.; Temkin, H. Portable flow-injection analyzer with liquid-core waveguide based fluorescence, luminescence, and long path length absorbance detector. *Analytica Chimica Acta* **2003,** *479*, 151-165.

144. Wang, S. L.; Fan, X. F.; Xu, Z. R.; Fang, Z. L. A simple microfluidic system for efficient capillary electrophoretic separation and sensitive fluorimetric detection of DNA fragments using light-emitting diode and liquid-core waveguide techniques. *Electrophoresis* **2005,** *26*, 3602-3608.

145. Zhao, Y. G.; Lin, Z. H.; Liao, H. P.; Duan, C. Y.; Meng, Q. J. A highly selective fluorescent chemosensor for Al3+ derivated from 8-hydroxyquinoline. *Inorganic Chemistry Communications* **2006,** *9*, 966-968.

146. Li, J. Z.; Dasgupta, P. K. Measurement of atmospheric hydrogen peroxide and hydroxymethyl hydroperoxide with a diffusion scrubber and light emitting diode-liquid core waveguide-based fluorometry. *Analytical Chemistry* **2000,** *72*, 5338-5347.

147. Li, J. Dasgupta, P.K.; Genfa, Z.; Hutterli, M.A. Field Measurement of Atmospheric Formaldehyde with a Diffusion Scrubber and Light emitting Diode-Liquid Core Waveguide based Fluorometry . *Field Analytical Chemistry and Technology* **2001,** *5,* 2-11.

148. Toda, K.; Dasgupta, P. K.; Li, J.; Tarver, G. A.; Zarus, G. M.; Ohira, S.-I. Measurement of Atmospheric Hydrogen Sulfide by Continuous Flow Fluorometry, *Anal. Sci.* **2001,** *17(Supp),* i407-i410

149. Li, Q. Y.; Dasgupta, P. K.; Temkin, H. K. Airborne bacterial spore counts by terbium-enhanced luminescence detection: Pitfalls and real values. *Environmental Science & Technology* **2008,** *42*, 2799-2804.

150. Genfa, Z.; Dasgupta, P. K. Hematin as a peroxidase substitute in hydrogen-peroxide determinations. *Analytical Chemistry* **1992,** *64*, 517-522.

151. Li, J. Z.; Dasgupta, P. K.; Tarver, G. A. Pulsed excitation source multiplexed fluorometry for the simultaneous measurement of multiple analytes. Continuous measurement of atmospheric hydrogen peroxide and methyl hydroperoxide. *Analytical Chemistry* **2003,** *75*, 1203-1210.

152. Manor, R. Datta, A. Dhar, A. Holtz, M.; Berg, J.; Gangopadhyay, S.; Dasgupta, P. K.; Temkin, H.; Veraraghavan, V.; Vijayraghavan, R.; Dallas, T. Microfabricated Liquid Core Waveguides for Microanalysis Systems *Proc. IEEE Sensors,* **2002**, 1, 660-664.

153. Datta, A.; Eom, I. Y.; Dhar, A.; Kuban, P.; Manor, R.; Ahmad, I.; Gangopadhyay, S.; Dallas, T.; Holtz, M.; Temkin, F.; Dasgupta, P. K. Microfabrication and characterization of Teflon AF-coated liquid core waveguide channels in silicon. *IEEE Sensors Journal* **2003,** *3*, 788-795.

154. Takeuchi, M.; Li, Q. Y.; Yang, B. C.; Dasgupta, P. K.; Wilde, V. E. Use of a capacitance measurement device for surrogate noncontact conductance measurement. *Talanta* **2008,** *76*, 617-620.

155. Ferguson, W. J.; Braunschweiger, K. I.; Braunschweiger, W. R.; Smith, J. R.; McCormick, J. J.; Wasmann, C. C.; Jarvis, N. P.; Bell, D. H.; Good, N. E. Hydrogen-ion buffers for biological-research. *Analytical Biochemistry* **1980,** *104*, 300-310.

156. Nichia Corporation, Specification for Nichia Chip Type UV LED Model NCSU033A(T). http://www.nichia.com/specification/led smd/NCSU033ATE. pdf (accessed May 25, 2008).

157. Hamamatsu Photonics, Metal Package PMT Photosensor Module H5784 Series. http://sales.hamamatsu.com/assets/pdf/parts H/H5784 series.pdf (accessed May 25, 2008).

158. Soroka, K.; Vithanage, R. S.; Phillips, D. A.; Walker, B.; Dasgupta, P. K. Fluorescence properties of metal-complexes of 8-hydroxyquinoline-5-sulfonic acid and chromatographic applications. *Analytical Chemistry* **1987,** *59*, 629-636.

159. Melanson, J. E.; Lucy, C. A. Violet (405 nm) diode laser for laser induced fluorescence detection in capillary electrophoresis. *Analyst* **2000,** *125*, 1049-1052.

160. Melanson, J. E.; Lucy, C. A. Enhanced detection of porphyrins by capillary electrophoresis-laser induced fluorescence. *Electrophoresis* **2002,** *23*, 1689-1694.

161. de Jong, E. P.; Melanson, J. E.; Lucy, C. A. Noncovalent labelling of myoglobin for capillary electrophoresis with laser-induced fluorescence detection by reconstitution with a fluorescent porphyrin. *Electrophoresis* **2004,** *25*, 3153-3162.

162. Vos, C. J.; Melanson, J. E.; Lucy, C. A. Violet diode laser for metal ion determination by capillary electrophoresis-laser induced fluorescence. Analytical Sciences 2001, 17, 225-227.

163. Melanson, J. E.; Boulet, C. A.; Lucy, C. A. Indirect laser-induced fluorescence detection for capillary electrophoresis using a violet diode laser. *Analytical Chemistry* **2001,** *73*, 1809-1813.

164. Jiang, J.; Lucy, C. A. Determination of glyphosate using off-line ion exchange preconcentration and capillary electrophoresis-laser induced fluorescence detection. *Talanta* **2007,** *72*, 113-118.

165. M. Hatcher, Sony ramps monthly GaN laser volume to 1.7m, April 27, 2008. Optics.org; http://optics.org/cws/article/industry/27746 (accessed May 25, 2008).

166. L. Wright, S. Goldwasser, Dissection of a Blu-ray reader assembly, March 8, 2007. http://www.repairfaq.org/sam/Blu-ray/site1/, see also http://www. fineartradiography.com/hobbies/lasers/blu-ray/diode.html (accessed May 25, 2008).

167. M. Taylor, Build a blue laser pointer. http://youtube.com/watch?v=R21hNxS78- I (accessed May 25, 2008).

168. Kipkay, Blu-ray laser phaser. http://youtube.com/watch?v=xfj1n8vPWCE (accessed May 25, 2008).

169. Prahl, S. Oregon Medical Laser Center. Optical Spectra: Coumarin 30. http://omlc.ogi.edu/spectra/PhotochemCAD/html/coumarin30.html (accessed May 25, 2008).

170. Paliwal, S.; Wales, M.; Good, T.; Grimsley, J.; Wild, J.; Simonian, A. Fluorescence-based sensing of p-nitrophenol and p-nitrophenyl substituent organophosphates. *Analytica Chimica Acta* **2007,** *596*, 9-15.

171. Blu-ray disc founders, August 2004. White Paper Blu-ray disc format. http://www.docstoc.com/docs/479157/Blu-ray-Disc-Format—General (accessed May 25, 2008)

172. Palacios, M. A.; Wang, Z.; Montes, V. A.; Zyryanov, G. V.; Hausch, B. J.; Jursikova, K.; Anzenbacher, P. Hydroxyquinolines with extended fluorophores: arrays for turn-on and ratiometric sensing of cations. *Chemical Communications* **2007,** 36, 3708-3710.

173. Zhao, Y. G.; Lin, Z. H.; Liao, H. P.; Duan, C. Y.; Meng, Q. J. A highly selective fluorescent chemosensor for Al3+ derivated from 8-hydroxyquinoline. *Inorganic Chemistry Communications* **2006,** *9*, 966-968.

174. Zhang, H.; Han, L. F.; Zachariasse, K. A.; Jiang, Y. B. 8-Hydroxyquinoline benzoates as highly sensitive fluorescent chemosensors for transition metal ions. *Organic Letters* **2005,** *7*, 4217-4220.

175. Phillips, D. A.; Soroka, K.; Vithanage, R. S.; Dasgupta, P. K. Enhancement and quenching of fluorescence of metal-chelates of 8-hydroxyquinoline-5-sulfonic acid. *Mikrochimica Acta* **1986,** *1*, 207-220.

176. Dasgupta, P. K.; Soroka, K.; Vithanage, R. S. Metal Ion Chromatography with Fluorescence Detection. *J. Liq. Chromatogr.* **1987,** *10*, 3287-3319.

177. Mulon, J.B. Destandau, E. Alain, V. Bardez, E. How can aluminium(III) generate fluorescence? *J. Inorg. Biochem*. ***2005***, 99, 1749–1755.

178. Moore, S.; Stein, W. H. Chromatography Of Amino Acids On Sulfonated Polystyrene Resins, *J. Biol. Chem.* **1951**, *192*, 663–681.

179. Spackman, D. H.; Stein, W. H.; Moore, S. Automatic recording apparatus for use in the chromatography of amino acids . *Anal. Chem.* **1958**, *30*, 1190–1206.

180. Lillig, B.; Engelhardt, H. In *Reaction Detection in Liquid Chromatography*; Krull, I. S., Ed.; Marcel Dekker Inc.: New York, 1986; pp 1-53.

181. Cassidy, R. M.; Elchuk, S.; Dasgupta, P. K. Performance of annular membrane and screen-tee reactors for postcolumn-reaction detection of metal-ions separated by liquid-chromatography. *Analytical Chemistry* **1987,** *59*, 85-90.

182. Dasgupta, P. K.; Vithanage, R. S.; Petersen, K. Pulsed reagent introduction through a membrane reactor for flow-injection systems. *Analytica Chimica Acta* **1988,** *215*, 277-282.

183. Hwang, H.; Dasgupta, P. K. Fluorometric flow-injection determination of aqueous peroxides at nanomolar level using membrane reactors. *Analytical Chemistry* **1986,** *58*, 1521-1524.

184. Dasgupta, P. K.; Genfa, Z.; Poruthoor, S. K.; Caldwell, S.; Dong, S.; Liu, S. Y. High-sensitivity gas sensors based on gas-permeable liquid core waveguides and long-path absorbance detection. *Analytical Chemistry* **1998,** *70*, 4661-4669.

185. Ganranoo, L.; Mishra, S. K.; Azad, A. K.; Shigihara, A.; Dasgupta, P. K.; Breitbach, Z. S.; Armstrong, D. W.; Grudpan, K. ; Rappenglueck, B. Measurement of nitrophenols in rain and air by two-dimensional liquid chromatography-chemically active liquid core waveguide spectrometry. *Anal.Chem.* **2010**, 82, 5838-5843.

186. Zhang, G.; Dasgupta, P. K.; Sigg, A. Determination of gaseous-hydrogen peroxide at parts-per-trillion levels with a nafion membrane scrubber and a single-line flow-injection system. *Analytica Chimica Acta* **1992,** *260*, 57-64.

187. Sata, T. *Ion Exchange Membranes: Preparation, Characterization, Modification and Application.* Royal Society Of Chemistry: London, U.K., 2004.

188. Berglund, I.; Dasgupta, P. K.; Lopez, J. L.; Nara, O. 2-Dimensional conductometric detection in ion chromatography -sequential suppressed and single column detection. *Analytical Chemistry* **1993,** *65*, 1192-1198.

189. Sjogren, A.; Dasgupta, P. K. 2-Dimensional conductometric detection in ion chromatography - analyte identification, quantitation of very weak acid anions, and universal calibration *Anal. Chem.* **1995**, *67*, 2110–2118.

190. Sjogren, A.; Dasgupta, P. K. A planar microelectrodialytic NaOH generator for eluite conversion after suppressed conductometric detection in ion chromatography. *Analytica Chimica Acta* **1999,** *384*, 135-141.

191. Al-Horr, R.; Dasgupta, P. K.; Adams, R. L. Two-dimensional detection in ion chromatography: Sequential conductometry after suppression and passive hydroxide introduction. *Analytical Chemistry* **2001,** *73*, 4694-4703.

192. Yang, B. C.; Zhang, F. F.; Liang, X. M.; Dasgupta, P. K. A multifunctional dual membrane electrodialytic eluent generator for capillary ion chromatography. *Journal of Chromatography A* **2009,** *1216*, 2412-2416.

193. Dasgupta, P. K.; Poruthoor, S. K. *Compr. Anal. Chem.* **2002**, *37*, 161–276.

194. Lu, C.; Rashinkar, S. M.; Dasgupta, P. K. Semicontinuous Automated Measurement of Organic Carbon in Atmospheric Aerosol Samples. *Analytical Chemistry* **2010,** *82*, 1334-1341.

195. Barron, L.; O'Toole, M.; Diamond, D.; Nesterenko, P. N.; Paull, B. Separation of transition metals on a poly-iminodiacetic acid grafted polymeric resin column with post-column reaction detection utilising a paired emitter-detector diode system. *Journal of Chromatography A* **2008,** *1213*, 31-36.

196. Michalski, R. Applications of Ion Chromatography for the Determination of Inorganic Cations. *Critical Reviews in Analytical Chemistry* **2009,** *39*, 230-250.

197. Dasgupta, P. K. In *Ion Chromatography*; Tarter, J. G., Ed.; Marcel Dekker: New York, 1987 pp 191-367.

198. Rose, D. J. Free-solution reactor for postcolumn fluorescence detection in capillary zone electrophoresis. *Journal of Chromatography* **1991,** *540*, 343-353.

199. Yamamoto, D.; Kaneta, T.; Imasaka, T. Postcolumn derivatization of proteins in capillary sieving electrophoresis/laser-induced fluorescence detection, *Electrophoresis* **2009**, *30*, 3780– 3785

200. Guo, L. H.; Qiu, B.; Jiang, Y. Y.; You, Z. Y.; Lin, J. M.; Chen, G. N. Capillary electrophoresis chemiluminescent detection system equipped with a two-step postcolumn flow interface for detection of some enkephalin-related peptides labeled with acridinium ester. *Electrophoresis* **2008,** *29*, 2348-2355.

201. Yang, B. C.; Chen, Y. J.; Mori, M.; Ohira, S.; Azad, A. K.; Dasgupta, P. K. Charge Detector for the Measurement of Ionic Solutes. *Analytical Chemistry* **2010,** *82*, 951-958.

202. Ghasemi, J.; Ahmadi, S.; Kubista, M.; Forootan, A. Determination of acidity constants of 4-(2-pyridylazo)resorcinol in binary acetonitrile plus water mixtures. *Journal of Chemical and Engineering Data* **2003,** *48*, 1178-1182.

203. Dionex Corporation. Application Note 131. December 1998.

BIOGRAPHICAL INFORMATION

Santosh K. Mishra, the elder son of Mr. Asha Pal Mishra and Mrs. Asha Mishra, has obtained his K-12 education at Atomic Energy Junior College, Mumbai, India. Ever since his initial days of education, his interests were in Science and Mathematics. Beginning in his primary school days, he has been academically oriented, always stood out for his scholastic performance and earned his way into the top ten percent of his class. He received B.Sc.-Chemistry degree (with distinction) from the S.I.E.S. College of Arts, Science and Commerce, University of Mumbai, India. His respectable educational credentials landed him in the Mumbai University Institute of Chemical Technology (MUICT or UDCT), the prestigious engineering college in India, to pursue Bachelor of Chemical Technology-Textile Technology (equivalent to Chemical Engineering with specialization in Textile Technology). At the end of the third year of course work at MUICT, he went to Century Textiles and Industries Ltd. (largest cotton mill in India) as an intern, to gain experience in the field of textile manufacturing. He was the first among his class at MUICT, to receive a job offer through campus interview (from Raymond Ltd, India's and world's largest wool fabric manufacturing company) five months before graduation. He graduated with B. Chem. Tech. - Textile Technology (with distinction) and joined Raymond Ltd. as an Assistant Manager trainee and learned various aspects of textile manufacturing. Soon he realized that graduate study plays an important role in advancement in professional life and made plans to go to the Florida Institute of Technology (FIT) where he performed his thesis research on the removal of pharmaceutical contaminants from water. After receiving his M.S. in Chemistry at FIT, he joined Prof. Purnendu (Sandy) Dasgupta Research Group to obtain his doctoral degree in Analytical Chemistry at the University of Texas at Arlington. There he conducted research to develop automated instrumentation for the measurement of atmospheric metals using capillary ion chromatography.